Physics Lib.

SEP 2 1 1935

DO NOT TAKE FROM LIBRARY
copy 2

THE PHYSICAL REVIEW

VOLUME 48 *Second Series* NUMBER 6

SEPTEMBER 15, 1935

Published for the

AMERICAN PHYSICAL SOCIETY

by the

AMERICAN INSTITUTE OF PHYSICS
Incorporated

LANCASTER, PA., AND NEW YORK, N. Y.

THE AMERICAN PHYSICAL SOCIETY

OFFICERS OF THE SOCIETY

R. W. WOOD, *President*
The Johns Hopkins University
Baltimore, Maryland

F. K. RICHTMYER, *Vice President*
Cornell University
Ithaca, New York

W. L. SEVERINGHAUS, *Secretary*
Columbia University
New York, New York

G. B. PEGRAM, *Treasurer*
Columbia University
New York, New York

JOHN T. TATE, *Editor*
University of Minnesota
Minneapolis, Minnesota

L. B. LOEB, *Local Secretary for the Pacific Coast*
University of California
Berkeley, California

THE PHYSICAL REVIEW

BOARD OF EDITORS

JOHN T. TATE, *Editor*

J. W. BUCHTA, *Assistant Editor*

Associate Editors

K. K. DARROW
J. C. HUBBARD
A. E. RUARK
A. ELLETT
L. A. TURNER
G. E. UHLENBECK
W. V. HOUSTON
R. S. MULLIKEN
I. I. RABI

THE PHYSICAL REVIEW, which was established in 1893, is a journal of experimental and theoretical physics. It is published for the American Physical Society by the American Institute of Physics Incorporated. There are two volumes annually with twelve issues in each volume.

Manuscripts for publication should be submitted to John T. Tate, University of Minnesota, Minneapolis, Minnesota.

Proof and all correspondence concerning papers in the process of publication, should be addressed to the Editorial Secretary, American Institute of Physics, 11 East 38th Street, New York, New York.

Subscription price: United States and Possessions and Canada, $15.00; Foreign, $16.50. Subscriptions and orders for back numbers should be addressed to Prince and Lemon Streets, Lancaster, Pennsylvania, or to the American Institute of Physics, 11 East 38th Street, New York, New York.

Advertising is not accepted for the *Physical Review* but attention is called to the *Review of Scientific Instruments with Physics News and Views*, a companion publication of the Institute, and a medium through which the field of physics can be reached most effectively. Rates and other information will be furnished on request to the Editorial Secretary.

Changes of address and complaints of failure to receive the *Physical Review*, in the case of members of the American Physical Society, should be addressed to the Treasurer; in the case of other subscribers, to the Editorial Secretary. New copies can be sent free in response to complaints of non-delivery only if notice of non-delivery is received within three months of date of issue.

The Physical Review is published semi-monthly at Prince and Lemon Streets, Lancaster, Pennsylvania.

Entered at the Post Office at Lancaster, Pennsylvania, as second class matter.

Acceptance for mailing at special rate of postage provided for in section 1103, Act of October 3, 1917, authorized September 6, 1926.

THE
PHYSICAL REVIEW
A Journal of Experimental and Theoretical Physics
VOL. 48, NO. 6 SEPTEMBER 15, 1935 SECOND SERIES

The Diffraction of X-Rays by Liquid Na-K Alloy in a Magnetic Field

C. W. HEAPS, *The Rice Institute*
(Received June 27, 1935)

Because magnetoresistance is found in the liquid Na-K alloy there is reason to expect that a magnetic field might modify the x-ray diffraction curve of the liquid. Experiment indicates that the diffraction is not changed by as much as two percent in a field of 2700 gauss. A test made to detect magnetostriction in the alloy indicates no volume change per unit volume greater than 3×10^{-7} in a field of 7800 gauss. The cause of magnetoresistance in the liquid does not, therefore, appear to lie in changes of molecular grouping caused by a magnetic field.

THE liquid alloy of sodium and potassium has recently been found to increase its resistance when placed in a magnetic field.[1] It also shows a fairly large Hall effect. The discovery of these galvanomagnetic effects in a liquid is a matter of some importance; it would now seem that a molecular lattice structure is not necessary for the production of the effects, although this structure has occasionally been suggested as fundamental in the phenomena. The empirical fact has been, heretofore, that strongly crystalline substances of low degree of symmetry (e.g., Bi, Sb, graphite) have the largest values of magnetoresistance. The Sommerfeld theory as developed by Houston[2] assumes the resistance of a metal to be due to deviations of the lattice from symmetry, such deviations being caused by impurities or thermal motions. If a magnetic field in any way affects the regularity of lattice structure we might expect magnetoresistance to appear.

There is at present a considerable body of evidence in favor of the view that liquids possess characteristic molecular structures. G. W. Stewart's idea[3] is that large numbers of molecules may be cooperating at any one instant of time to form temporary lattice arrangements in the liquid. Although this viewpoint is not necessary in order to explain x-ray diffraction curves for liquids there are a number of reasons why it is a plausible hypothesis. If it is accepted we might expect a magnetic field to affect either the number of molecules which at any one time are cooperating, the time of their cooperation, or the orientation (crystalline axis) of the group. Hence, following the general lines of Houston's theory, the field might be expected to change the resistance of the liquid. If the field produces any of the suggested effects on molecular grouping, the x-ray diffraction curve of the liquid would be modified, provided the effects are large enough. It seemed worth while, therefore, to investigate the effect of a magnetic field on the x-ray diffraction curve of the liquid Na-K alloy.

EXPERIMENT

The x-ray spectrometer was equipped with Soller slits and an ionization chamber made of seamless steel tubing filled with argon at about 20 atmospheres pressure. A celluloid window

[1] Fakidow and Kikoin, Physik. Zeits. d. Sowjetunion **3**, 381 (1933); J. E. Armstrong, Phys. Rev. **47**, 391 (1935).
[2] W. V. Houston, Zeits. f. Physik **48**, 449 (1928).
[3] G. W. Stewart, Rev. Mod. Phys. **2**, 116 (1930).

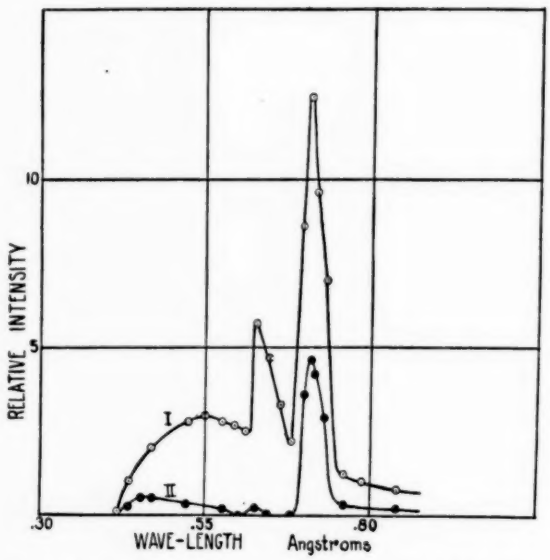

FIG. 1. Effect of filter on the x-ray spectrum of Mo. Curve I, no filter; curve II, with ZrO_2 filter.

admitted the rays. The ionization current was measured by the use of a Western Electric D-96475 electrometer tube in an amplifying circuit as described by Harnwell and Van Voorhis.[4] The sensitivity was adjusted to be about 40,000 divisions per volt and an input resistance of 10^{10} ohms was used. The circuit was carefully shielded and readings were not taken until about two hours after the filament current had been turned on. Under these conditions the galvanometer drift was negligible and random fluctuations were seldom more than two mm.

The x-rays were produced by a Coolidge tube with water-cooled molybdenum target. A potential of about 30 kv was used. The tube was enclosed in a lead box provided with a small hole through which the x-ray beam could pass. A filter of ZrO_2 placed over this hole produced approximate monochromatization of the beam. Fig. 1 shows the spectrum of the rays obtained with a calcite crystal, with and without the filter.

The liquid alloy contained approximately 35 percent sodium, this proportion having been found by Armstrong to give an alloy with fairly large magnetoresistance. The cell for holding the alloy was about 1 mm thick. It was made by

[4] G. P. Harnwell and S. N. Van Voorhis, Rev. Sci. Inst. **5**, 244 (1934).

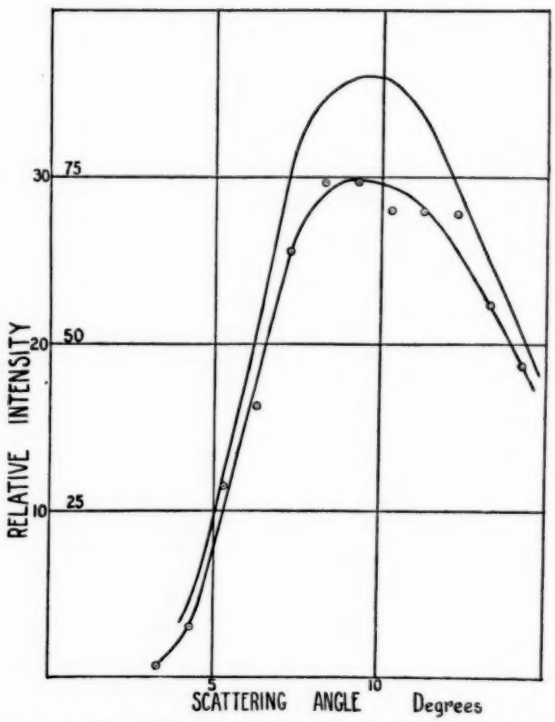

FIG. 2. Scattering by Na-K alloy. For the upper curve obtained without filter, the right-hand scale of ordinates is to be used. For the lower curve, obtained with filter, the left-hand scale is used. The experimental points all refer to the lower curve.

bending a thin glass rod into suitable contour and cementing thin mica plates to both sides of this framework. The scattering of the empty cell was small; however it was carefully measured for the various angles and subtracted from the total scattering after the cell was filled. This difference was assumed to be the scattering of the alloy. To fill the cell it was placed mouth downward in an evacuated tube. The alloy, in a side bulb, was now decanted into the tube. When air was admitted the alloy was forced up into the cell. This cell was mounted on the spectrometer table between the poles of an electromagnet.

Fig. 2 shows the scattering curves obtained with and without the filter. The points are averages of a number of observations taken with random distribution. A magnetic field of 2700 gauss produced no measurable effect on the form of either curve. In testing the effect of the magnetic field the following procedure was adopted. The galvanometer zero was first noted, then a lead shutter was opened to admit the x-ray beam through the Soller slits to the specimen. The

scattered beam passed through the second set of slits into the ionization chamber and produced a definite deflection of the galvanometer. The magnetic field was now switched on and careful observation made to see whether the deflection changed. Then the field was switched off, the shutter closed, and the galvanometer zero checked again. In no case could any effect of the magnetic field be detected. Tests were made at 1° intervals for both curves of Fig. 2, a field of 2700 gauss being used. An effect as large as two percent could have been detected in the case of the largest deflections.

Discussion of Results

The diffraction of x-rays by Na-K alloys has been investigated previously by K. Banerjee,[5] who used the Mo $K\alpha$ radiation and a photographic method. Banerjee finds a maximum at 11° 28′. In the present work the maximum is at about 9.5°. The scattering of the points at the maximum in Fig. 2 appears to be rather too large for high accuracy; however, repeated trials indicated a definitely smaller angle for the maximum than was found by Banerjee. The reason for the discrepancy is not evident. It may be mentioned, however, that thin, flattened, glass tubes, such as Banerjee used to contain his alloy, could not be used in the present work because their scattering was comparable to that of the alloy. Using the Bragg formula the spacing of diffracting centers in the liquid turns out to be 4.3 Angstrom units, according to the present data, instead of 3.5 as given by Banerjee.

The absence of any effect of a magnetic field indicates that no appreciable modification of molecular groupings is produced. Hence the magnetoresistance of the alloy cannot be explained on these grounds. The possibility remains that certain structural changes may occur which are too small to be detected by the x-ray method. Ferromagnetic crystals when magnetized give an unchanged x-ray spectrum although definite structural changes occur, as is evidenced by the presence of magnetostriction.

An attempt was made to detect magnetostriction in the Na-K alloy. A quantity of the material under oil in a glass bulb was placed between the poles of an electromagnet and subjected to a field of 7800 gauss. The oil meniscus in a fine capillary tube connected to the bulb was observed under a microscope. It was estimated that if any magnetostriction occurred the volume change per unit volume must have been less than 3×10^{-7}, the limit of accuracy of the experiment. This is a smaller volume change than is found to exist in ferromagnetic materials.

The conclusion appears to be that in this alloy a magnetic field does not produce a resistance change by modification of any molecular groupings or spacings in the liquid. The main cause of magnetoresistance is thus to be sought in the Lorentz forces which modify the electron free paths.

[5] K. Banerjee, Ind. J. Phys. **3**, 399 (1928).

SEPTEMBER 15, 1935 PHYSICAL REVIEW VOLUME 48

The Transmutation Functions for Some Cases of Deuteron-Induced Radioactivity[1]

Ernest O. Lawrence, Edwin McMillan and R. L. Thornton, *Radiation Laboratory, Department of Physics, University of California, Berkeley*

(Received July 1, 1935)

When nuclei are bombarded with deuterons, a commonly observed type of reaction is that resulting in proton emission and the conversion of the nuclei into isotopes of mass number one unit greater. Many such reactions give beta-radioactive products. The variation of the transmutation cross section with deuteron energy has been studied for the radioactivity thus produced in Na, Al, Si and Cu, with deuteron energies ranging from 0 to 3.6 MV. In all these cases it is found that the excitation curve is too flat to be explained by the Gamow theory, while it is fitted very well by a theoretical curve derived by Oppenheimer and Phillips. This is based on the idea that the nucleus can capture the neutron from the deuteron without requiring the penetration of the deuteron through the nuclear Coulomb barrier. The form of the theoretical curve depends on the binding energy of the deuteron; a value between 2.0 and 2.4 MV is required by the experimental results.

Introduction

IN THE original investigations of the radioactivity induced in sodium[2] and aluminum[3] by deuteron bombardment, observations of the voltage excitation curves up to a deuteron energy of 1.9 MV were made. In this range the experimental curves can be fitted reasonably well by the Gamow[4] nuclear penetration function, which has been found to describe so well many other nuclear reactions produced by α-particle and proton bombardment. It was noticed, however, in the case of aluminum, for which the experimental data were more detailed, that the experimental points corresponding to the lowest deuteron energies lie above the theoretical curve when it is made to fit the high energy points. The true significance of this was not realized until the experiment was repeated with a deuteron beam of much greater energy, extending the excitation curve for aluminum up to 3.4 MV.

It was then found that the differential excitation function for aluminum beyond 2 MV, instead of rising with a rapidly increasing slope as predicted by the Gamow theory, goes up at a much more modest rate. The part of the curve between 2 and 3.3 MV is in fact a straight line when plotted against the range of the deuterons. Curves of similar shape were found for the sodium reaction, and some others that will be described later. (See Figs. 2–5.)

These observations indicated that some new description of the mechanism of these reactions was necessary. If one should attempt to explain the experimental results while retaining the usual picture of a simple penetration of the bombarding particle through the nuclear potential barrier, it would be necessary to suppose either that a conglomeration of unresolved resonance levels happened to give this particular shape to the curve, or else that the deuterons were going over the top of the barrier at a remarkably low energy. The first of these suppositions is made highly improbable by the facts that the curves are smooth and monotonic, and are of similar shape for several different reactions. The second would require an abnormally large nuclear radius. Duncanson and Miller[5] find 9 MV for the height of the Al potential barrier to α-particles; one would expect the height for deuterons to be half as great, and therefore beyond the energy range covered in these experiments.

At this point Professor Oppenheimer became interested in the problem from a theoretical standpoint, and found that the experimental results are not at all mysterious, but are just what must be expected for reactions of the type investigated when the small stability of the deuteron is taken into account. A full account of the theory is given by Professor Oppenheimer and M. Phillips in the paper immediately following this one. We shall return to a discussion of the mechanism of reaction involved and its application in this case after devoting some attention to the experiments.

Reactions Studied

The formation of radioactive bodies from sodium and aluminum by deuteron bombardment has been shown[2, 3] to occur almost certainly according to the reactions:

$$Na^{23}+H^{2}\rightarrow Na^{24}+H^{1}, \quad (1)$$

$$Al^{27}+H^{2}\rightarrow Al^{28}+H^{1}. \quad (2)$$

Recently H. W. Newson,[6] working in this laboratory, has found that an active product of 2.8 hours half-life, isotopic with silicon, is made from silicon under deuteron bombardment. The reaction concerned is presumably:

$$Si^{30}+H^{2}\rightarrow Si^{31}+H^{1}. \quad (3)$$

Finally, we have observed that copper with deuterons gives an activity of about 12 hours half-life, which is probably the same substance as the active copper isotope produced by neutron bombardment, whose half-life is given as 10 hours by Amaldi *et al.*[7] We also found a shorter

[1] This work was first reported at the Washington meeting of the National Academy of Sciences. Abstract in Science **81**, 421 (1935).

[2] Ernest O. Lawrence, Phys. Rev. **47**, 17 (1935).

[3] Edwin McMillan and Ernest O. Lawrence, Phys. Rev. **47**, 343 (1935).

[4] Gamow, *Atomic Nuclei and Radioactivity* (Oxford University Press, 1931). This is based on the wave-mechanical idea of the "diffraction" of particle waves through potential barriers, which was first applied to a nuclear problem (α-radioactivity) by Gurney and Condon and independently by Gamow.

[5] W. E. Duncanson and H. Miller, Proc. Roy. Soc. **A146**, 413 (1934).

[6] H. W. Newson, Bull. Am. Phys. Soc. **10**, No. 4, p. 8 (1935).

[7] E. Amaldi, O. D'Agostino, E. Fermi, B. Pontecorvo, F. Rasetti and E. Segrè, Proc. Roy. Soc. **A149**, 522 (1935).

period, but cannot be sure that it arises from copper without further work, taking greater care to eliminate the ubiquitous carbon and nitrogen contamination effects. Only the long period activity will be considered in this paper. It is weak compared to that of sodium; after equal exposure to a 3.6-MV deuteron beam a copper target shows about 1/200 the activity of a sodium target. Nevertheless it is very much larger than one would expect for an element of such high atomic number (29) without some modification of the ordinary theory of nuclear penetration. The reaction of formation is probably:

$$Cu^n + H^2 \rightarrow Cu^{n+1} + H^1, \qquad (4)$$

where n may be 63 or 65 depending on which of the two stable copper isotopes is the parent substance.

It will be noticed that all these reactions are of the same type, in which a deuteron is captured and a proton emitted, converting the bombarded nucleus into its next higher isotope. This sort of process can also be described by saying that the nucleus snatches a neutron away from the deuteron, leaving the proton free to escape, and it is in terms of this description that the theory of Oppenheimer and Phillips is to be understood. Many such reactions with radioactive products are now known. The four listed above[8] were chosen for the present study on purely mechanical grounds, in that the substances concerned can be obtained in the form of very thin uniform foils, as required by the experimental technique used.

Experimental Method

In order to obtain a voltage-yield curve for a reaction giving a radioactive product, one measures the intensity of activation of a number of samples exposed to bombardment by particles of different energies. The relative bombarding current and exposure time must be accurately known for each sample, a requirement which is most easily and satisfactorily met by activating them simultaneously. This was done by using as a target a stack of thin foils of the substance being investigated, through which the activating deuteron beam was sent. The energy of the deuterons traversing any particular foil is then determined by their initial energy and the stopping power of the preceding foils, and the measured activities give directly the differential excitation curve.

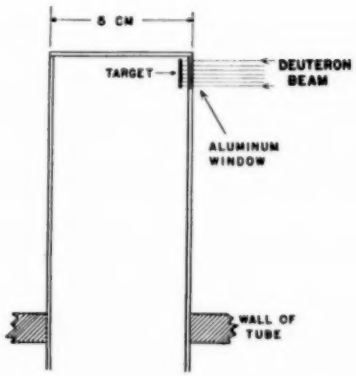

Fig. 1. Arrangement for bombarding targets.

An apparatus of the type developed by Lawrence and Livingston[9] was used to produce a beam of high speed deuterons.[10] The beam was allowed to emerge from the vacuum through a thin aluminum window (8 mm air equivalent stopping power), mounted on a brass grid near the end of a tube built into the side of the apparatus, as shown in Fig. 1. The target was placed next to the window, and the space between them was evacuated during the bombardment. Deuteron currents between 1 and 2 microamperes and exposure times from 5 minutes to 1.5 hours were used.

Measurements

The initial energy of the deuteron beam was deduced from its range in air, determined visually

[8] One other case of particular interest has recently been examined by M. C. Henderson (Bull. Am. Phys. Soc. **10**, No. 4, p. 6 (1935)). Magnesium with deuterons gives two active bodies, by the reactions:

$$Mg^{26} + H^2 \rightarrow Mg^{27} + H^1, \qquad (5)$$

$$Mg^{26} + H^2 \rightarrow Na^{24} + He^4. \qquad (6)$$

Making use of the widely different decay periods, he obtained the separate excitation curves of the two reactions, and found that reaction (5) follows a curve of the type described in this paper, while reaction (6) follows a Gamow curve. Theoretically one expects just this sort of behavior, since in reaction (6) the deuteron as a whole must penetrate into the Mg^{26} nucleus.

[9] Ernest O. Lawrence and M. Stanley Livingston, Phys. Rev. **45**, 608 (1934).

[10] Since we shall have many occasions in the future to refer to this apparatus, we feel that it should have a name. The term "magnetic resonance accelerator" is suggested. In this, the last two words imply the essential principle of operation, while the first word is added to distinguish it from the apparatus of Sloan and Lawrence (Phys. Rev. **38**, 2021 (1931)), which can be called a "linear resonance accelerator." The word "cyclotron," of obvious derivation, has come to be used as a sort of laboratory slang for the magnetic device.

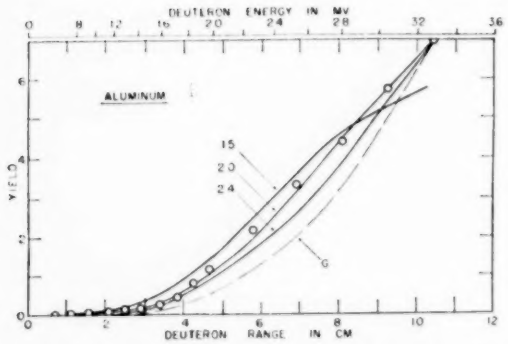

FIG. 2. Differential excitation curve of the radioactivity induced in aluminum ($Z=13$) by deuteron bombardment. Circles, experimental points. Solid lines, Oppenheimer-Phillips functions with the values of I given by the numbers, in MV. Dashed line, Gamow function.

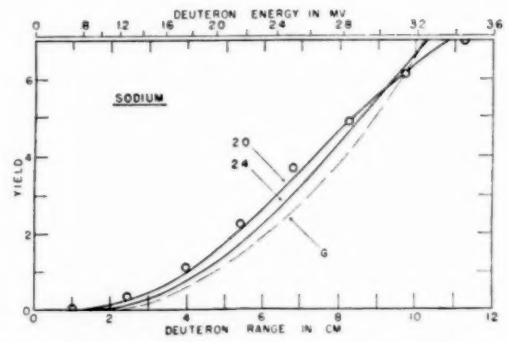

FIG. 3. Differential excitation curve of the sodium radioactivity ($Z=11$). Notation same as in Fig. 2. The ordinate of the highest energy experimental point is probably too low.

by observing the end of the streak of blue luminescence that it produces. Since the maximum air path available (see Fig. 1) was less than the range of the beam, aluminum foils were put next to the window, of such a thickness as to reduce the range to less than 4.5 cm. The stopping power of these foils was determined by weighing. The error in the range measurements made by this method was certainly not greater than 5 mm.

The stopping powers of the foils which were to be activated were determined by means of a polonium source mounted on a micrometer screw and a Wynn-Williams counter, the displacement of the counts-against-distance curve on interposing a foil being taken as its stopping power. An error of about 0.2 mm is possible in these measurements.

The activities of the foils were observed by a quartz-fiber electroscope in an ionization chamber provided with a thin aluminum window to admit β-particles. All the activities were large compared to the natural background, and these determinations should be precise to within one or two percent. The time of making each reading was recorded, making it possible to correct for the decay of the active products. In plotting the results, points with ordinates proportional to the corrected activities are put at abscissas corresponding to the centers of the foils. This method of plotting would be precise only if the curves were straight lines, but it is easy to see that the error introduced by the curvature is negligible with the spacing of points used.

Details of the various cases investigated are given below:

Aluminum (Fig. 2)

Range of deuteron beam in air (at 20°C) = 11 cm. Stopping power of individual foils (pure aluminum) = 11.5 mm. Since the active product has a half-life of about 156 sec., it decayed by a factor of about 7 in the 7 min. needed to measure the activities of all the foils, but the half-life is well enough known that this can be corrected for with very little error. The part of the curve below 4.5 cm deuteron range is taken from the results of reference 3, which were obtained with a shorter initial range, the ordinate scales being adjusted to make the two curves fit at 4.5 cm. The abscissas of the low-range points taken in this way are obviously more precise than those obtained by the passage of a long-range beam through a great thickness of foils.

Sodium and silicon (Figs. 3 and 4)

Range of beam = 12 cm. Stopping power of foils = 14.5 mm. The foils used were of mica, whose composition is given by the formula H_2 (K, Na) $Al_3 Si_3 O_{12}$. This substance after exposure to deuterons contains several active bodies; there are some short periods that practically vanish within an hour, as well as the 2.8-hour silicon product, and the 15.5- and 13.5-hour sodium and potassium products. Of the latter two, the sodium activity is much the stronger, even though the amount of sodium is less than that of potassium in ordinary micas (Na/K ~ 10–30 percent). A subsidiary experiment shows this. Targets of NaCl and KCl were given equal exposures (checked by the equality of the 40 min. chlorine activities induced), and observed 20 hours later.

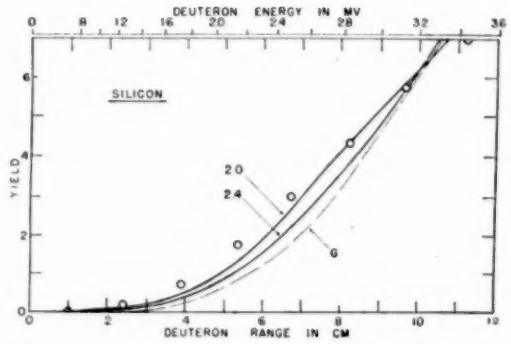

FIG. 4. Differential excitation curve of the silicon radioactivity ($Z=14$). Notation same as in Fig. 2. The ordinate of the highest energy experimental point is probably too low.

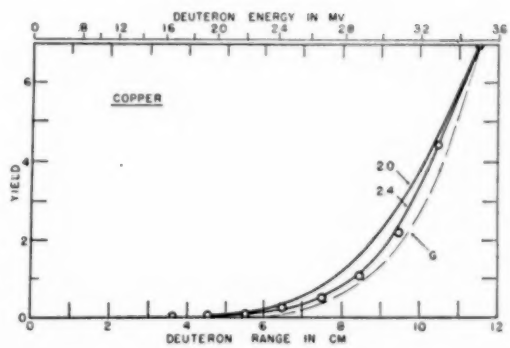

FIG. 5. Differential excitation curve of the long-period copper radioactivity ($Z=29$). Notation same as in Fig. 2.

The NaCl was found to have 70 times the activity of the KCl. Therefore in mica the greater susceptibility of the sodium to activation far outweighs its smaller abundance, and we can assume with little error that the whole long period activity arises from sodium.

The activities of the foils were measured 2 and 20 hours after activation, in order to disentangle the silicon and sodium effects. The total activities (sum of all foils) observed for silicon and sodium, corrected for decay back to the end of the activation (1.5 hours at 1 microampere) were 6 and 1.8 divisions/sec., respectively, corresponding to about 3 and 0.9 microcuries of active substances. The saturation activities after a very long exposure would be 8 and 13 microcuries.

The measured values of the activities of the highest energy foil are probably too low. This error arises from the forward recoil momentum imparted to the activated nuclei by the colliding deuterons, which, as shown in reference (3), drives the active material forward in the direction of the beam with an average range of the order of a millimeter air equivalent. As a result, an appreciable part of the activity of the first foil is transferred on to the second one. For the second and succeeding foils the loss in activity on one side is nearly compensated by the gain on the other from the preceding one. Aluminum is not subject to this error, since even the first foil is preceded by the aluminum window. Copper has such a heavy nucleus that the recoil range is small, and the error produced is negligible.

Copper (Fig. 5)

Range of beam = 10 cm and 12 cm. Stopping power of foils (pure copper) = 9.8 mm. This curve was obtained in two sections. The part from 0 to 10 cm was done at a time when the apparatus was not set to give a beam of the highest energy, and the extension up to 12 cm was made later, the two ordinate scales being adjusted to make the curves fit together at 9.5 cm.

The activities were measured 3 hours after bombardment, when only the long period copper activity remained. The total activity (all foils), expressed as that after a very long exposure to 1 microampere of 12 cm deuterons, was 14 divisions/sec. or about 7 microcuries.

Since the stopping power of copper relative to that of air varies with the velocity of the particles, the air equivalent thickness of the foils measured with polonium α-particles is slightly in error for some parts of the deuteron range. The necessary correction, which increases the effective stopping power for the highest energy and decreases it for the lowest, was made according to the values given by Mano.[11] The corresponding correction for aluminum and mica is negligible.

DISCUSSION OF THE THEORY AND ITS FIT WITH EXPERIMENT

The essence of the theoretical explanation of these results given by Oppenheimer and Phillips lies in the fact that reactions of the above type can occur without requiring the penetration of a charged particle through the nuclear Coulomb potential barrier which opposes the entry of the

[11] G. Mano, J. de phys. et rad. **5**, 628 (1934).

deuteron. The mechanism postulated can be described in the following way: Consider the deuteron as built of a proton and neutron, with the binding energy I. Because of the wave nature of the particles, this structure is not confined within a sharply limited volume, but there is a finite chance that the neutron or proton may be found some distance away from the center of mass. This chance decreases rapidly with the distance. When the deuteron is projected against a nucleus, the proton is held back by the Coulomb field. This distorts the probability distribution of the proton in such a way that for a given distance of the deuteron center of mass from the nucleus, the chance of finding it in the center of the nucleus is very much reduced. On the other hand, the neutron is immune to the action of the electrostatic field, and its probability distribution can overlap the center of the nucleus; this distribution is in fact distorted by the forces involved in the deceleration of the neutron, in such a way as to increase its density on the side toward the nucleus. Therefore the neutron has a relatively larger chance of being within the nucleus, and while there of undergoing a reaction in which it becomes bound, forming a new nucleus. The extension of the neutron distribution varies with I, becoming greater as I decreases. It is the relatively small value of I (~ 2 MV) that causes the slow energy variation of this type of reaction, by flattening out the neutron probability distribution.

The actual shape of the function giving the variation of the neutron-penetration with energy depends on the value of I. Since this most probably lies between 2.0 and 2.4 MV (see appendix), the curves for these two cases have been compared with the experimental values. They are plotted as solid lines on Figs. 2–5. On Fig. 2 (aluminum) the curve for $I=1.5$ MV is plotted also. The ordinates of the theoretical curves are adjusted to make them fit at the highest experimental points, except in the cases of sodium and silicon where the measured values of these are almost certainly too low because of recoil effects (see the special discussion of these cases).

The Gamow function:

$$(1/v^2)e^{-4\pi^2 Z e^2/hv}, \qquad (7)^{12}$$

where Z = atomic member, v = deuteron velocity, is also plotted on the figures for comparison. In this connection it should be emphasized that the power of v which multiplies the exponential, although usually given as $1/v^2$, is not definitely determinable without a rather detailed knowledge of the forces acting during the reaction. Depending on these, it may vary between 1 and $1/v^2$. We have used $1/v^2$, which gives the flattest curve, in order to show that even in this extreme case the function is too steep to fit the experimental results.

On the other hand, the results of Oppenheimer and Phillips show a very satisfactory agreement with the observed values. Consider first the case of aluminum. This is the most trustworthy experimentally; with pure aluminum foils the activity is very large compared to that of any possible contamination, and there is no error in the highest point caused by recoil. It is seen that the Oppenheimer-Phillips function with $I=2.0$ fits extremely well, while with $I=1.5$ and $I=2.4$ it is off by more than the experimental error.

The fit for sodium and silicon is also best for $I=2.0$. Here the possibility of experimental error is somewhat greater, and the apparent deviation in the case of silicon between 1.5 and 2.5 MV may not be real. The results for these two elements are of chief interest in showing that this type of excitation curve is not a characteristic of any particular reaction, but of a class of reactions. The comparative values for sodium and silicon show also that the steepness of the curves increases with Z, as it should.

For copper the fit seems to be best with $I=2.4$. Here, because the greatest variation of the function occurs in a narrower voltage range, the different theoretical curves are not as widely separated as in the other cases and the apparent better agreement with $I=2.4$ may not be real. We can give an explanation for it, which, however, we do not wish to emphasize unduly. Oppenheimer and Phillips point out that the theory is subject to small modifications whose evaluation would require an intimate knowledge of the nuclear structure, and which would be in such a direction as to increase the value of I giving the best fit; the magnitude of these modifications would be least for elements of large Z. The result of this would be to make the form of the theory

[12] Eq. (1), reference 3, which purports to give this function, contains a typographical error.

used here require a larger value of I for copper ($Z=29$) than for the other elements studied ($Z=11$, 13 and 14).

Such refinements are hardly justified at present. We can, however, make some conclusions that we feel are definitely beyond the possible uncertainties of both the experimental results and the theory. They are first, that the theory proposed by Oppenheimer and Phillips is adequate to explain the observed excitation curves while the Gamow theory is not, and second that the value of the deuteron binding energy consonant with this explanation is 2 MV or slightly larger.

The acceptance of this reaction mechanism as correct leads to another very important conclusion. Just as the variation of the transmutation yield with energy for a given atomic number is slower than expected, likewise the variation with atomic number for a given energy is slower. This has the consequence that it will be possible, with the available deuteron energies, to produce nuclear reactions much farther up the periodic table than one could have hoped before.

The interest and cooperation of Professor Oppenheimer and M. Phillips in this work has been of great value to us, and it is with real pleasure that we acknowledge it. We also express our appreciation of the helpful financial support given by the Research Corporation, the Chemical Foundation, and the Josiah Macy Junior Foundation.

Appendix on the Binding Energy of the Deuteron

The binding energy of the deuteron can in principle be calculated precisely from the disintegration energies of various reactions. Actually the results are subject to some uncertainty, because of possible errors in the values given for reaction energies and nuclear masses. In particular, there are intrinsic difficulties in measuring the energies of reactions involving neutrons. As an example of this sort of calculation we have chosen a set of reactions which can be combined so as to make most of the masses cancel out, and in which the direction of the uncertainty in the measurement of the energies is known, so that definite upper and lower limits can be set. These are:

$$Li^7+H^1\rightarrow 2He^4+17.06\pm0.06 \text{ MV}, \quad (8)^{13}$$

$$Li^6+H^2\rightarrow 2He^4+22.06\pm0.07 \text{ MV}, \quad (9)^{13}$$

$$H^2+H^2\rightarrow H^1+H^3+3.97\pm0.02 \text{ MV}, \quad (10)^{13}$$

$$Li^7+H^2\rightarrow 2He^4+n+14.60\pm0.25 \text{ MV}, \quad (11)^{13}$$

$$H^2+H^2\rightarrow He^3+n+2.8\pm0.2 \text{ MV}, \quad (12)^{14}$$

$$Li^6+H^1\rightarrow He^3+He^4+3.5\pm0.3 \text{ MV}, \quad (13)^{15}$$

$$Li^6+n\rightarrow H^3+He^4+4.6\pm0.3 \text{ MV}. \quad (14)^{16}$$

The energies of the particles emitted in reactions (8) to (11) have been measured with the greatest precision, and the reaction energies deduced from these are known with corresponding precision, except in the case of reaction (11). This is a three-body disintegration, and it was assumed that the most energetic α-particle comes off with the greatest energy allowed by the momentum laws. If this ideal limit is not actually attained, the reaction energy must be greater, and therefore the value given is a lower limit.

The energy given for reaction (14) was calculated from the observed H^3 range, using Mano's[11] range-energy relation. In a reaction of this type, involving the capture of a neutron, it is known, particularly from Kurie's[17] work, that some energy may be radiated during the capture; therefore the reaction energy given is a lower limit.

Since three of these reactions involve a neutron, three independent values of the deuteron binding energy can be obtained from them. The combinations giving the greatest cancelation of masses are:

$$(8)-(11), \text{ giving } H^1+n-H^2=2.46\pm0.3,$$

$$(13)-(9)-(12), \text{ giving } H^1+n-H^2=2H^2-He^4-21.36\pm0.4,$$

$$(14)-(9)-(10), \text{ giving } H^1+n-H^2=2H^2-He^4-21.43\pm0.4.$$

H^1+n-H^2 is the binding energy sought. The only masses occurring on the other side of the equations are in the combination $2H^2-He^4$, which is equivalent to 23.8 ± 0.2 MV using the new values,[18] and to 23.4 ± 0.2 MV using the old ones. Putting the first of these into the equations, the three values obtained for the binding energy are:

$$(8)-(11),\ I=2.46\pm0.3,$$

$$(13)-(9)-(12),\ I=2.44\pm0.45,$$

$$(14)-(9)-(10),\ I=2.37\pm0.45.$$

Recalling that the energies given for the reactions (11) and (14) are lower limits, one sees that the first value of I is an upper limit, and the third is a lower limit.

These values can be compared with that obtained by Chadwick and Goldhaber[19] from the process:

$$H^2+h\nu(2.6 \text{ MV})\rightarrow H^1+n+0.5 \text{ MV},$$

giving $I=2.1$ MV. The possible error in the measurement of the energy given to the ejected proton is uncertain, but may be some tenths of a million volts. The observed cross section for this reaction is smaller than that calculated from the theory of Bethe and Peierls,[20] using $I=2.1$; the value of I required by the theory to fit the observed cross section is 2.4.

[13] Oliphant, Kempton and Rutherford, Proc. Roy. Soc. **A149**, 406 (1935).
[14] Dee and Gilbert, Proc. Roy. Soc. **A149**, 200 (1935).
[15] Oliphant, Kinsey and Rutherford, Proc. Roy. Soc. **A141**, 722 (1933).
[16] Chadwick and Goldhaber, Nature **135**, 65 (1935); Taylor and Goldhaber, Nature **135**, 341 (1935).
[17] Kurie, Phys. Rev. **47**, 97 (1935).
[18] Aston, Nature **135**, 541 (1935).
[19] Chadwick and Goldhaber, Nature **134**, 237 (1934).
[20] Bethe and Peierls, Proc. Roy. Soc. **A148**, 146 (1935).

Note on the Transmutation Function for Deuterons

J. R. OPPENHEIMER AND M. PHILLIPS, *University of California, Berkeley*

(Received July 1, 1935)

We consider the effect of the finite size and ready polarizability of the deuteron on the probability of transmutations involving the capture of the neutron. These have as a consequence that the Coulomb repulsion of the nucleus is less effective than for alpha-particles or protons, and that the corresponding transmutation functions increase less rapidly with deuteron energy. We treat the collision by the adiabatic approximation and obtain quantitative results for this energy dependence which are in good agreement with experiment.

MANY elements can be rendered radioactive by deuteron bombardment, the reaction involving the capture of a neutron and the liberation of a proton:

$$ {}_{n}A^{m}+H^{2}\rightarrow {}_{n}A^{m+1}+H^{1}. \qquad (1) $$

Four reactions of this type have been studied in detail by Lawrence, McMillan and Thornton.[1] The transmutation functions which are found increase smoothly with deuteron energy, but the increase is far less rapid than we should expect on the basis of the familiar considerations of Gamow[2] on the penetration of charged particles through the potential barrier of the nuclear Coulomb field. To account even roughly for the observations on this basis, we are forced to assume that the Coulomb potential breaks down at very large distances ($\sim 1.5\times 10^{-12}$ cm for copper). The transmutation function is thus anomalous when compared to that for protons and alpha-particles, and it is natural to associate this anomaly with the structure of the deuteron, particularly its low stability. We wish to show in this paper that when this is taken into account, it does in fact provide a satisfactory explanation of the experiments.

For neutron capture to be possible the neutron must have an appreciable probability of coming within the range of the nuclear forces. But this condition can be satisfied even when the center of mass of the deuteron lies beyond the range of these forces. It is this possibility which leads to an explanation of the fact that even with such a highly charged element as copper nuclear transmutations can occur for deuteron energies of the order of 2 MV.

The quantitative treatment of the corresponding collision problem is complicated, not only by our ignorance of the detailed forces involved, but by the complete inapplicability of the Born approximation. For the velocity of the deuteron is not large compared to the internal velocity of proton and neutron; the effective time of collision of the deuteron is long compared to its period. We have thus to use the adiabatic approximation: the relative motion of proton and neutron is approximately given by the solution of the wave equation when the distance of the center of mass of the deuteron from the nucleus is held fixed; the center of mass moves in an effective potential which is the energy $\mathcal{E}(X)$ of the relative motion; and the perturbation which induces the inelastic impacts of the transmutation is the term in the kinetic energy neglected in this zeroth approximation. In fact the cross section for the transmutation is then given, with a proper normalization of the wave functions, by

$$ \sigma = 1/\hbar^{2}\,|\int\int dp\,dn\,\bar{\psi}_{f}(p,n) \times[\hbar^{2}/4M\Delta_{X}+W-I-\mathcal{E}(X)]\psi_{i}(x,X)\,|^{2}. \qquad (2) $$

Here p and n are the coordinates of proton and neutron, $x=p-n$ their relative coordinates, X the coordinates of the center of mass of deuteron measured from the nucleus as origin. Further ψ_i is the approximate adiabatic wave function for the initial state (normalized to unit flux); ψ_f the wave function for the final state, in which the neutron is captured and the proton is flying off with a considerable kinetic energy; and W, I, $2M$ are kinetic energy, binding energy and mass of

[1] Lawrence, McMillan and Thornton, preceding article. We are greatly indebted to the authors for the opportunity of seeing their experimental results, and for many helpful discussions.

[2] Gamow, *Atomic Nuclei and Radioactivity* (Oxford University Press, 1931).

the deuteron. We wish to evaluate the dependence of this cross section on the energy of the deuteron, insofar as this can be done without a detailed knowledge of the structure of the nucleus and the nature of the nuclear forces.

The reactions (1) are highly exothermic, and we may therefore neglect the dependence of the final wave function for the proton on the deuteron energy; except in the immediate neighborhood of the nucleus we can take for the final wave function of the proton a plane wave. Further, the final wave function for the neutron will vanish except in the immediate neighborhood of the nucleus. Since the neutron is far more stably bound in the nucleus than in the deuteron, it is reasonable to neglect the finite extension of the corresponding wave function. The effect of this neglect will be to make the value of the binding energy of the deuteron which best fits the experimental curves somewhat lower than the true value, but the error should be small, especially for an atomic number as high as that of copper. We shall take then

$$\psi_f \sim e^{i/\hbar(2ME)^{\frac{1}{2}}p}\delta(n), \tag{3}$$

except for very small values of p. Here E is the energy imparted to the proton by the disintegration.

The essential energy dependence of σ is determined by the form of ψ_i. The adiabatic approximation gives

$$\psi_i = u(x, X)\varphi(X), \tag{4}$$

where $u(x, X)$ is the wave function for the relative coordinates x, when the center of mass X is fixed, and $\varphi(X)$ is the wave function for the motion of the center of mass. If V_0 be the potential between neutron and proton, and V_N the nuclear potential, then these functions are determined by the wave equations

$$\{\hbar^2/M\Delta_x + \mathcal{E}(X) - V_0(x) - V_N(x, X)\}u = 0, \tag{5}$$

$$\{\hbar^2/4M\Delta_X + W - I - \mathcal{E}(X)\}\varphi = 0. \tag{6}$$

According to the familiar arguments of Wigner, V_0 is given by an extremely narrow and deep trough, and is equivalent, as Bethe and Peierls[3] have observed, to the boundary condition for

$$\partial \ln u/\partial x)_{x=0} = -(MI)^{\frac{1}{2}}/\hbar. \tag{7}$$

For V_N we shall take the Coulomb repulsion of the proton, and neglect the specifically nuclear forces in the immediate neighborhood of the nucleus; for these the adiabatic approximation can hardly be valid, and they could have a sensible effect on the transmutation function only if resonance occurred; the experimental curves afford no evidence for this.

According to (3) we need consider u only for $n=0$, $x=2X$. If we now determine u, $\mathcal{E}$ and φ by the Wentzel-Kramers-Brillouin method, we find, with sufficient approximation,

$$u(2X, X) = a(X)\exp\left\{-\frac{2X(WI)^{\frac{1}{2}}}{\hbar v}\theta\left(\frac{Ze^2}{XI}-1\right)\right\}$$

$$\mathcal{E}(X) = -I + Ze^2/X \tag{8}$$

$$\varphi(X) = \frac{b(W, X)}{v}\exp\left\{-\frac{2Ze^2}{\hbar v}f\left(\frac{XW}{Ze^2}\right)\right\}.$$

Here Z is the nuclear charge, v the deuteron velocity, $W = Mv^2$ the deuteron energy, and the functions f and θ are defined by

$$f(\alpha) = \cos^{-1}(\alpha)^{\frac{1}{2}} - (\alpha(1-\alpha))^{\frac{1}{2}},$$

$$\theta(z) = \frac{1+z}{(z)^{\frac{1}{2}}}\cot^{-1}(z)^{\frac{1}{2}} - 1, \qquad z>1$$

$$= (2(1-z))^{\frac{1}{2}} - 1 + \frac{1+z}{(z)^{\frac{1}{2}}}\left(\tan^{-1}\left(\frac{2z}{1-z}\right)^{\frac{1}{2}} - \tan^{-1}(z)^{\frac{1}{2}}\right), \qquad 0<z<1 \tag{9}$$

$$= (2(1-z))^{\frac{1}{2}} - 1 + \frac{1+z}{(-z)^{\frac{1}{2}}}\left(\tanh^{-1}\left(\frac{-2z}{1-z}\right)^{\frac{1}{2}} - \tanh^{-1}(-z)^{\frac{1}{2}}\right). \qquad z<0$$

[3] Bethe and Peierls, Proc. Roy. Soc. **A148**, 146 (1935).

Further $a(X)$, $b(W, X)$ are slowly varying functions. Far from the turning points $X_1=Ze^2/2I$, $X_2=Ze^2/W$, they are given by

$$a(X)=(I-Ze^2/2X)^{-\frac{1}{4}};\ b(W, X)=(Ze^2/X-W)^{-\frac{1}{4}}.$$

Since, as we shall see, the values of X which contribute essentially to the matrix integrals for σ vary little with W, the contribution of a and b to the transmutation function will be neglected.

We can thus write

$$\psi_i(2X, X)\sim 1/v \exp\left\{-\frac{2Ze^2}{\hbar}\left(\frac{M}{I}\right)^{\frac{1}{2}}F\left(\frac{W}{I}, \frac{IX}{Ze^2}\right)\right\}, \quad (10)$$

where

$$F(q, y)=y\theta(1/y-1)+q^{-\frac{1}{2}}f(qy). \quad (11)$$

Regarded as a function of X, F has a rather sharp minimum. The position of this minimum varies little with deuteron energy in the range 1.5 MV to 3 MV, and lies roughly at $Ze^2/2I$. The breadth of the corresponding maximum of $\psi_i(2X, X)$ decreases slowly with W, but since this breadth is of the same order as the wavelength $\hbar/(2ME)^{\frac{1}{2}}$ of the proton wave function, this variation will affect the magnitude of the matrix integral very little. The effect of the variation of a and b and of the logarithmic derivatives of u and ϕ which appear in the integrals for σ could in principle be taken into account by obtaining accurate solutions of the wave equations (5), (6); but without a detailed knowledge of the energy of the proton E, and the form of the final neutron wave function, such refinements would be illusory. Throughout the range $I/2<W<2I$,

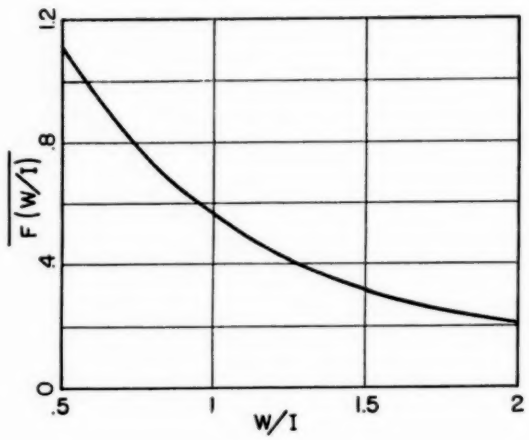

FIG. 1.

the variation of σ with W is given essentially by

$$\sigma\sim\frac{1}{v^2}\exp\left\{-\frac{4Ze^2}{\hbar}\left(\frac{M}{I}\right)^{\frac{1}{2}}\overline{F\left(\frac{W}{I}\right)}\right\}, \quad (12)$$

where $\overline{F(W/I)}$ is the minimum value of $F(W/I, IX/Ze^2)$. A plot of $\overline{F(W/I)}$ is given in Fig. 1.

The form of the transmutation functions given by (12) still depends upon the value of I. This is known to be roughly 2 MV, and this value gives satisfactory agreement with the experimental curves of Lawrence, McMillan and Thornton. In Fig. 2 of their paper Eq. (12) is plotted for three values of I (1.5 MV, 2 MV, 2.4 MV) for the aluminum reaction. It is seen that the agreement with the experimental values is best for $I\sim 2$ MV. The approximations in the theoretical treatment would tend to favor rather too low a value of the binding energy of the deuteron.

The Radioactivity of Solids Determined by Alpha-Ray Counting

GLADYS D. FINNEY, *Physics Department, University of California at Berkeley*
AND
ROBLEY D. EVANS, *Physics Department, Massachusetts Institute of Technology*

(Received June 11, 1935)

The complete theory of alpha-ray counting for thin and thick radioactive sources is developed. Tables of the numerical constants required for the interpretation of practical measurements are given. Apparatus and experimental verification of the theory are described. Several new methods for determining the thorium content of geological samples are described. Analyses of a suite of igneous rocks show Th contents between 3.9 and 16.5×10^{-6}g Th per g, with an average Th/U ratio of 7. Therefore thorium is more important in age and geothermal problems than uranium.

I. INTRODUCTION

RECENT refinements in detection technique permit ionization measurements[1] on the alpha-rays emitted by all ordinary materials because of their natural contamination by traces of radioactive substances. Accurate alpha-ray measurements permit the determination of the thorium content of geological specimens, hence lead toward satisfactory solutions of such basic problems as the age of igneous rocks, the age of the stellar system as determined from meteorite analyses, and the excessive, radioactivity-derived internal heat of the earth.

Feebly radioactive sources such as igneous rocks emit the order of one alpha-ray per cm² per hour. Any measurements are therefore subject to statistical fluctuations due to the random time of emission of these alpha-rays. Ionization measurements are further impaired by ionization fluctuations due to the variation in residual track length of the emitted alpha-rays, which must be compounded with the effects of random rate of emission in accord with the statistical theory of independently random processes.[2] Ionization measurements must also deal with the unavoidable background due to cosmic-ray and local gamma-ray ionization in the detecting chamber.

These difficulties are circumvented by counting the individual alpha-rays with a detector which is unresponsive to cosmic or local gamma-radiation. Precision is then limited only by the statistical fluctuations in the rate of emission of alpha-rays, and by the accuracy of the computations dealing with the finite thickness of the source. The statistical problem concerning several alpha-emitters of widely different half-periods but in radioactive equilibrium has been treated by Adams.[3] The equations describing thickness corrections for sources containing any number of radioactive elements are here developed and confirmed by direct experiments.

II. THEORY OF PARTICLE COUNTING

Consider the section of a radioactive solid bounded by the planes AA' and BB' in Fig. 1, and surmounted by absorbers of thickness a_1 and a_2 cm. The source emits N alpha-rays per cm³ per sec., of mean range R air-cm (i.e., measured in air at 0°C, 760 mm Hg). The full alpha-ray range in the source would be μR cm, and in the absorbers $\mu_1 R$, and $\mu_2 R$, respectively. The source is $\mu\tau$ cm (or τ air-cm) thick and some of the alpha-rays which it emits are observable in the detecting chamber located above the plane DD'.

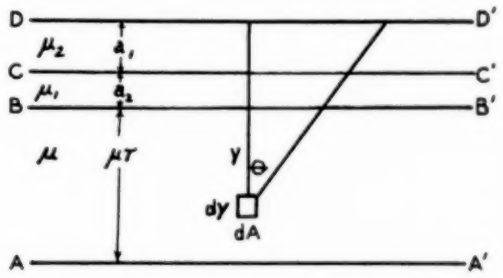

FIG. 1. Geometry for Eqs. (1) *et seq. Errata:* Subscripts for a_1 and a_2 should be interchanged.

[1] Evans, Phys. Rev. **45**, 29, 38 (1934).
[2] Evans and Neher, Phys. Rev. **45**, 144 (1934).
[3] N. I. Adams, Jr., Phys. Rev. **44**, 651 (1933).

A. Thin sources

There are $N\,dy\,dA$ alpha-rays per sec. emitted in all directions from the volume element $dydA$ located y cm below BB'. Alpha-rays which have equivalent air ranges of r or less below the interface DD', hence residual ranges equal to or greater than $(R-r)$ in the detecting chamber above DD', will be emitted within a cone of half-angle θ, or fractional solid angle $(1-\cos\theta)/2$, where $r\cos\theta=y/\mu+a_1/\mu_1+a_2/\mu_2$. Hence the number of such rays from the elementary volume is $N\,dy\,dA(1-\cos\theta)/2$, and n_a' the total number of such rays per cm² of surface of a source of large area (where edge effects are negligible) is obtained by integrating over y between the limits: $y=0$, and $y=\mu\tau$

$$n_a'=\frac{N}{2}\int_0^{\mu\tau}(1-\cos\theta)dy$$

$$=\frac{N}{2}\int_0^{\mu\tau}\left[1-\frac{y/\mu+a_1/\mu_1+a_2/\mu_2}{r}\right]dy \qquad (1)$$

$$=\frac{N\mu\tau}{4}\left[\frac{2(r-a)-\tau}{r}\right] \quad \text{where}$$

$$a\equiv a_1/\mu_1+a_2/\mu_2\cdots\text{air cm.} \qquad (2)$$

Now if the detecting instrument above DD' responds only to alpha-rays having a residual range equal to or greater than ρ air-cm, then the number of counted alpha-rays per cm² per sec. is given by Eq. (2) when $r=R-\rho$, that is:

$$n'_a=(N\mu\tau/4)\cdot[2(R-\rho-a)-\tau]/(R-\rho), \qquad (3)$$

which is the counting rate for thin sources surmounted by absorbers.[4]

If the thin source has an area A then the total alpha-ray counting rate is $n_a'A$. When d is the density of the source, its total mass $m=\mu\tau Ad$, and $n_a''\mu\tau Ad=n_a'A$, where n_a'' is the total alpha-ray counting rate per g of source. Therefore:

$$n_a''=n_a'/\mu\tau d$$
$$=(N''/4)[2(R-\rho-a)$$
$$-(m/\mu Ad)]/(R-\rho), \qquad (4)$$

where $N/d\equiv N''$ alpha-rays emitted per sec. per g of source. When an infinitely thin source is used without an absorber $\tau=m=a=0$, and Eq. (4) reduces to $n''=N''/2$. Only in this limiting case is the counting rate independent of R. Under these conditions the alpha-ray counting rate is a direct measure of the rate of helium production, hence could be directly combined with a helium analysis on a bulk rock specimen to determine its age.

N and N'' may be expressed in terms of the fractional concentration of radioactive material Q g per g, its decay constant λ sec.$^{-1}$, its atomic weight W, and the density d of the source; thus:

$$N=6.06\times10^{23}Q\lambda d/W, \qquad (5)$$

$$N''=N/d=6.06\times10^{23}Q\lambda/W. \qquad (6)$$

When the source thickness increases to $\tau=R-\rho-a$, any further increase in thickness will not increase the counting rate because even the alpha-rays directed normal to the plane DD' will emerge with residual ranges less than ρ and hence cannot be counted. The thickness $\tau=R-\rho-a$ is the transition between thin sources, whose theory has been given above, and thick sources, which are treated later. The variation in counting rate with source thickness may be obtained by employing Eq. (3) to derive the ratio of n_a' the counting rate above a thin source to n_a the rate above a thick source, both having the same absorber a superposed.

The counting rate n_a for thick sources (i.e., $\tau\geqslant R-\rho-a$) follows from Eq. (3) for a source of critical thickness $\tau=R-\rho-a$. Substituting, we find:

$$n_a=(N\mu/4)(R-\rho-a)^2/(R-\rho). \qquad (7)$$

Dividing Eq. (3) by Eq. (7) we obtain the variation in counting rate with source thickness.

$$n_a'/n_a=\tau[2(R-\rho-a)-\tau]/(R-\rho-a)^2$$
$$=1-[1-\tau/(R-\rho-a)]^2 \qquad (8)$$
$$\equiv1-(1-F_\tau)^2, \qquad (9)$$

where F_τ is the fractional thickness $\tau/(R-\rho-a)$ of the source, and $0\leqslant F_\tau\leqslant1$, as $0\leqslant(n_a'/n_a)\leqslant1$. In Fig. 2, the ordinates at the right are n_a'/n_a, when the abscissae are F_τ.

B. Thick sources

Sources are called thick when $\tau\geqslant R-\rho-a$, in which case the counting rate is independent of source thickness and is given by Eq. (7).

[4] Evans, Phys. Rev. **45**, 29 (1934).

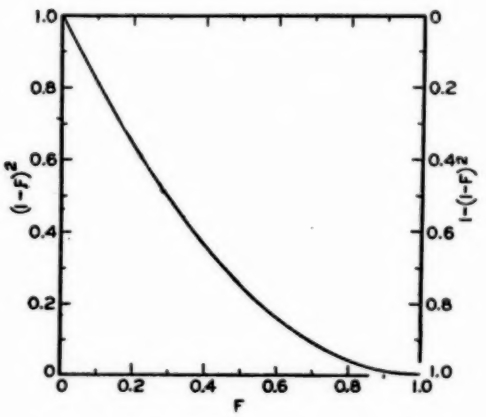

FIG. 2. Left-hand ordinates show fractional counting rate from thick sources surmounted by absorbers of fractional thickness $F_a=a/(R-\rho)$; see Eq. (11). Right-hand ordinates show fractional counting rate from thin sources having a fractional thickness $F_\tau=\tau/(R-\rho-a)$; see Eq. (9).

The variation with absorber thickness of the counting rate due to a thick source is best computed in terms of the counting rate n for zero absorption. Thus from Eq. (7):

$$n_a/n=(R-\rho-a)^2/(R-\rho)^2$$
$$=[1-a/(R-\rho)]^2 \qquad (10)$$
$$\equiv(1-F_a)^2, \qquad (11)$$

where F_a is the fractional thickness $a/(R-\rho)$ of the absorber, and $0\leqslant F_a\leqslant 1$, as $0\leqslant(n_a/n)\leqslant 1$. In Fig. 2, the ordinates at the left are n_a/n when the abscissae represent F_a.

Combining Eq. (8) for $a=0$, with Eq. (10), we find:

$$n'/n+n_a/n=1-[1-\tau/(R-\rho)]^2$$
$$+[1-a/(R-\rho)]^2. \qquad (12)$$

Hence if the thin source has a thickness τ, and no absorber, its counting rate n' may be immediately obtained from curves for the counting rate n_a due to a thick source with an absorber of thickness a equal to τ. Or, analytically, Eq. (12) reduces to:

$$n'/n+n_a/n=1 \quad \text{when} \quad \tau=a. \qquad (13)$$

Eq. (13) holds for each particular alpha-ray range R, hence also for the integrated effects of several alpha-ray emitters in the same source. It is the basic correspondence theorem correlating the theories of thin and thick sources, and its use halves the numerical calculations required for applications to sources emitting alpha-rays from many or all members of the U, Th and Ac series. It can, of course, be verified by inspection of the geometry involved.

It has been shown previously[4] that the decreased counting rate due to alpha-particle straggling in the solid is almost completely offset by the gain in counting rate occasioned by the symmetrical character of the error function describing straggling. The fractional loss is $\Delta n/n=\frac{1}{2}(\rho_3)^2$, where $\rho_3\gamma$ is Brigg's range straggling coefficient. The fractional loss is thus always less than 0.3 percent.

III. Total Counting Rate for Sources Containing Many Radioactive Elements

Measurements on chemically prepared materials containing only one alpha-ray emitting element are easily interpreted by Eqs. (3) and (7). A more complicated case is met in measurements of the total alpha-ray emission from materials containing all members of the U, Th and Ac radioactive series, such as rocks. We shall consider the case of thick sources; values for thin sources may be readily obtained by use of the correspondence theorem of Eq. (13).

We shall regard the specimen as sufficiently old to have reached radioactive equilibrium. Then the number of alpha-rays produced per cm^3 per sec. is essentially the same for each member of a radioactive decay series. Substituting[5] the decay constant and atomic weight of U and of Th in Eq. (5) we find:

$$N_U=\frac{6.06\times10^{23}\times4.77\times10^{-18}}{238.14}\cdot U\cdot d$$
$$=1.21\times10^4\ U\cdot d. \qquad (14)$$

$$N_{Th}=\frac{6.06\times10^{23}\times1.7\times10^{-18}}{232.12}\cdot Th\cdot d$$
$$=0.44\times10^4\ Th\cdot d. \qquad (15)$$

$$N_{Ac}=0.04N_U=0.05\times10^4\ U\cdot d. \qquad (16)$$

[5] Kovarik and Adams, Phys. Rev. **40**, 718 (1932) give $\lambda=4.865\times10^{-18}$ sec.$^{-1}$ for UI. When corrected for AcU, this value becomes 4.77×10^{-18} sec.$^{-1}$. Geiger and Rutherford, Phil. Mag. **20**, 691 (1910), and H. Fesefeldt, Zeits. f. Physik **86**, 605 (1933), find $\lambda=1.7\times10^{-18}$ sec.$^{-1}$ for Th. A. v. Grosse, Phys. Rev. **42**, 565 (1932) reviews the work on Ac and recommends 0.04 for the Ac/U activity ratio.

Since each alpha-ray body in the U series emits 1.21×10^4 U$\cdot d$ alphas per sec., the total counting rate for a thick source containing only the U series would be:

$$(1.21\times10^4\ \mathrm{U}\cdot\mu\cdot d/4)\Sigma(R-\rho-a)^2/(R-\rho)$$

where the summation extends over all the range values R which are members of the uranium series.

In a natural source, such as a granitic rock, the Th and Ac series will be present also, hence similar expressions must be written for them. The total observed counting rate n_a will then be due to terms from the U plus Ac series and from the Th series, or

$$n_a=v_a\mathrm{U}+w_a\mathrm{Th} \tag{17}$$

where U and Th are the uranium and thorium concentrations in g per g of source. Writing

$$H\equiv\Sigma(R-\rho-a)^2/(R-\rho) \tag{18}$$

we have:

$$\begin{aligned} v_a&=(1.21\times10^4\mu d/4)H_{\mathrm{U}}\\ &\qquad+(0.05\times10^4\mu d/4)H_{\mathrm{Ac}}\\ &=[3.03H_{\mathrm{U}}+0.12H_{\mathrm{Ac}}]10^3\mu d \end{aligned} \tag{19}$$

$$w_a=[1.11H_{\mathrm{Th}}]10^3\mu d \tag{20}$$

where the summations are made over the members of the U, Th and Ac series as indicated, and H for the CC′C″ bodies considers their respective branching ratios.

The computation of H_{U}, H_{Ac} and H_{Th} may be considerably simplified by the following devices. Let Δj be a numerical parameter defined as the ratio of the number of alpha-rays per second from any element, such as Ra, to the number from its parent, in this case U I. Then, without practical error, $\Delta j=1$ for all alpha-emitting elements, except those in the CC′C″ branches, when radioactive equilibrium is present. For Ra C, $\Delta j=0$ (accurately, 0.0004); for Ra C′, $\Delta j=1$ (0.9996); for Th C, $\Delta j=0.35$; for Th C′, $\Delta j=0.65$; for Ac C, $\Delta j=1$ (0.997); and for Ac C′, $\Delta j=0$ (0.003). To account analytically for branching we therefore introduce the parameter Δj into Eq. (18), obtaining:

$$H=\Sigma\Delta j(R-\rho-a)^2/(R-\rho) \tag{21}$$

$$\begin{aligned} &=\Sigma\Delta j(R-\rho)[1-a/(R-\rho)]^2\\ &=\Sigma R\cdot\Delta j+a^2\Sigma\Delta j/(R-\rho)-(\rho+2a)\Sigma\Delta j. \end{aligned} \tag{22}$$

TABLE I. *Mean range R in air at 0°C and 760 mm Hg; and Δj, j, Pj, Qj (see Eq. (23)) for all alpha-ray emitters in the U, Ac and Th series.*

	R	Δj	j	P_j	$Q_j(\rho=0.5)$
URANIUM SERIES					
Ra C′	6.51₂[1]	0.9998[2]	1	6.51	0.1665
Ra A	4.38[1]	1	2	10.89	0.425
Ra C (av)	3.80[2]	0.0002[2]	2	10.89	0.425
Rn	3.80[1]	1	3	14.69	0.728
Ra F	3.61[1]	1	4	18.30	1.050
Ra	3.16[3]	1	5	21.46	1.426
UI I	3.05[3]	1	6	24.51	1.818
Io	2.97[3]	1	7	27.48	2.223
U I	2.51[3]	1	8	29.99	2.721
ACTINIUM SERIES					
Ac C′	6.17[4]	0.003[5]	0	0	0
Ac A	6.08[4]	1	1	6.08	0.179
An (av)	5.29[4]	1	2	11.37	0.388
Ac C (av)	5.04[4]	0.997[5]	3	16.41	0.608
Rd Ac	4.36[5]	1	4	20.77	0.867
Ac X	4.07[5]	1	5	24.84	1.147
Pa	3.42[5]	1	6	28.26	1.489
Ac U	3.0[4]	1	7	31.26	1.889
THORIUM SERIES					
Th C′	8.09[1]	0.65[5]	0.65	5.26	0.0857
Th A	5.31[1]	1	1.65	10.57	0.294
Tn	4.71[1]	1	2.65	15.28	0.532
Th C	4.45[1]	0.35[5]	3	16.84	0.620
Th X	4.06[5]	1	4	20.90	0.901
Rd Th	3.74[3]	1	5	24.64	1.210
Th	2.66[3]	1	6	27.30	1.673

[1] Lewis and Wynn-Williams, Proc. Roy. Soc. **A136**, 349 (1932).
[2] Rutherford, Wynn-Williams, Lewis and Bowden, Proc. Roy. Soc. **A139**, 617 (1933).
[3] Rutherford, Chadwick and Ellis, *Radiations from Radioactive Substances* (1930), p. 26. The extrapolated ionization ranges R_i there given are converted to mean ranges using the relation[5] $R_i-R=0.042(R_i-1.51)^{\frac{1}{2}}$ cm.
[4] Evans, Phys. Rev. **45**, 29 (1934), estimated from the half-period, A. v. Grosse, Phys. Rev. **42**, 565 (1932), and the Geiger-Nuttall relation using Geiger's, Zeits. f. Physik **8**, 45 (1921), data for the Ac series.
[5] Kurie and Knopf, Phys. Rev. **43**, 311 (1933), give the extrapolated ionization range R_i in air at 0°, 760 mm as 2.71 ± 0.03 cm. The mean range is estimated by deducting $0.042(R_i-1.51)^{\frac{1}{2}}$ cm [Briggs, Proc. Roy. Soc. **A114**, 313 (1927); Kurie, Phys. Rev. **41**, 701 (1932); Evans, Phys. Rev. **45**, 29 (1934)]. Using Lewis and Wynn-Williams (reference 1, Table I) relationship, $R_2-R=0.8\rho-0.06$, where ρ is the straggling coefficient ($\rho\equiv\rho_{AX}$ used by Briggs) one obtains $R=2.67$ for Th. G. H. Henderson and Nickerson, Phys. Rev. **36**, 1344 (1930) obtained a lower value $R_i=2.59\pm0.05$ cm at 15°C, 760 mm, while Geiger, Zeits. f. Physik **8**, 45 (1922) found $R_i=2.90$ cm at 15°C, 760 mm.

Now we define $P_j\equiv\Sigma R\cdot\Delta j$, $Q_j\equiv\Sigma\Delta j/(R-\rho)$, and $j\equiv\Sigma\Delta j$; then Eq. (22) becomes:

$$H=P_j+a^2Q_j-j(\rho+2a). \tag{23}$$

In evaluating P_j, Q_j and j the summation extends only over those alpha-rays having $R\geqslant a+\rho$, since only these contribute countable rays. Table I gives the values of R, Δj, j, P_j, and Q_j for all alpha-rays in the U, Ac and Th series.

As an example, consider a thick radioactive source containing only the Th series. Let the minimum detectable track $\rho=0.5$ air-cm and the absorber $a=4$ air-cm. Then only alpha-rays having $R\geqslant4.5$ air-cm may be counted. From Table I this is seen to include Th C′, Th A and Tn, but neither Th C nor shorter members. Reading across the row corresponding to the shortest

TABLE II. *Dependence on absorber thickness, a air-cm, of the relative counting rate v_a/v for the U plus Ac series in equilibrium, w_a/w for the Th series, and v_a/w_a the ratio of U plus Ac series to Th series counts.* All values correspond to $\rho=0.5$ air-cm. Values of v_a and w_a (see Eqs. (19) and (20)) are also given.

a	$v_a/10^3\mu d$	$w_a/10^3\mu d$	v_a/w_a	v_a/v	w_a/w
0	82.1	27.0	3.04	1.000	1.000
1	40.4	15.52	2.60	0.493	0.575
2	15.62	7.75	2.02	0.1905	0.287
3	5.63	3.36	1.68	0.0687	0.124
4	2.12	1.40	1.51	0.0258	0.052
5	0.529	0.633	0.84	0.00645	0.0236
6	0	0.237	0	0	0.0089

countable emitter, Tn, we find $j=2.65$, $P_j=15.28$, $Q_j=0.532$. Hence by Eq. (23), $H_{\mathrm{Th}}=15.28+(4)^2\times0.532-2.65(0.5+2\times4)=1.26$. Finally, from Eqs. (17) and (20), the number of alpha-rays counted per sec. per cm² of source surface is $n_a=w_a\mathrm{Th}=1.11\times10^3 H_{\mathrm{Th}}\mu d\cdot\mathrm{Th}=1.40\times10^3\mu d\cdot\mathrm{Th}$, when $a=4$, $\rho=0.5$ air-cm. This value will be found in Table II.

Writing subscripts 1 and 2 to characterize two values of absorber thickness, a_1 and a_2, we may write the equations for absorption measurements which might permit separation of the U and Th effects, and hence provide a direct measure of either or both of these elements.

$$n_1=v_1\mathrm{U}+w_1\mathrm{Th},\quad n_2=v_2\mathrm{U}+w_2\mathrm{Th}. \tag{24}$$

Combining these equations we obtain:

$$\mathrm{Th}=(n_1/w_1)(n_2/n_1-v_2/v_1)/(w_2/w_1-v_2/v_1), \tag{25}$$

$$\mathrm{U}=(n_1/v_1)(w_2/w_1-n_2/n_1)/(w_2/w_1-v_2/v_1), \tag{26}$$

$$\mathrm{Th/U}=(v_1/w_1)(n_2/n_1-v_2/v_1)/(w_2/w_1-n_2/n_1), \tag{27}$$

$$n_1/n_2=(w_1/w_2)(v_1/w_1+\mathrm{Th/U})/(v_2/w_2+\mathrm{Th/U}). \tag{28}$$

Here n_1 and n_2 are values which can be observed experimentally, while v_1, v_2, w_1, w_2 are computed theoretically, or obtained experimentally by internal standardization, as described in Section IV.

Numerical examination of Eqs. (25), (26), (27), (28) quickly shows that an impossibly high experimental precision is required if U and Th concentrations are to be obtained from experiments in which the two absorbers differ in thickness by only about an air-cm. If, however, a_1 approaches zero, while a_2 is made the order of 5 or 6 air-cm, then separation of U and Th becomes possible even for quite feebly radioactive sources. Due to the low background counting rate attainable in counting experiments these measurements become possible, whereas they are forbidden by the relatively high gamma- and cosmic-ray background if ionization methods are employed.[4]

It will be noticed by comparison with Eqs. (19) and (20) that Eqs. (25) and (26) express the Th and U content in terms of $(1/\mu d)$ since the product μd occurs once in each term involving v or w. Experimentally, the effective stopping power $(1/\mu)$, is not readily determinable for rocks, particularly if they are coarse grained. The product μd can be approximated, however, from the Bragg-Kleeman rule which gives

$$\mu d_g=d_a W_g^{\frac{1}{2}}/W_a^{\frac{1}{2}}, \tag{29}$$

where $d_a=$ density of air at 0°C, 760 mm; $d_g=$density of the mineral grain; $W_g^{\frac{1}{2}}=$sum of the atomic percent times the square root of the atomic weight of each of the chemical constituents of the mineral grain; $W_a^{\frac{1}{2}}=$the similarly computed mean square root of the atomic weight for air. Direct measurements of μd for mica have been made by Briggs[6] and by G. H. Henderson[6] who obtained 1.547×10^{-3}g/cm² and 1.659×10^{-3}g/cm², respectively. Computations of μd for mica have been given by G. H. Henderson[6] and by Kerr-Lawson,[6] who found 1.629×10^{-3}g/cm² and 1.639×10^{-3}g/cm², respectively. Since $W_g^{\frac{1}{2}}$ is about 4.79 for mica (Kerr-Lawson) we may say that within an uncertainty of about ±3 percent

$$\mu d_g=3.4\times10^{-4}W_g^{\frac{1}{2}}. \tag{30}$$

This value is also obtained when the known values of d_a and $W_a^{\frac{1}{2}}$ are substituted in Eq. (29).

For practical applications of Eqs. (24) to (28) we need tables of v_2/v_1, w_2/w_1, and the values of v and w when $a=0$. These are obtained from the data of Table I combined with Eqs. (19) and (20), and are given in Table II for the case in which $\rho=0.5$ air-cm, which is an easily

[6] G. H. Briggs, Proc. Roy. Soc. **A114**, 341 (1927). G. H. Henderson, Proc. Roy. Soc. **A145**, 563 (1934). D. E. Kerr-Lawson, Univ. of Toronto Studies, Geological Series, No. 24, p. 54 (1927). Each of the values of μd quoted above has been corrected to 0°C, 760 mm Hg pressure.

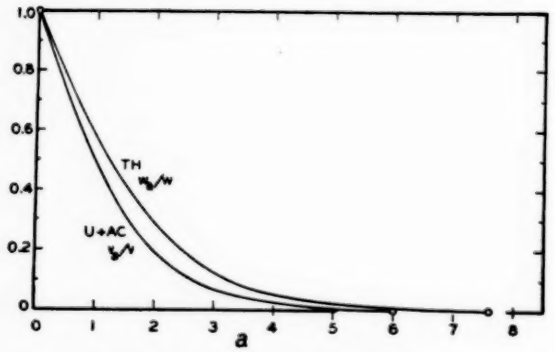

FIG. 3. Dependence of the relative counting rate v_a/v for the U plus Ac series in equilibrium, and w_a/w for the Th series, on absorber thickness a air-cm, when $\rho=0.5$ air-cm.

obtained experimental condition. Table II corresponds to Eqs. (24) to (28) when $a_1=0$, $a_2=a$; $v_1=v_0\equiv v$, $w_1=w_0\equiv w$; and $v_2\equiv v_a$, $w_2\equiv w_a$. Fig. 3 shows graphically the dependence of v_a/v and w_a/w on a.

IV. Determination of the Thorium Content of Geological Specimens

Completely satisfactory experimental methods are available for determining the radium (hence uranium) content of rocks.[7] Geological age and thermal problems also require accurate knowledge of the thorium content of rocks. The results of Section III lead to several new methods for determining the thorium content of rocks[8] by counting the alpha-rays emitted from the rock surface.

Method A rests on absorption measurements and the use of Eq. (25). The value of μd for the source may be estimated from Eq. (30), or obtained experimentally by internal standardization, that is, by adding a known amount of a finely powdered Th mineral such as monazite sand to a powdered rock specimen and determining the change in the observed counting rate.

Method B also involves absorption measurements, but employs Eq. (27) to evaluate the Th/U ratio. This method is independent of the value of μd for the source, but must be combined with a separate determination of U by emanation measurements. These can be made with high precision. The method B is really equivalent to a

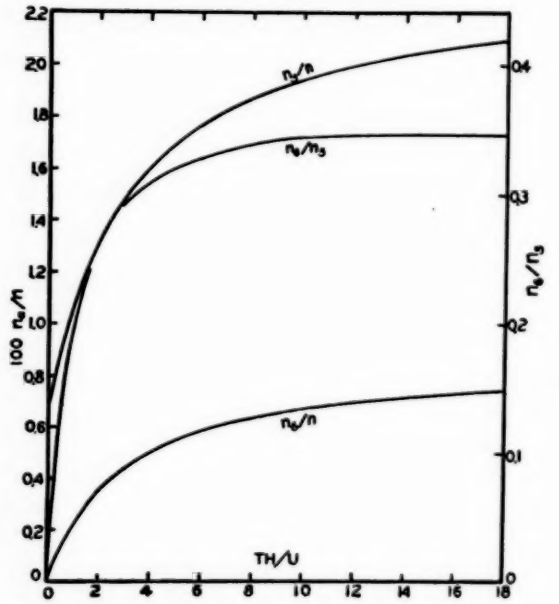

FIG. 4. Left-hand ordinates: ratio n_a/n of counting rates with and without absorbers; curve n_5/n for $a=5$ air-cm, curve n_6/n for $a=6$ air-cm. Right-hand ordinates: ratio n_6/n_5 of counting rates with $a=6$ to $a=5$ air-cm absorption. Abscissae: Th/U ratio in g per g.

combination of method A with a determination of μd by means of Eq. (26) and the independently measured uranium content. Fig. 4 shows the dependence of the relative counting rate n_a/n with 5 and 6 air-cm absorbers to the counting rate with no absorber, and also n_6/n_5 the relative counting rate with 6 air-cm and with 5 air-cm absorbers, each as a function of the Th/U ratio. It will be noted that the method is best suited to Th/U ratio less than about 6; for higher Th/U ratios, method C is preferable.

Method C is especially applicable to very weak sources in which absorption measurements would reduce the counting rate to an impractically low value. It is, therefore, generally applicable even when methods A and B become objectionally inaccurate due to statistical fluctuations in the counting rates. It consists of simply measuring the total counting rate from a source with no absorber, hence by Eq. (24) and Table II:

$$n=(82.1\mathrm{U}+27.0\mathrm{Th})10^3\mu d. \qquad (31)$$

As in method A, μd is evaluated by internal standardization using either a thorium or a uranium mineral, or μd is estimated from Eq. (30). In the latter case, it must be remembered

[7] Evans, Rev. Sci. Inst. **6**, 99 (1935).
[8] Evans, Finney, Kip and Mugele, Phys. Rev. **47**, 791 (1935).

that if a coarsely powdered rock is used as a source, the density of the source d in Eq. (31) is less than the density d_g of the individual grains treated in Eq. (30). Since the ratio d/d_g is not easily measured, the method of internal standardization gives a more reliable value of μd. A separate measurement of the uranium content is then used with Eq. (31) for the determination of the thorium content of the specimen. Since knowledge of the U content is always required in age or thermal problems, this involves no additional work and is therefore not objectionable.

Where ΔTh is the known change in Th content, introduced as an internal standard, and Δn is the corresponding change in the counting rate n, we have

$$\text{Th} = n(\Delta\text{Th}/\Delta n) - (v_a/w_a)\text{U} \qquad (32)$$

$$= n(\Delta\text{Th}/\Delta n) - 3.04\text{U}(\text{when } a=0). \qquad (33)$$

Method D. For sufficiently strong sources a fourth method is available. This consists of a single measurement of the counting rate with an absorber sufficiently thick ($a+\rho=6.5$ air-cm at 0°C 760 mm) to stop all but the 8.08 air-cm alpha-ray from Th C′. This method is really a special limiting case of method A, for when $v_2=0$, i.e., complete U series absorption, Eq. (25) leads to:

$$\text{Th} = n_2/w_2 = 4.22\times10^{-3} n_a/\mu d \qquad (\text{for } a=6,\ \rho=0.5), \qquad (34)$$

where n_a is the counting rate per cm² per sec., and μd is obtained either by internal standardization or from Eq. (30). Taking $\mu d = 1.63\times10^{-3}$, as for mica, we then have $\text{Th} = 2.6 n_a$. If the source is a granitic rock having 10^{-5}g Th per g the total counting rate through the 6 air-cm absorber will then be $10^{-5}\times150\times3600/2.6 = 2.8$ alphas per hr. per 150 cm², which is detectable on the apparatus described in Section V. For sources containing as much as 10^{-4} g Th per g the method becomes quite accurate, as statistical fluctuations are then much less pronounced.

V. Apparatus for Counting Alpha-Rays from Large Surface Areas

The counting chamber (Fig. 5) is a parallel plate condenser having a lower collecting electrode 10 cm in diameter. This electrode is surrounded at a distance of 1 mm by a circular guard ring 2.5 cm wide. The edges of both are beveled to reduce the electrostatic capacity of the collector. The upper electrode is 2 cm above the lower collecting plate, and is mounted on a brass ring supported by Bakelite blocks. In the early experiments a grid of parallel, gauge 40, German silver wires spaced 5 mm apart was used. The alpha-ray source was mounted immediately over it with the active face downward and the active area defined by a circular opening in a brass mask which rested on the upper electrode ring and supported the source.

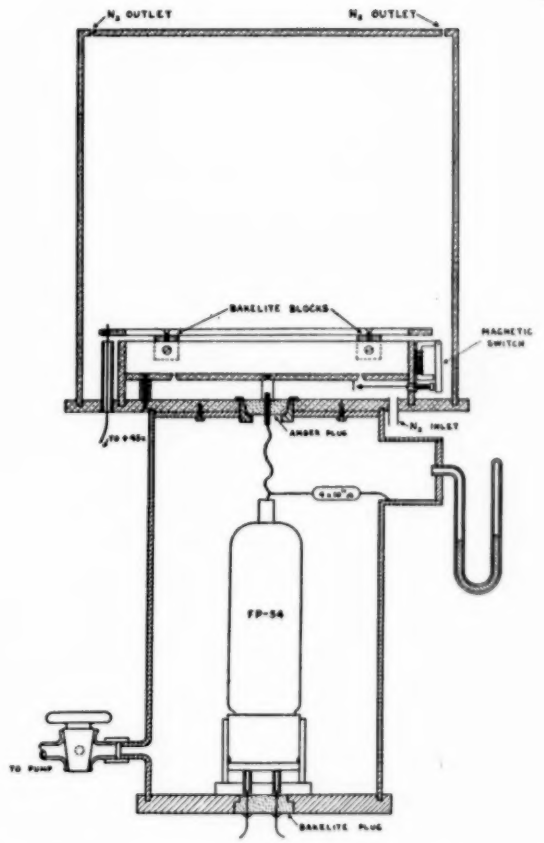

FIG. 5. Construction of the counting chamber, source holder, and electrometer-tube housing. Accurately to scale.

The source is either a flat surface polished onto a hand specimen of a rock; a chemically prepared precipitate painted onto an aluminum disk by using ethyl alcohol as a diluent; or a finely ground rock powder painted on in the same way. The source is covered with a sheet of thin aluminum or gold leaf (stopping power 0.03 air-cm) fastened to the periphery of the source disk

with vaseline. This covering provides a uniform electrostatic field normal to the surface of the source, and prevents minute free grains of the source from dropping into the counting chamber. Gold leaf will not prevent the escape of Rn and Tn from polished rock surfaces, but direct tests by several methods show that the powdered rock sources do not permit the escape of a significant amount of emanation.

Satisfactory electrical operation can be realized without the use of this covering foil, even when the wire grid is removed from below it, but we have always used the foil in order to provide exactly reproducible collecting fields for all specimens. In this case it is best to remove the wire grid, making the foil which covers the source act as the upper electrode of the collecting chamber. This procedure also eliminates the absorption of alpha-rays by the wires of the grid and by the gas between the source and the grid, and avoids the uncertainties of penetration of the collecting field beyond the wires of the grid. The equations of Section III permit accurate correction for the small absorption in the foil. For absorption measurements, aluminum foils are placed directly between the source and the chamber, and nearly in contact with the source.

In addition, powdered sources similarly prepared on Al foils may be placed directly on the lower collecting electrode with their active surfaces facing upward into the counting chamber. It is thus possible to utilize over 150 cm^2 of active source material.

The lead from the lower collecting electrode passes through an amber insulator into an evacuated iron tube-housing patterned after Bearden's[9] apparatus. The amplifying circuit follows the methods of DuBridge and Brown,[10] and the output galvanometer deflection is continuously photographed with a telechron driven drum camera nearly identical with that developed for string electrometer measurements by Evans.[7] Eastman P.M.C. No. 2 contrast bromide emulsion on smooth single-weight paper, 5 inches wide, is used for recording. The drum is 12 inches in diameter and rotates once an hour, hence the travel is 1.6 cm per min.

This high film speed permits recording the full form of the alpha-ray deflection and gives a distinctive hump with a steep initial slope, corresponding to the ballistic period of the galvanometer; a maximum height corresponding to the range of the alpha-ray in the chamber; and an exponential return to the undeflected position, corresponding to the electrostatic time constant of the collecting system. From measurements on the shape of the return curve, and knowledge of the value of the grid resistance (4×10^{11} ohms), the electrostatic capacity of the collecting system and its leads is found to be 36 cm.

The sensitivity[11] is such that a 1 cm alpha-ray produces a 1 cm deflection of the galvanometer. The maximum noise level fluctuations are about 2 to 3 mm hence, while shorter alpha-rays can be clearly identified, we have taken ρ as 0.5 air-cm (0°C 760 mm of air) for then there can be no ambiguity.

Radioactively dead nitrogen, from tanks stored longer than one month, is flowed continuously through the collecting chamber and its cylindrical brass housing at a rate of about 20 cm^3 per minute, which causes no appreciable pressure rise in the chamber. This excludes room air from the apparatus and eliminates resultant contamination. Great care must be taken in preparing sources, and in all operations with the apparatus, to avoid traces of contamination. Numerous control and background runs accompany every measurement of any source, in order to avoid contamination effects. The parts of the counting chamber are readily removable for cleaning, and average background counting rates of 5 alphas per hour are realizable, while 10 per hour is an easily reproduced routine standard. The maximum resolvable counting rate is the order of 350 alphas per hour, and various classes of rock specimens normally run between 20 and 200 alphas per hour per 50 cm^2 of surface area.

The entire apparatus except the camera is housed in a double-walled masonite case for protection from temperature variations, and all electrical parts are electrostatically shielded.

[9] Bearden, Rev. Sci. Inst. **4**, 271 (1933).
[10] DuBridge and Brown, Rev. Sci. Inst. **4**, 532 (1933).

[11] The apparatus has been moved from the University of California to the Massachusetts Institute of Technology, where, with the assistance of Mr. Howard Tatel, a Western Electric 7567-A electrometer tube has been substituted for the FP-54 formerly employed.

The galvanometer spot is automatically moved across the camera slit so that successive hours' records lie side by side on a single photograph. Two methods, each telechron controlled, have been successfully used. By means of a 22 contact, rotary, magnetic telephone relay, which is fed hourly impulses from contacts on the minute and second hands of a telechron clock, the plate resistance and hence the galvanometer zero may be shifted over suddenly once each hour. Alternatively, the galvanometer lamp, mounted on a traveling carriage, may be moved uniformly by means of a screw-thread driven at any speed by a gear on the minute hand shaft of a telechron motor. The former method was used for over 2200 hours of photographic records without any failures, but the latter method has proved preferable at very high sensitivities, because of the low and critical value of the plate circuit resistance.

VI. Experimental Results

Analyses of suites of rock specimens, protactinium sources, kolm, etc., will be separately reported in other journals. In addition we have measured the alpha-ray emission from artificial rock sources in order to verify the theoretical equations of Section III. The specimens were prepared by mixing small amounts of a weak uranium ore (carnotite) and a weak thorium ore (monazite) with plaster of Paris, and have been previously described in connection with ionization measurements on alpha-rays emitted by solids.[12] The uranium series sources contain 2.53×10^{-5} g U per g and 2.53×10^{-6} g U per g; the thorium series sources 4.25×10^{-5} g Th per g and 4.25×10^{-6} g Th per g.

Taking the value of μd_g from Eq. (30), and measuring d for the plaster of Paris ($=1.32$ g cm^{-3}), it is found that the observed counting rate, within the statistical fluctuation of ±3 to 5 percent occasioned by the random emission of alpha-rays, is equal to that predicted by the equations of Section III.

Further calibration tests were made by adding known small amounts of the uranium and thorium series to powders of igneous rocks, in the course of repeated internal standardization tests. Here again the experimental observations are in close agreement with Eqs. (30), (32), and the analog of Eq. (32) for the uranium series. The agreement in the case of the thorium standards tends to support the Geiger-Rutherford value of the Th decay constant which was chosen[5] in Section III as more probable than Kirsch's lower value.[13]

In general, the thorium analyses of igneous rocks have shown values between 3.9 and 16.5×10^{-6} g Th per g, and Th/U ratios ranging between 3.2 and 10.6, and averaging about 7. These results have been confirmed by independent measurements of the U and Th content of these specimens by the emanation method[14] and the γ-ray method.[15] They focus attention on the great importance of a reliable routine method for the determination of the Th content of geological materials, because for Th/U ratios greater than 4 the Th series produces more helium and more thermal energy than the U series, and hence is of greater importance geophysically.

The experimental work and a preliminary theory for thin absorbers which is equivalent to the present general theory was completed at the University of California during the National Research Council Fellowship tenure (1932–1934) of one (E) of the authors. The generous support and encouragement given this program by Professor Leonard B. Loeb is particularly appreciated.

[12] Evans, Phys. Rev. **45**, 38 (1934).

[13] G. Kirsch, Physik. Zeits. **31**, 1017 (1930).

[14] Evans, Finney, Kip and Mugele, Phys. Rev. **47**, 791 (1935); Physics (1935), in preparation.

[15] Evans and Mugele, Phys. Rev. **47**, 427 (1935).

Double Beta-Disintegration

M. GOEPPERT-MAYER, *The Johns Hopkins University*

(Received May 20, 1935)

From the Fermi theory of β-disintegration the probability of simultaneous emission of two electrons (and two neutrinos) has been calculated. The result is that this process occurs sufficiently rarely to allow a half-life of over 10^{17} years for a nucleus, even if its isobar of atomic number different by 2 were more stable by 20 times the electron mass.

1. INTRODUCTION

IN a table showing the existing atomic nuclei it is observed that many groups of isobars occur, the term isobar referring to nuclei of the same atomic weight but different atomic number. It is unreasonable to assume that all isobars have exactly the same energy; one of them therefore will have the lowest energy, the others are unstable. The question arises why the unstable nuclei are in reality metastable, that is, why, in geologic time, they have not all been transformed into the most stable isobar by consecutive β-disintegrations.

The explanation has been given by Heisenberg[1] and lies in the fact that the energies of nuclei of fixed atomic weight, plotted against atomic number, do not lie on one smooth curve, but, because of the peculiar stability of the α-particle are distributed alternately on two smooth curves, displaced by an approximately constant amount against each other (the minimum of each curve is therefore at, roughly, the same atomic number). For even atomic weight the nuclei of even atomic number lie on the lower curve, those with odd atomic number on the higher one. One β-disintegration then brings a nucleus from a point on the lower curve into one of the upper curve, or *vice versa*. The nuclei on the upper curve are all of them unstable. But it may happen that a nucleus on the lower curve, in the neighborhood of the minimum, even though it is not the most stable one, cannot emit a single β-particle, since the resultant isobar, whose energy lies on the upper curve, has higher energy. This nucleus would then be metastable, since it cannot go over into a more stable one by consecutive emission of two electrons. This explanation is borne out by the fact that almost only isobars of even difference in atomic number occur.

A metastable isobar can, however, change into a more stable one by simultaneous emission of two electrons. It is generally assumed that the frequency of such a process is very small. In this paper the propability of a disintegration of that kind has been calculated.

The only method to attack processes involving the emission of electrons from nuclei is that of Fermi[2] which associates with the emission of an electron that of a neutrino, a chargeless particle of negligible mass. Thereby it is possible to explain the continuous β-spectrum and yet to have the energy conserved in each individual process by adjusting the momentum of the neutrino. In this theory the treatment of a β-disintegration is very similar to that of the emission of light by an excited atom.

A disintegration with the simultaneous emission of two electrons and two neutrinos will then be in strong analogy to the Raman effect, or, even more closely, to the simultaneous emission of two light quanta,[3] and can be calculated in essentially the same manner, namely, from the second-order terms in the perturbation theory. The process will appear as the simultaneous occurrence of two transitions, each of which does not fulfill the law of conservation of energy separately.

The following investigation is a calculation of the second-order perturbation, due to the interaction potential introduced by Fermi between neutrons, protons, electrons and neutrinos. As far as possible the notation used is that of Fermi. For a more detailed discussion and justification of this mathematical form and the assumptions involved reference must be made to Fermi's paper.

[1] W. Heisenberg, Zeits. f. Physik **78**, 156 (1932).

[2] E. Fermi, Zeits. f. Physik **88**, 161 (1934).

[3] M. Goeppert-Mayer, Ann. d. Physik (V) **9**, 273 (1931).

2. The Mathematical Apparatus

The nucleus is assumed not to contain any electrons and neutrinos but to be built up out of neutrons and protons only. Neutron and proton are regarded as not essentially different from one another, but to represent two different quantum states of the heavy particle. The two kinds of light particles outside of the nucleus, the electrons and neutrinos are treated according to the method of superquantization. The stationary states of the electrons are taken to be those of positive energy H_s in the Coulomb field of the nucleus, described by four Dirac functions $\psi_s=(\psi_s^1, \psi_s^2, \psi_s^3, \psi_s^4)$. Since the neutrinos are not affected by the field of the nucleus their eigenfunctions are represented by plane Dirac waves $\varphi_\sigma=(\varphi_\sigma^1, \varphi_\sigma^2, \varphi_\sigma^3, \varphi_\sigma^4)$ with energies K_σ. The Pauli principle is assumed to hold for both electrons and neutrinos, so that the number N_s of electrons in a stationary state s and the number M_σ of neutrinos in a stationary state σ can be 0 or 1 only.

A quantum state N of the total system is then determined by these numbers N_s, M_σ and by the quantum state n, with energy W_n of the nucleus; n means in this case not only the quantum states in the ordinary sense but includes the quantum states of all possible isobars. The energy of a quantum state N is given by

$$E_N=\sum_s N_s H_s+\sum_\sigma M_\sigma K_\sigma+W_n. \tag{1}$$

The interaction energy between the heavy particles within the nucleus and the light particles without is constructed in such a way that the transition from neutron to proton is necessarily accompanied by the emission of an electron and a neutrino and *vice versa*. A matrix element of H corresponding to the transition of a neutron with eigenfunction u_n to a proton with eigenfunction v_m is different from 0 only if at the same time two numbers N_s, M_σ change from 0 to 1, and is then given by

$$H_M^N=H_{m\cdots 1_s\cdots 1_\sigma\cdots}^{n\cdots 0_s\cdots 0_\sigma\cdots}$$

$$=(-1)^{N_1+\cdots+N_{s-1}+M_1+\cdots+M_{\sigma-1}}\bar{\psi}_s\delta\varphi_\sigma^* H_{nm}, \tag{2}$$

with the abreviation

$$\bar{\psi}\delta\varphi^*=-\psi^{*1}\varphi^{*2}+\psi^{*2}\varphi^{*1}+\psi^{*3}\varphi^{*4}-\psi^{*4}\varphi^{*3}, \tag{3}*$$

$$H_{nm}=g\int v_m^* u_n d\tau. \tag{4}$$

The functions ψ and φ are taken at the place of the nucleus, the assumption being made that they do not vary considerably over its range. For an "allowed" transition $\int v_m^* u_n d\tau$, taken over the volume of the nucleus, has the order of magnitude 1. The value of the proportionality constant g can be roughly obtained by equating calculated and observed intensity of β-disintegration. Fermi determines it to be

$$g=4\times 10^{-50}\ \text{cm}^3\ \text{ergs}. \tag{5}$$

3. Calculations

The probability of simultaneous emission of two electrons and two neutrinos is obtained from the second order terms of the perturbation theory. In this approximation the amplitude of the transition probability is given by

$$a_M^N=\sum_K \frac{H_K^N H_M^K}{E_K-E_N}\left\{\frac{e^{(2\pi i/h)(E_M-E_N)t}-1}{E_M-E_N}-\frac{e^{(2\pi i/h)(E_M-E_K)t}-1}{E_M-E_K}\right\}. \tag{6}$$

We want to consider transitions of such a type that in the beginning state, N, no electrons or neutrinos are present; in the end state, M, the charge of the nucleus has been increased by 2, that is two neutrons have been transformed into protons, and two electrons have been emitted into states s and t, two neutrinos into states σ and τ. The intermediate state K then must be such that one neutron has changed into a proton, one electron and one neutrino have been emitted. This means that the intermediate state k of the nucleus is a quantum state of the isobar with atomic number larger by 1 than the original nucleus. The assumption that ordinary β-disintegration is energetically impossible means that $W_{kn}=W_k-W_n>-mc^2$; the first denominator E_K-E_N in (6) will therefore always be positive. The process of double β-disintegration is, however, energetically permissible if $W_{mn}=W_m-W_n<-2mc^2$. In this case the second

* A star denotes the conjugate complex of a quantity.

denominator, $E_M - E_N$, the difference of energy between beginning and end state, will, for those processes for which the energy is conserved, approach zero, and only then has $a_M{}^N$ appreciable values. As in the theory of radiation the second term in the bracket in (6) can then be neglected with respect to the first, since $E_M - E_K$ has always a finite value.

The summation over the intermediate states of the light particles can be made explicitly; there are only four intermediate states possible, namely, electron s may have been emitted before or after electron t, and neutrino σ before or after neutrino τ. The power of -1 in the operators $a_s{}^*$, $b_\sigma{}^*$ introduces a difference in sign in the different cases. The result is:

$$a_M{}^N = \pm\sum_k H_{nk}H_{km}\left\{\left[\frac{1}{W_{kn}+H_s+K_\sigma}+\frac{1}{W_{kn}+H_t+K_\tau}\right]\bar{\psi}_s\delta\varphi_\sigma{}^*\bar{\psi}_t\delta\varphi_\tau{}^*\right.$$
$$\left.-\left[\frac{1}{W_{kn}+H_s+K_\tau}+\frac{1}{W_{kn}+H_t+K_\sigma}\right]\bar{\psi}_s\delta\varphi_\tau{}^*\bar{\psi}_t\delta\varphi_\sigma{}^*\right\}\frac{\exp\left[(2\pi i/h)(W_{mn}+H_s+H_t+K_\sigma+K_\tau)t\right]-1}{W_{mn}+H_s+H_t+K_\sigma+K_\tau}. \quad (7)$$

To obtain the transition probability $|a_M{}^N|^2$ has to be summed over all possible states s, σ, t and τ. The first step to this is to average the absolute value squared of (7) over all possible directions of the plane waves of the neutrino. This is done most easily by assuming that the neutrinos are confined to a large space Ω. In that case, neglecting the neutrino mass, $\overline{\varphi_\sigma{}^\nu\varphi_\sigma{}^\mu} = (1/4\Omega)\delta_{\nu\mu}$. We obtain terms of the type

$$\overline{|\bar{\psi}_s\delta\varphi_\sigma{}^*|^2} = (1/4\Omega)(\bar{\psi}_s\psi_s), \quad \overline{\bar{\psi}_s\delta\varphi_\sigma{}^*\cdot\bar{\psi}_t{}^*\delta\varphi_\sigma} = (1/4\Omega)(\bar{\psi}_s\psi_t),$$

where the abbreviation $(\bar{\psi}_s\psi_t) = \sum_\nu \psi_s{}^\nu{}^*\psi_t{}^\nu$ has been used.

Furthermore, from the properties of the ψ's, the relativistic eigenfunctions of the Coulomb field, it follows that, if the spin of the state s is parallel to that of t,

$$|(\bar{\psi}_s\psi_t)|^2 = (\bar{\psi}_s\psi_s)(\bar{\psi}_t\psi_t);$$

if the spins of states s and t are antiparallel

$$|\bar{\psi}_s\psi_t|^2 = 0.\dagger$$

We therefore obtain

$$|a_M{}^N|^2 = \frac{1}{16\Omega^2}A(\bar{\psi}_s\psi_s)(\bar{\psi}_t\psi_t)\cdot\frac{4\sin^2\left[(\pi/h)(W_{mn}+H_s+H_t+K_\sigma+K_\tau)t\right]}{(W_{mn}+H_s+H_t+K_\sigma+K_\tau)^2},$$

where A is the following abbreviation:

For parallel spin of states s and t,

$$A = A_1 = \left|\sum_k H_{nk}H_{km}\left[\frac{1}{W_{kn}+H_s+K_\sigma}+\frac{1}{W_{kn}+H_t+K_\tau}-\frac{1}{W_{kn}+H_s+K_\tau}-\frac{1}{W_{kn}+H_t+K_\sigma}\right]\right|^2. \quad (8a)$$

For antiparallel spin

$$A = A_2 = \left|\sum_k H_{nk}H_{km}\left[\frac{1}{W_{kn}+H_s+K_\sigma}+\frac{1}{W_{kn}+H_t+K_\tau}\right]\right|^2$$
$$+\left|\sum_k H_{nk}H_{km}\left[\frac{1}{W_{kn}+H_s+K_\tau}+\frac{1}{W_{kn}+H_t+K_\sigma}\right]\right|^2. \quad (8b)$$

Here the sum over k runs over all possible quantum states of the intermediate isobar.

† This is true only for ψ functions with the angular quantum number $j = 1/2$ in the neighborhood of $r = 0$, with which we are concerned. But all other ψ's are negligible at these distances from the origin.

The summation over all possible states of the neutrinos is now replaced by an integration over the energies K_σ, K_τ. The number of neutrino states whose energy lies between K_σ and $K_\sigma+dK_\sigma$ is given by

$$(8\pi\Omega/h^3c^3)K_\sigma^2 dK_\sigma.$$

In the first integration, i.e., over K_τ, only those energies contribute which lie in the neighborhood of the place $E_M-E_N=0$, which corresponds to conservation of energy. The integral becomes proportional to the time t in the usual manner. By neglecting the dependence of A on the energies, the probability of emission of one electron into state s, one into the state t becomes

$$P^{st}=(1/t)\sum_{\sigma,\tau}|a_M{}^N|^2=(8\pi^4/h^7c^6)A(\bar{\psi}_s\psi_s)(\bar{\psi}_t\psi_t)\int K_\sigma^2(W_{mn}+H_s+H_t+K_\sigma)^2dK_\sigma$$
$$=(4\pi^4/15)(A/h^7c^6)(\bar{\psi}_s\psi_s)(\bar{\psi}_t\psi_t)(W_{nm}-H_s-H_t)^5. \quad (9)$$

Finally the summation over s and t is replaced by a double integration over the energy, that is over the continuous spectrum of the electron in the Coulomb field of the nucleus. It is somewhat more convenient to express the energies in units of mc^2, namely, to introduce the dimensionless quantities $mc^2\epsilon=W_{nm}>0$, $mc^2h_s=H_s$, $mc^2h_t=H_t$.

According to Fermi the value of ψ at the outer edge of the nucleus, that is at a distance $\rho=9\times10^{-13}$ cm from the center has to be used; the sum of $(\bar{\psi}_s\psi_s)$ over all states with a fixed direction of spin and energy in the range dh_s is given by:

$$\sum_{dh_s}\psi_s(\rho)\psi_s(\rho)=\frac{16\pi}{|\Gamma(3+2S)|^2}\frac{m^3c^3}{h^3}\left(\frac{4\pi mc\rho}{h}\right)^{2S}\cdot h_s(h_s^2-1)^{\frac{1}{2}+S}$$
$$\exp\left[\pi\gamma\frac{h_s}{(h_s^2-1)^{\frac{1}{2}}}\right]\left|\Gamma\left(1+S+i\gamma\frac{h_s}{(h_s^2-1)^{\frac{1}{2}}}\right)\right|^2 dh_s, \quad (10)$$

where Z is atomic number, $\gamma=Z/137$, $S=(1-\gamma^2)^{\frac{1}{2}}-1$. S is for any occurring value of nuclear charge negative and small compared to 1; $\gamma=0.3$, $S=-0.05$ correspond to $Z\leq41$. (10) can therefore be approximated by a much simpler form by neglecting S against $1/2$ in the exponent of (h_s^2-1) and S against 1 in the Γ-function, since

$$\exp\left(\pi\gamma\frac{h_s}{(h_s^2-1)^{\frac{1}{2}}}\right)\left|\Gamma\left(1+i\gamma\frac{h_s}{(h_s^2-1)^{\frac{1}{2}}}\right)\right|^2\leq2\pi\gamma\frac{h_s}{(h_s^2-1)^{\frac{1}{2}}}.$$

The transition probability of the nucleus obtained by summation of (9) over all states and the two cases of parallel and antiparallel spin of the electrons, then turns out to be

$$P=\frac{4^6\pi^8\gamma^2}{15|\Gamma(3+2S)|^4}\frac{m^{11}c^{10}}{h^{13}}\left(\frac{4\pi mc\rho}{h}\right)^{4S}(A_1+A_2)\int_1^{\epsilon-1}h_s^2\int_1^{\epsilon-h_s}h_t^2(\epsilon-h_s-h_t)^5dh_tdh_s \quad (11)$$
$$=\frac{4^6\pi^8\gamma^2}{6\cdot7\cdot15|\Gamma(3+2S)|^4}\frac{m^{11}c^{10}}{h^{13}}\left(\frac{4\pi mc\rho}{h}\right)^{4S}(A_1+A_2)F(\epsilon-2),$$

where

$$F(x)=x^7\left(1+\frac{1}{2}x+\frac{1}{9}x^2+\frac{1}{9.10}x^3+\frac{1}{2\cdot9\cdot10\cdot11}x^4\right).$$

ϵ is the difference of energy between the beginning and end states of the nucleus in units mc^2. A_1 and A_2 are given by (8); they contain the dependence of the process on the energy levels of the intermediate nucleus. It turns out, however, that the values of those energies do not greatly influence the probability. Roughly one can put

$$A_1+A_2 \simeq \left|\frac{H_{nk}H_{km}}{W_k-W_n}\right|^2 \sim \frac{g^4}{m^2c^4},$$

with g given by (5). Numerical evaluation for $Z=31$ leads to

$$P=1.15\times10^{-35}F(\epsilon-2) \text{ sec.}^{-1}$$
$$=3.6\times10^{-28}F(\epsilon-2) \text{ year}^{-1}. \quad (12)$$

As seen from the general formula (11) P is almost independent of Z.

The value of F for some arguments is given in the following table:

$\epsilon=$	4	6	8	10
$F(\epsilon+2)=$	0.37×10^{2}	9.2×10^{4}	3.4×10^{6}	4.2×10^{7}
$\epsilon=$	12	20		
$P(\epsilon-2)=$	3.3×10^{8}	1×10^{11}		

The author wishes to express her gratitude to Professor E. Wigner for suggesting this problem, and for the interest taken in it.

SEPTEMBER 15, 1935 PHYSICAL REVIEW VOLUME 48

The Infrared Absorption Spectra of the Linear Molecules Carbonyl Sulphide and Deuterium Cyanide

PAUL F. BARTUNEK AND E. F. BARKER, *University of Michigan*

(Received June 28, 1935)

Carbonyl sulphide. The discovery of new vibration-rotation bands in the infrared absorption spectrum of carbonyl sulphide has made it possible to determine the vibrational energy level scheme of the molecule. The agreement between theory and experiment is quite satisfactory. *Deuterium cyanide.* The fundamental bands of deuterium cyanide ω_2 at 570 cm^{-1} and ω_3 at 2630 cm^{-1} have been measured with grating spectrometers. The former has a strong zero branch at 570.16 cm^{-1}, and the fine structure lines on each side are well separated. From the line spacing the moment of inertia of the molecule is found to be 22.92×10^{-40} gram cm^2. A comparison of this value with the corresponding one for HCN, i.e., 18.72×10^{-40} gram cm^2, permits the calculation of the internuclear distances. From the positions of these two bands, together with those of the observed fundamentals of HCN, the zeroth order quadratic potential energy expression is computed.

THE infrared absorption spectrum of carbonyl sulphide (COS) has been investigated by Cassie and Bailey[1] who found ten unresolved bands in the region 1–20μ using a prism spectrometer. Vegard[2] has deduced from x-ray measurements that the molecule is linear with interatomic separations C–O of 1.10 Angstrom units and C–S of 1.96 Angstrom units. The calculated moment of inertia is 178×10^{-40} gram cm^2.

The perturbed expression for the vibrational energy is

$$E \text{ (vibration)}=\nu_1V_1+\nu_2V_2+\nu_3V_3+X_{11}V_1^2$$
$$+X_{22}V_2^2+X_{33}V_3^2+X_{12}V_1V_2+X_{13}V_1V_3$$
$$+X_{23}V_2V_3+X_{ll}l^2+\text{constant}$$

where the V's are the vibrational quantum numbers, l is the azimuthal quantum number, and ν_1 to X_{ll} are constants. If ten bands which involve these constants in an independent way are located experimentally the ten constants may be calculated and the energy level system for the molecule determined. This is of fundamental importance because it provides the correlating network and serves to predict new absorption bands.

This problem is similar to that of HCN which has been developed through a number of experimental researches to a fairly complete solution.[3, 4, 5, 6, 7, 8] Recently Herzberg and Spinks[9]

[1] Bailey and Cassie, Proc. Roy. Soc. **A135**, 375 (1932).
[2] Vegard, Zeits. f. Krist. **77**, 411 (1931).
[3] Burmeister, Verh. d. D. Phys. Ges. **15**, 589 (1913).
[4] Barker, Phys. Rev. **23**, 200 (1924).
[5] Badger and Binder, Phys. Rev. **37**, 800 (1931).
[6] Brackett and Liddel, Smith. Inst. **85**, No. 5 (1931).
[7] Choi and Barker, Phys. Rev. **42**, 777 (1932).
[8] Adel and Barker, Phys. Rev. **45**, 277 (1934).
[9] Herzberg and Spinks, Proc. Roy. Soc. **A147**, 434 (1934).

have photographed two HCN bands at λ10,385 and λ11,645 under high resolution. The moment of inertia obtained from the fine structure observed is 18.70×10^{-40} gram cm². By assuming the C–H distance to be the same as in acetylene, i.e., 1.06 Angstrom units, they found the atomic distance C–N to be 1.15 Angstrom units. These dimensions may be determined in a more reliable manner by comparing the spectra of HCN and DCN. We have observed two of the fundamental bands of the latter molecule, and have completely resolved one of them, thus obtaining a precise measure of the moment of inertia.

Adel[10] gives an analysis of vibrational isotope effects in three particle systems showing how the infrared spectra of two or more isotopic molecules can be applied to the analysis of their quadratic potential energy function making the assumption that the molecular force field is invariant under an isotopic change of mass. We are now able to compute these potential constants for HCN and DCN.

Three infrared spectrometers were available. The first, which is equipped with a rocksalt prism and gratings having 2400 and 4800 lines per inch has been described by Barker and Meyer.[11] It was used for the region $1-10\mu$. The second is a recording instrument with a KBr prism set up by Randall and Strong[12] and is particularly adapted for rapid exploration out to 20μ. The third spectrometer has a grating with 1200 lines per inch and a KBr foreprism, the optical system having been described by Hardy.[13] It was used for analyzing the bands at 17.5μ and 19μ.

Two absorption cells were used. The first is twenty cm in length with KBr windows, and the second is twenty-five cm in length with windows of rocksalt.

Carbonyl sulphide was prepared by treating 50 cm³ of concentrated water solution of KSCN with a cold mixture of 520 grams of concentrated H_2SO_4 and 400 cm³ of water. The gas COS is given off at 25°C (contaminated with a few impurities in slight amount namely CO_2, CS_2 and H_2S) according to the reaction;[14] $KSCN + H_2O + 2H_2SO_4 \rightarrow COS + KHSO_4 + NH_4HSO_4$.

[10] Adel, Phys. Rev. **46**, 222 (1934).

[11] Barker and Meyer, Trans. Faraday Soc. **25**, 912 (1929).
[12] Randall and Strong, Rev. Sci. Inst. **2**, 585 (1931).
[13] Hardy, Phys. Rev. **38**, 2162 (1931).
[14] Mellor, *Comprehensive Treatise in Chemistry.*

TABLE I. *Observed bands of carbonyl sulphide.*

Observed by Barker & Bartunek				Observed by Cassie & Bailey						Raman lines observed by Dadieu & Kohlrausch		
Band no.	(cm^{-1})	Band no.	(cm^{-1})	Band no.	(cm^{-1})	Assignment	Band no.	(cm^{-1})	Assignment	Line no.	(cm^{-1})	Assignment
1	4101	9	1558.6	1	4084	$2\omega_3$	9	—	$3\omega_2$	1	2233	$2\omega_1+\omega_2$
2	3739	10	1530.4	2	3742	$2\omega_1+\omega_3$	10	—	$\omega_3-\omega_2$	2	2055	ω_3
3	3096	11	1047.4	3	3095	$2\omega_2+\omega_3$	11	1051	$2\omega_2$	3	1383	$\omega_1+\omega_2$
4	2919	12	859.2	4	2904	$\omega_1+\omega_3$	12	859	ω_1	4	1041	$2\omega_2$
5	2575	13	526.6	5	—	$\omega_2+\omega_3$	13	—	$1_1\rightarrow2_2$	5	859	ω_1
6	2050.5	14	521.5	6	2079	ω_3	14	527	ω_2	6	678	$2\omega_1-2\omega_2$
7	1892	15	514.3	7	1898	$2\omega_2+\omega_1$	15	—	$1_1\rightarrow2_0$	7	524	ω_2
8	1710			8	1718	$2\omega_1$						

TABLE II. *Carbonyl sulphide bands.*

Observed	Calculated	Assignment	Observed	Calculated	Assignment
4101*	4101	$2\omega_3$	514.3	516	$1_1\rightarrow2_0$
3739	3779	$2\omega_1+\omega_3$		Raman lines	
3096	3094	$2\omega_2+\omega_3$	2233	2227	$2\omega_1+\omega_2$
2919*	2919	$\omega_1+\omega_3$	2055	2050.5	ω_3
2575*	2575	$\omega_2+\omega_3$	1383	1380.7	$\omega_1+\omega_2$
2050.5*	2050.5	ω_3	1041	1037.5	$2\omega_2$
1892*	1892	$2\omega_2+\omega_1$	859	859.2	ω_1
1710*	1710	$2\omega_1$	678	672.5	$2\omega_1-2\omega_2$
1558.6*	1558.6	$3\omega_2$	524	521.5	ω_2
1530.4	1529	$\omega_3-\omega_2$		Constants	
1047.4	1037.5	$2\omega_2$	$\nu_1=863.4$	$X_{11}=-4.2$ $X_{12}=-2.35$	$X_{ll}=2.65$
859.2*	859.2	ω_1	$\nu_2=518.95$	$X_{22}=-.10$ $X_{13}=9.3$	
526.6*	526.6	$1_1\rightarrow2_2$	$\nu_3=2050.5$	$X_{33}=0$ $X_{23}=3.$	
521.5*	521.5	ω_2			

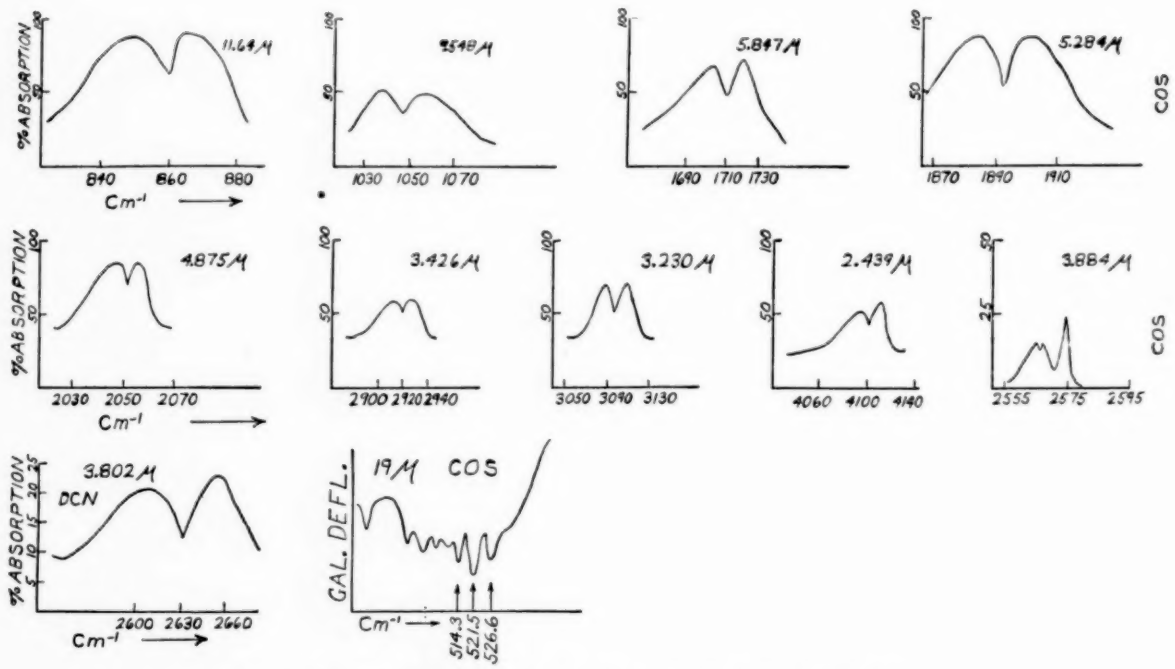

FIG. 1. Carbonyl sulphide bands and the deuterium cyanide band ω^3.

The products were passed from the generating flask through a trap immersed in a mixture of ice and salt which condenses the greater part of the CS_2, then through a 33 percent solution of KOH to precipitate CO_2 and H_2S, and finally through traps containing $CaCl_2$ and P_2O_5. The dry gas was then condensed with liquid air and stored in a five liter reservoir.

The deuterium cyanide was supplied by the California Isotope Company in a small glass capsule containing a mixture of about 40 percent DCN and 60 percent HCN.

The readings were taken in the usual in and out method for all the bands with the exception of the 17.5μ band of DCN, the 14μ band of HCN and the 19μ region of COS. In these cases the cell was in the beam permanently during the time deflections were taken. It was then removed and the "background" mapped on the same day. Care was always taken of course to insure a pure spectrum. The Nernst glower was used as a source of continuous radiation. The calibration of the spectrometers is in terms of the water vapor lines in the region of 6μ.

The results for carbonyl sulphide are shown in Fig. 1 and Tables I and II. Table I gives the observed bands in terms of wave numbers with the bands observed by Cassie and Bailey[1] for comparison. At the end of the table the Raman lines observed by Dadieu and Kohlrausch[15] are listed.

The 2.67μ band is not reproduced. It is very irregular due to superposition of the CO_2 and H_2S bands in the same region since it is impossible to remove every trace of these substances from the gas. It is extremely difficult to judge the position of the center but it seems to be at 3739 cm^{-1}. Cassie and Bailey[1] found a band in this region which they list as 3742 cm^{-1}. This band was not used in calculating the constants. The two bands 1558.5 cm^{-1} and 1530 cm^{-1} are also not reproduced. Both have sharp zero branches similar to the 2575 cm^{-1} band. Two of the three zero branches in the 19μ region are upper stage transitions from the first excited state to the second excited states. These are clearly shown on the photographic record, Fig. 1. The proportion of molecules in the first excited state at room temperature is 17 percent which is sufficient to account for the upper stage absorption.

Table II gives the observed and calculated positions of the infrared bands and Raman lines,

[15] Dadieu and Kohlrausch, Physik. Zeits. **33**, 165 (1932).

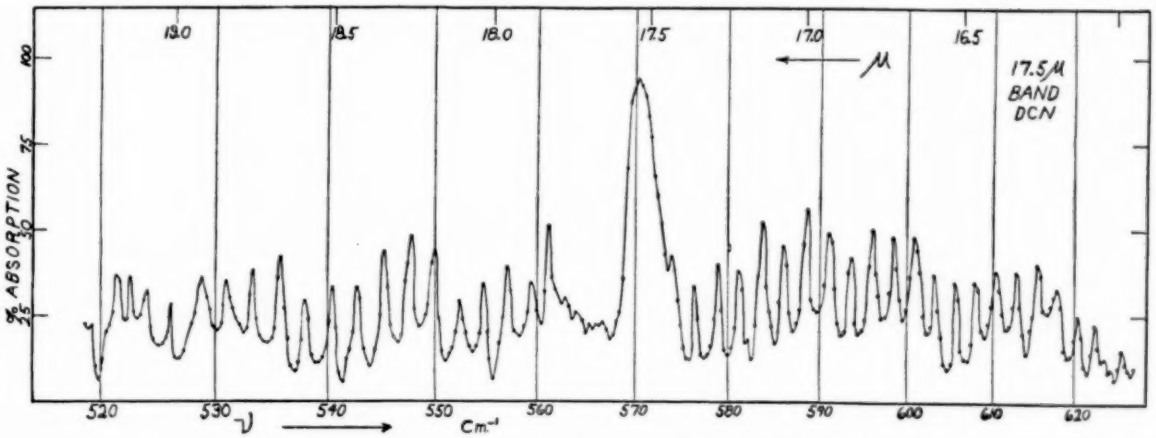

FIG. 2. Rotation lines of the 17.5μ region of deuterium cyanide.

the calculated values of the ten constants being obtained from the bands marked with asterisks. These constants are given at the end of the table.

The results for deuterium cyanide are shown in Fig. 2 indicating the fine structure of the 17.5μ region; in Fig. 1 where the fundamental band ω_3 appears; and in Tables III and V. Table III gives the observed and calculated positions of the rotation lines of DCN while Table IV gives similar results for HCN. The calculated values in these tables were obtained from the formula $\nu=\nu_0+Am+Bm^2+Cm^3$ the constants ν_0, A, B and C being obtained empirically. The ordinal number "m" is counted from the band center. The constants are for DCN $\nu_0=569.10$; $A=2.425$; $B=0.0013$; $C=-0.00003$ and for HCN $\nu_0=712.07$; $A=2.952$; $B=0$; $C=0$.

The part of the band immediately to the low frequency side of the zero branch is somewhat irregular due to the superposition of the upper stage bands of DCN. The rather sharp intense

TABLE III. *Rotation lines of the* 17.5μ *band of DCN zero branch* 570.16 cm^{-1}.

R Branch $\Delta J=+1$				*P* Branch $\Delta J=-1$				*R* Branch $\Delta J=+1$				*P* Branch $\Delta J=-1$		
Obs.	Calc.	Res.	m	Obs.	Calc.	Res.	m	Obs.	Calc.	Res.	m	Obs.	Calc.	Res.
—	571.53	—	1	—	—	—	13	600.76	600.78	−.02	13	537.86	537.87	−.01
573.74	573.96	−0.22	2	564.52	564.26	0.26	14	603.17	603.22	−.05	14	535.53	535.48	.05
576.28	576.39	−.11	3	561.81	561.83	−.02	15	605.66	605.67	−.01	15	533.17	533.11	.06
578.84	578.82	.02	4	559.41	559.42	−.01	16	608.05	608.11	−.06	16	530.83	530.75	.08
581.06	581.26	−.20	5	556.98	557.00	−.02	17	610.45	610.54	−.09	17	528.36	528.40	−.04
583.67	583.69	−.02	6	554.62	554.61	.01	18	612.94	613.00	−.06	18	526.02	526.04	−.02
586.25	586.13	.12	7	552.29	552.19	.10	19	615.60	615.44	.16	19	523.86	523.71	.15
588.59	588.56	.03	8	549.98	549.80	.18	20	617.99	617.88	.11	20	521.51	521.36	.15
591.15	591.02	.13	9	547.69	547.41	.18	21	620.56	620.32	.24	21	—	—	—
593.60	593.45	.15	10	545.10	545.01	.09	22	622.71	622.76	−.05	22	—	—	—
595.94	595.90	.04	11	542.59	542.63	−.04	23	624.88	625.21	−.33	23	—	—	—
598.31	598.34	−.03	12	540.37	540.24	.13								

TABLE IV. *Rotation lines of the* 14μ *band of HCN zero branch* 712.28 cm^{-1}.

R Branch $\Delta J=+1$				*P* Branch $\Delta J=-1$				*R* Branch $\Delta J=+1$				*P* Branch $\Delta J=-1$		
Obs.	Calc.	Res.	m	Obs.	Calc.	Res.	m	Obs.	Calc.	Res.	m	Obs.	Calc.	Res.
—	715.02	—	1	—	—	—	14	753.35	753.40	−.05	14	670.69	670.74	−.05
717.86	717.97	−0.11	2	706.33	706.17	0.16	15	756.29	756.35	−.06	15	667.66	667.79	−.13
720.81	720.93	−.12	3	703.23	703.21	.02	16	759.25	759.30	−.05	16	664.66	664.84	−.18
723.78	723.88	−.10	4	699.60	700.26	−.66	17	762.23	762.25	−.02	17	661.69	661.89	−.20
726.77	726.83	−.06	5	697.25	697.31	−.06	18	765.24	765.21	.03	18	658.75	658.93	−.18
729.80	729.78	.02	6	694.24	694.36	−.12	19	768.28	768.16	.12	19	656.08	655.98	.10
732.85	732.73	.12	7	691.38	691.41	−.03	20	770.99	771.11	−.12	20	653.19	653.03	.16
735.93	735.69	.24	8	688.42	688.45	−.03	21	774.07	774.06	.01	21	650.33	650.08	.25
738.72	738.64	.08	9	685.48	685.50	−.02	22	777.18	777.01	.17	22	647.02	647.13	−.11
741.85	741.59	.26	10	682.57	682.55	.02	23	779.97	779.97	.00	23	—	644.17	—
744.69	744.54	.15	11	679.69	679.60	.09	24	782.78	782.92	−.14	24	—	641.22	—
747.55	747.49	.06	12	676.57	676.65	−.08	25	785.84	785.87	−.03	25	—	638.27	—
750.44	750.45	−.01	13	673.49	673.69	−.20	26	788.81	788.82	−.01	26	—	—	—

TABLE V. *Average separations of the rotation lines.*

DCN 17.5μ BAND $\frac{R(m)-P(m)}{2m}$	m	HCN 14μ BAND $\frac{R(m)-P(m)}{2m}$	DCN 17.5μ BAND $\frac{R(m)-P(m)}{2m}$	m	HCN 14μ BAND $\frac{R(m)-P(m)}{2m}$
2.305 cm^{-1}	2	2.883 cm^{-1}	2.416	14	2.952
2.412	3	2.930	2.416	15	2.954
2.429	4	3.023	2.413	16	2.956
2.408	5	2.952	2.414	17	2.957
2.421	6	2.973	2.414	18	2.958
2.426	7	2.962	2.414	19	2.953
2.413	8	2.969	2.412	20	2.954
2.414	9	2.958	—	21	2.946
2.425	10	2.964	—	22	2.958
2.425	11	2.955	Average 2.414 cm^{-1}		Average 2.955 cm^{-1}
2.414	12	2.958	$I=22.92\times10^{-40}$ g cm^2		$I=18.72\times10^{-40}$ g cm^2
2.419	13	2.959			

line at 561.07 cm^{-1} is probably the zero branch of the transition $1_1\rightarrow2_0$ where the subscript indicates the l value. The upper stage transition $1_1\rightarrow2_2$ probably lies somewhere within the zero branch of that from the ground state $0_0\rightarrow1_1$. At room temperature about 14 percent of the molecules are in the first excited state. This is sufficient to account for the presence of upper stage zero branches.

Table V gives the average separations of the lines from which the moment of inertia about the center of gravity is calculated. Values of $(R(m)-P(m))/2m$ are given for both HCN and DCN, with the calculated moments of inertia.

A search was made for the other two fundamentals ω_1 and ω_3 as well as for harmonics. Because of the rather small amount of gas available the only other band observed was ω_3 at 2630 cm^{-1}.

In the case of HCN because of the strong absorption of carbon dioxide in the background, readings could not be taken for a short space as the deflections dropped to zero. Because of the regularity of the lines the missing line was interpolated and found to agree very well with the calculated value.

The expression for the moment of inertia of this linear triatomic molecule about its center of gravity is

$$I=m_1x^2+m_2y^2-\frac{1}{m_1+m_2+m_3}(m_1^2x^2+m_2^2y^2-2m_1m_2xy)$$

where x is the H–C distance and y is the C–N distance. m_1, m_2 and m_3 are the masses of the hydrogen, nitrogen and carbon atoms, respectively. Introducing the isotopic masses m_1 and m_1' and solving the two equations simultaneously we obtain the interatomic separations, $x=1.06\times10^{-8}$ cm and $y=1.15\times10^{-8}$ cm.

The theory of small oscillations may be applied, considering the molecule as a group of uncoupled simple harmonic oscillators of which two are linear and one is plane isotropic in a plane perpendicular to the axis of the molecule. The normal modes of vibration are well known. We shall use coordinates somewhat different from those defined by Adel[10] in order to preserve the same meaning of these coordinates for both isotopes. Let r represent the distance from the central atom to the line joining the end atoms measured parallel to the displacement of the particles in the perpendicular vibration. Let q measure the relative separation of the hydrogen and carbon atoms, and z measure the relative displacement of the carbon and nitrogen atoms. In the perpendicular vibration let y_1, y_2 and y_3 represent the displacements of the hydrogen, nitrogen and carbon atoms. Then the kinetic energy is

$$T=\tfrac{1}{2}m_1\dot{y}_1^2+\tfrac{1}{2}m_2\dot{y}_2^2+\tfrac{1}{2}m_3\dot{y}_3^2.$$

The expression for r in terms of y_1, y_2 and y_3 and the internuclear distances is

$$r=y_1y/r_0+y_2x/r_0-y_3 \quad \text{where} \quad r_0=x+y.$$

Since the momentum is conserved as well as the moments of momenta about any point one has two additional relations

$$m_1\dot{y}_1+m_2\dot{y}_2+m_3\dot{y}_3=0 \quad \text{and} \quad m_1\dot{y}_1x-m_2\dot{y}_2y=0.$$

In terms of r the kinetic energy becomes $T=\frac{1}{2}\mu_r\dot{r}^2$ where

$$\mu_r=1\Big/\left[\frac{1}{m_2}\left(\frac{x}{r_0}\right)^2+\frac{1}{m_1}\left(\frac{y}{r_0}\right)^2+\frac{1}{m_3}\right].$$

For the longitudinal vibrations x_1, x_2 and x_3 represent the displacements from equilibrium of the hydrogen, nitrogen, and carbon atoms, respectively. Then

$$q=x_3-x_1; \quad z=x_2-x_3;$$

and

$$m_1\dot{x}_1+m_2\dot{x}_2+m_3\dot{x}_3=0.$$

In this case the kinetic energy is $T=\frac{1}{2}m_1\dot{x}_1^2+\frac{1}{2}m_2\dot{x}_2^2+\frac{1}{2}m_3\dot{x}_3^2$ or in terms of $\dot{q}$ and $\dot{z}$, $T=\frac{1}{2}\mu_q\dot{q}^2+\frac{1}{2}\mu_z\dot{z}^2+\frac{1}{2}\cdot 2\mu_{qz}\dot{q}\dot{z}$ where

$$\mu_q=\frac{m_1(m_2+m_3)}{S}; \quad \mu_z=\frac{m_2(m_1+m_3)}{S}; \quad \mu_{qz}=\frac{m_1m_2}{S}$$

and $S=m_1+m_2+m_3$, the total mass of the molecule. The potential energy is subject to the geometric symmetry of the molecule. It may be written $V=\frac{1}{2}(k_{11}q^2+k_{22}r^2+2k_{13}qz+k_{33}z^2)$. The secular determinant of the normal coordinate transformation factors into a linear and a quadratic expression, and yields the following set of equations,

$$\lambda_1+\lambda_3=\frac{\mu_qk_{33}+\mu_zk_{11}-2\mu_{qz}k_{13}}{\mu_q\mu_z-\mu_{qz}^2},$$

$$\lambda_1\lambda_3=\frac{k_{11}k_{33}-k_{13}^2}{\mu_q\mu_z-\mu_{qz}^2},$$

$$\lambda_2=k_{22}/\mu_r.$$

In normal coordinates the kinetic and potential energies assume the forms

$$T=\tfrac{1}{2}(\dot{Q}^2+\dot{R}^2+\dot{Z}^2), \quad V=\tfrac{1}{2}(\lambda_1Q^2+\lambda_2R^2+\lambda_3Z^2).$$

The normal vibrations expressed in wave numbers are $\nu_i=(1/2\pi c)(\lambda_i)^{\frac{1}{2}}$. The constant k_{22} may be computed from ω_2 of HCN and DCN and is nearly the same for both as would be expected. Using the fundamentals ω_1 and ω_3 of HCN and the fundamental ω_3' of DCN the unobserved fundamental ω_1' of DCN can be calculated as well as the other three constants k_{11}, k_{13} and k_{33}. There are two sets of constants because the equations are quadratic. These are

$k_{22}=0.8071\times10^5$		$k_{22}=0.8071\times10^5$		dynes/cm
$k_{11}=5.6987$ "		$k_{11}=5.6981$ "		
$k_{13}=6.443$ "	Or	$k_{13}=-0.30491$ "		
$k_{33}=25.34$ "		$k_{33}=18.065$ "		

k_{13} represents the interaction between the extreme atoms, and should be small. Hence the second set is the more plausible.

The observed and calculated values of the wave numbers for the fundamental bands of HCN and DCN are as follows:

Observed wave numbers	*Calculated wave numbers*
$\omega_1=2089.0$ cm^{-1}	$\omega_1=2089.6$ cm^{-1}
$\omega_2=712.1$	$\omega_2=712.8$
$\omega_3=3312.9$	$\omega_3=3312.3$
$\omega_1'=$ —	$\omega_1'=1896.7$
$\omega_2'=569.1$	$\omega_2'=568.6$
$\omega_3'=2630.0$	$\omega_3'=2629.5.$

SEPTEMBER 15, 1935 PHYSICAL REVIEW VOLUME 48

Absorption Spectrum of Tin Sulphide

E. N. SHAWHAN, *Mendenhall Laboratory of Physics, Ohio State University*

(Received July 8, 1935)

The absorption spectrum of tin sulphide between 3200A and 4600A has been photographed at moderate dispersion and between 4000A and 4600A at high dispersion. The system in the near ultraviolet may be represented by the formula:

$$\nu=28{,}336.2+332.77(v'+\tfrac{1}{2})-1.42(v'+\tfrac{1}{2})^2-488.25(v''+\tfrac{1}{2})+1.47(v''+\tfrac{1}{2})^2.$$

This formula is not in agreement with that given by Butkow and Tschassowenny who seem to have incorrectly assigned the system origin. A new system has been located in the visible which is limited by predissociation to two v'' progressions. These bands are given by the formula:

$$\nu=23{,}287.67+367.5(v'+\tfrac{1}{2})-488.25(v''+\tfrac{1}{2})+1.47(v''+\tfrac{1}{2})^2.$$

The observed isotope structure of the strong bands in this system confirms their vibrational assignment.

Introduction

OUR knowledge of the band spectra of the metallic sulphides seems quite meager when compared with the information available on the spectra of the oxides of the metals. This is perhaps in part due to the difficulties involved in obtaining spectra of sulphides in emission. Some progress has been made in several cases where it is possible to obtain absorption spectra. Wilhelm[1] has reported the spectrum of MgS and given its vibrational analysis. The absorption spectra of ZnS, CdS and HgS have been studied by Sen-Gupta.[2] He observed only regions of continuous absorption, which indicates that the potential curves of the excited states of these molecules either have shallow minima or none at all. Shapiro, Gibbs and Laubengayer[3] made a vibrational analysis of the absorption spectrum of GeS and identified heads due to four isotopes of germanium. Rochester and Howell[4] have given a rather complete vibrational analysis of the extensive absorption spectrum of PbS and indicate that the rotational analysis is in progress.

A short report on the vibrational analysis of the band spectrum of SnS in absorption has been published by Butkow and Tschassowenny.[5] They report only two band systems, one lying between 2580 and 3164A and the other between 3277 and 3799A. They give the band-head formula in each case without recording data on the bands observed. One would expect the spectrum of SnS to resemble that of PbS. The fact that the spectrum of PbS extends into the near infrared and includes at least five systems suggested that a further critical examination of the spectrum of SnS might reveal other systems lying farther toward the visible.

Experimental

Chemically pure tin sulphide (SnS) contained in a graphite tube about 50 cm long and 2 cm in internal diameter, open to the air at the ends, was heated by means of a Hoskins carbon resistance furnace operated at 25 volts a.c. and about 300 amperes. The temperature was varied between 800 and 1100°C. A five-hundred watt projection lamp provided a source of continuous radiation which was passed through the tin-sulphide vapor and then focused on the slit of the spectrograph.

The spectrum between 3200A and 4000A was photographed on an E-1 quartz spectrograph giving a dispersion of 6 to 12A/mm over this range. The times of exposure with this spectrograph ranged up to a half-hour. A Littrow mounted concave grating with a radius of curvature of ten feet, giving a dispersion of 5.6A/mm in the first order was used to photograph the region between 3400A and 4650A. In order properly to develop the bands near the red end of the spectrum it was necessary to increase the vapor pressure until the light on the slit appeared distinctly yellow. At a somewhat lower temperature the violet end of the spectrum could be photographed in about an hour.

For still higher dispersion between 4000A and 4650A this portion of the spectrum was photographed in the first order of a 21-ft. concave grating in a Paschen-Runge mount. This grating is ruled with 30,000 lines to the inch and gives a dispersion of 1.25A/mm in the first order. The SnS was introduced into an iron tube approximately 80 cm long and 1 cm in internal diameter. This tube was heated to about 1000°C in two nichrome-wound Hoskins furnaces placed end to end. As in the previous case a five-hundred watt projection lamp provided the continuous radiation which was passed through the iron tube containing the SnS vapor.

Results

Two band systems were observed, one in the ultraviolet extending from about 3250A to 4300A, and the other in the visible between approximately 4200A and 4600A. The system in the near ultraviolet probably includes the bands observed in this region by Butkow and Tschassowenny.[5] Their near ultraviolet system extended as far toward shorter wave-lengths but not as far to the red. The system in the visible does not seem to have been previously reported. It is confined to a few fairly strong bands degraded to the red as are all other bands in the spectrum.

[1] H. A. Wilhelm, Iowa State Coll. J. Sci. **6**, 475 (1932).
[2] P. K. Sen-Gupta, Proc. Roy. Soc. **A143**, 438 (1934).
[3] C. V. Shapiro, R. C. Gibbs and A. W. Laubengayer, Phys. Rev. **40**, 354 (1932).
[4] G. D. Rochester and H. G. Howell, Proc. Roy. Soc. **A148**, 157 (1935).
[5] K. Butkow and W. Tschassowenny, Zeits. f. Physik **90**, 53 (1934).

The rotational structure of the stronger bands is resolved on the high dispersion plates.

A number of weak heads, scattered through the portion of the spectrum explored, were measured but could not be classified. Those falling in the region photographed on the 21-ft. grating were examined on the high dispersion plates. Most of them were found to be due to the accidental grouping of rotation lines occurring in the complex structure resulting from the overlapping of bands corresponding to the numerous isotopes of tin. The few unclassified heads that cannot be accounted for in this manner may belong to fragmentary systems. A number of unclassified heads[6] have also been observed in the spectrum of SnO.

Near ultraviolet system

Table I gives the wave numbers of the heads in the near ultraviolet system, together with their estimated intensities, the values of v' and v'' and the departures of the observed wave numbers from those calculated from the formula:

$$\nu = 28{,}336.2 + 332.77(v'+\tfrac{1}{2}) - 1.42(v'+\tfrac{1}{2})^2 - 488.25(v''+\tfrac{1}{2}) + 1.47(v''+\tfrac{1}{2})^2.$$

At a temperature of about 1000°C this system is characterized by strong v' and v'' progressions which allow the values of v' and v'' to be assigned with confidence. At lower temperatures the bands corresponding to the higher v'' values are noticeably weaker. Higher temperatures failed to reveal additional bands.

TABLE I. *Bands observed in near ultraviolet system.*

I	v'	v''	$\nu_{obs.}$	$\nu_{obs.}-\nu_{calc.}$	I	v'	v''	$\nu_{obs.}$	$\nu_{obs.}-\nu_{calc.}$
0	1	10	23865.5	−2.1	2	4	3	27637.3	−0.3
2	1	9	24329.0	+2.5	10	0	1	27773.1	−0.1
0	3	10	24520.6	+1.6	4	3	3	27791.8	−0.9
0	2	9	24650.1	−2.5	1	5	4	27957.8	+1.6
0	1	8	24788.3	0.0	10	1	1	28102.9	−0.2
1	0	7	24923.6	+0.5	4	0	0	28259.1	+0.6
0	3	9	24975.2	−2.6	4	3	2	28271.4	−0.9
1	2	8	25115.2	−0.2	8	2	1	28430.2	0.0
3	1	7	25253.8	+0.8	0	10	6	28559.7	−2.5
1	4	9	25296.3	−2.9	8	1	0	28589.2	+0.8
5	0	6	25391.5	+0.8	6	4	2	28594.3	+0.8
6	1	6	25720.5	−0.2	1	3	1	28753.4	−1.1
7	0	5	25862.8	+0.5	7	2	0	28915.8	+0.3
4	1	5	26190.7	−0.6	1	4	1	29075.2	−0.7
8	0	4	26337.5	+0.6	6	3	0	29239.5	−0.3
3	3	6	26369.4	−2.6	2	5	1	29393.4	−1.0
1	2	5	26517.7	−0.7	1	10	4	29504.5	−1.8
0	5	7	26548.5	−2.8	5	4	0	29560.5	−0.7
10	0	3	26811.0	−0.1	2	9	3	29677.7	−0.8
3	3	5	26845.6	−1.5	5	6	1	29710.3	+0.1
4	2	4	26989.2	−1.5	1	8	2	29852.0	+1.3
0	1	3	27139.8	−1.5	5	5	0	29880.1	+0.3
1	4	5	27167.3	+2.7	3	7	1	30022.1	−1.0
10	0	2	27291.7	+0.9	1	9	2	30159.8	+1.8
2	3	4	27315.7	−0.5	3	6	0	30195.5	0.0
5	2	3	27468.5	+0.1	2	8	1	30332.8	−0.3
5	1	2	27621.0	+0.2	1	7	0	30508.2	−0.2

TABLE II. *Intensity distribution in near ultraviolet system.*

v' \ v''	0	1	2	3	4	5	6	7	8	9	10
0	4	10	10	10	8	7	5	1			
1	10	10	5	0		4	6	3	0	2	0
2	10	8		5	4	1			1	0	
3	10	1	4	4	2	3	3			0	0
4	8	1	6	2		1				1	
5	5	2			1			0			
6	3	5									
7	1	3									
8		2	1								
9			1	2							
10					1		0				

Watson and Loomis[7] found difficulty in measuring the heads of the bands in the far ultraviolet system of SnO because of the overlapping of bands corresponding to the five abundant and six less abundant isotopes of tin. The values of ρ for the various tin isotopes are larger for SnS than for SnO, but most of the bands in this system are so near the system origin that the heads corresponding to the several isotopes are nearly coincident and the observed heads are fairly sharp. Near the limits of the system the heads appear somewhat diffuse but the spreading is not sufficient to allow the individual isotope heads to be distinguished.

The intensity distribution of the bands in this system is shown in Table II. There is a rather open Condon parabola to be expected from the difference in the values of ω_e' and ω_e''. Inside this parabola, and separated from it by weaker bands, is another group of fairly strong bands. This effect[4] is quite marked in the A system of PbS.

Comparison with earlier work. Butkow and Tschassowenny[5] gave the following formula for the bands between 3277A and 3799A:

$$\nu = 30{,}280.5 + 315.6(v'+\tfrac{1}{2}) - 0.59(v'+\tfrac{1}{2})^2 - 484.5(v''+\tfrac{1}{2}) + 0.50(v''+\tfrac{1}{2})^2.$$

This formula accounts for only a few of the strong bands observed in this region of the spectrum during this investigation. It may be that the lower temperatures used by these investigators, 600 to 840°C, were not sufficient to develop properly the bands near the red end of

[6] F. C. Connelly, Proc. Phys. Soc. **45**, 780 (1933).

[7] F. W. Loomis and T. F. Watson, Phys. Rev. **45**, 805 (1934).

the system, leading to an incorrect assignment of the system origin, which necessarily gives an incorrect value for ω_e'. The (0,0) band of the formula as given by Butkow and Tschassowenny with origin at 30,280.5 becomes the (6,0) band of the system proposed here with ν_e as 28,336.2. Their formula fits only bands which may be assigned values of v' equal to or greater than 6 in our formula.

Butkow and Tschassowenny represented the bands between 2580A and 3164A by the formula:

$$\nu = 34{,}868.3 + 288.3(v'+\tfrac{1}{2}) - 1.255(v'+\tfrac{1}{2})^2 - 484.5(v''+\tfrac{1}{2}) + 0.50(v''+\tfrac{1}{2})^2.$$

At the temperatures used in this investigation SnS vapor is almost opaque to light in the far ultraviolet. No attempt was made to repeat their observations in this region.

Visible system

In the vicinity of 4300A there are three strong bands and six less intense, all degraded toward the red. These bands may be represented by the formula:

$$\nu = 23{,}287.67 + 367.5(v'+\tfrac{1}{2}) - 488.25(v''+\tfrac{1}{2}) + 1.47(v''+\tfrac{1}{2})^2.$$

The vibrational assignments of the bands, estimated intensities, and differences between the observed and calculated wave numbers are given in Table III. No bands have been observed which

TABLE III. *Bands in visible system.*

v' \ v''	0	1	2	3	4	5
0	(10) 23531.89 (+0.09)	(10) 23046.51 (+0.02)	(6) 22563.78 (−0.34)	(1) 22084.34 (−0.35)		
1	(10) 23899.34 (+0.04)		(2) 22931.78 (+0.16)	(4) 22452.38 (+0.19)	(1) 21976.65 (−0.05)	(0) 21501.87 (−0.28)

seem to correspond to values of v' higher than 1. In view of the fact that the (0,2) band is fairly strong, this can be explained only by supposing that the potential curve of the upper state of this system is crossed by a repulsive state just beyond $v'=1$. The conclusion that there is predissociation is supported by the fact that the rotational structure of the (1,0) band seems to terminate abruptly about 200 cm^{-1} from the head.

The vibrational assignments of the three strong bands are qualitatively confirmed by the observed isotope structure. The lines of the (0,0) band are sharp and single near the head, but become broader and appear to split into several partially resolved components at a considerable distance from the head. On the other hand, the lines of the (1,0) band are rather diffuse near the head but become sharper toward the tail of the band. The structure of the (0,1) band is quite complex. The displacements of the lines of any isotopic molecule from those of the most abundant molecule may be expressed by the approximation,

$$\nu^i - \nu = (\rho-1)\nu_v + 2(\rho-1)\nu_r.$$

The value of $x_e'\omega_e'$ is not known but it is certainly small and the system origin must be in the vicinity of 23,580 cm^{-1}. Hence ν_v and ν_r have opposite signs for the (1,0) band and the same signs for the (0,0) and (0,1) bands. The lines of all isotopes should coincide because of the cancelation of the rotational and vibrational displacements at about 160 cm^{-1} from the head of the (1,0) band. This cancellation does not occur in the (0,0) and (0,1) bands. The lines of the (0,0) band are fairly sharp because of its proximity to the system origin but become broader at increasing distances from the head due to the combined rotational and vibrational displacements.

The rotational analysis of the bands in this system is in progress and will be the subject of a later report.

Grateful acknowledgment is made to Professor Alpheus W. Smith and Dr. R. V. Zumstein for their many helpful suggestions.

Note added in proof: While this paper was in the press Rochester (Proc. Roy. Soc. **A150**, 668 (1935)) also reported on the band spectrum of stannous sulphide. He assigns the origin of the visible system at 23,211.8 cm^{-1} whereas our analysis indicated that it is at about 23,580 cm^{-1}. Our data on these band heads taken from the high dispersion spectrograms are inconsistent with his assignment.

A Mass Spectrum Analysis of the Products of Ionization by Electron Impact in Nitrogen, Acetylene, Nitric Oxide, Cyanogen and Carbon Monoxide

JOHN T. TATE, P. T. SMITH AND A. L. VAUGHAN, *Department of Physics, University of Minnesota*

(Received June 29, 1935)

A *mass spectrograph*, designed for the identification of the products of ionization and dissociation by electron impacts in molecular gases is described.

Ionization potential of nitrogen. A direct comparison in a nitrogen-argon mixture showed that the ionization potential of nitrogen is at least 0.04 volt less than that of argon. The ionization potential is therefore not greater than 15.65 volts, though it may be lower by as much as 0.1 volt.

Analysis of ionization and dissociation products in C_2H_2, NO, and C_2N_2. The ions formed by electron impacts in these gases together with their appearance potentials in volts are as follows:

Ion	$C_2H_2^+$	C_2H^+	C_2^+	CH^+	C^+	H^+	
App. pot.	11.2	17.8	23.8	22.2	24.5	21.7,	25.6
Est. error	±0.1	±0.2	±0.3	±0.5	±1.0	±1.0	±1.0

Ion	NO^+	N^+	NO^{++}
App. pot.	9.5	22.0	44
Est. error	±0.1	±0.5	±1.0

Ion	$C_2N_2^+$	C_2N^+	CN^+	C_2^+
App. pot.	14.1	19.8	21.3	18.6
Est. error	±0.1	±0.5	±0.3	±0.5

Negative O^- ions appear in NO as reported by Tate and Smith. An ion of mass 27 found in C_2H_2 is ascribed to $C^{12}C^{13}H_2$. The abundance ratio $C^{13} : C^{12}$ was calculated to be 1 : 100.

I. THE MASS SPECTROGRAPH

IN THE studies here to be described of the effects of electron impacts in various gases a mass spectrograph was used to identify the ionized products of the impacts.

The mass spectrograph which is shown diagrammatically in Figs. 1 and 2 is similar to that described by Bleakney.[1] Since many of the gases to be studied are dissociated at the hot filament it was necessary to shut off the filament, except for the first small diaphragm in the cylinder A, in a separate compartment provided with a separate pump. The scheme is shown in Fig. 1. Since the pressure is kept lower on the filament side of A than in the main tube the products of dissociation were kept from diffusing into the region where impact ionization and dissociation were being studied.

[1] W. Bleakney, Phys. Rev. **40**, 496 (1932).

A magnetic field of about 900 gauss parallel to the axis of the tube was provided by a large solenoid surrounding the tube and coaxial with it. This field served the double purpose of maintaining the electron beam from the filament in line and of providing the magnetic field for the analyzer.

Electrons from the tungsten filament F are accelerated by a constant drawing out potential between F and A. S_1 is at the same potential as A. A variable potential V_a is applied between the filament F and the slits S_2, S_3 and S_4 which are all at ground potential. The electrons with energy of approximately V_a electron-volts then enter the region between the plates P_1 and P_2 which form part of the analyzer shown in end section in Fig. 2. Here a few of them suffer impacts with the gas molecules but the majority go straight through to the electron trap which is, in

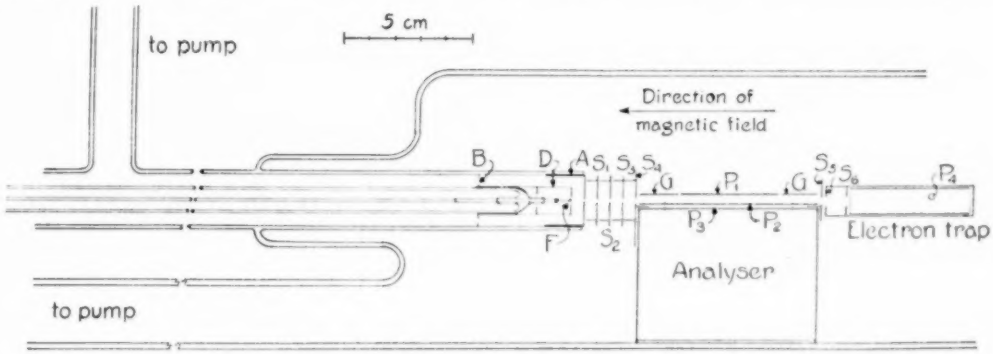

FIG. 1. Diagram of the apparatus as viewed from the side.

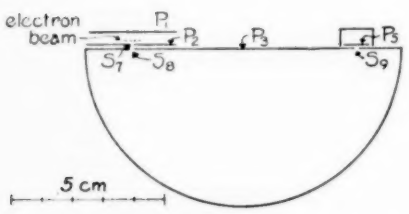

FIG. 2. Diagram as viewed from the end with electron gun removed. S_1, S_2, S_3 and S_4—1×6 mm; S_7—0.2×50 mm; S_8 and S_9—0.155×50 mm.

turn, connected with a galvanometer. The pressure of the gases to be studied is so low (10^{-4} to 10^{-6} mm Hg) that a very small fraction of the electrons experience single impacts, and multiple impacts are negligible.

The ions produced in the region between P_1 and P_2 are drawn downward by a small potential V_0 (about 2 volts) applied between P_1 and P_2. This potential is so applied that the space through which the electron beam passes is maintained at ground potential. There is a long slit in P_2 (Fig. 2) through which a narrow sheet of ions may pass. These are further accelerated by a variable potential V_1 between P_2 and P_3, are bent around in the magnetic field and pass through the slit S_9 to the collector P_5. The current to P_5 is measured with a Compton electrometer or vacuum tube amplifier. The resolving power of the analyzer (ratio of $\Delta(m/e)$ to (m/e) is about 1/40).

All of the metal parts of the spectrograph are of tantalum or tungsten with Pyrex insulation. The tube is mounted in an electric furnace which in turn is mounted in the center of a water-cooled solenoid.

The tube was evacuated and baked at a temperature of about 400°C, for many hours and the baking process was repeated at frequent intervals. The spectrograph itself forms a good ionization gauge. The residual pressure, before admitting the gas to be studied, was less than 10^{-7} mm Hg. The gases were admitted through a long capillary and allowed to flow continuously out through the pumps.

In making an m/e analysis of the ions their velocity was varied by varying V_1 in steps of 0.1 or 0.05 volt and the current to P_5 plotted as a function of V_1 (see Fig. 3, for example). When the appearance potential of a particular type of ion is to be determined V_1 is set for the collection of that ion and the electron velocity varied by varying V_a. The ion current is then plotted as a function of V_a. This type of curve is shown in Fig. 4.

II. Ionization Potential of Nitrogen

The precise value of the ionization potential of the nitrogen molecule has for several years been a matter of some concern both to those interested in electron collision phenomena and to band spectroscopists. Determinations of the threshold energies electrons must have in order that they be capable of producing ions in a gas are subject always to uncertainties introduced by the shape of the ionization curves near the threshold. These uncertainties have two causes: the first a lack of sharpness in the velocity distribution of the electrons themselves and the second a lack of knowledge about the actual probability-of-ionization as a function of velocity in the neighborhood of the threshold.

The first cause of uncertainty can be removed by an independent determination of the velocity distribution but the second is more refractory and is particularly troublesome in the case of molecules for which the sharpness of onset of ionization depends on the shapes of the potential-energy curves for the molecule and molecular ion and the relative positions of their minima with respect to internuclear separations. The result is that the estimate of ionization potential will depend on the sensitiveness of the measuring instruments and any value so obtained usually represents an upper limit.

The present determination of the ionization potential of nitrogen was made by using a mixture of nitrogen and argon in the mass spectrograph and by measuring simultaneously the number of N_2^+ and of A^+ ions collected for a number of electron energies near the threshold energy. The advantage of using argon as a calibrating gas is that its ionization potential differs from that of nitrogen by only about 0.1 volt yet the mass spectrograph permits a complete separation of the A^+ and N_2^+ ions and a determination of their relative abundance.

This method of estimating the ionization potential of nitrogen eliminates all uncertainty relative to contact potentials and velocity distribu-

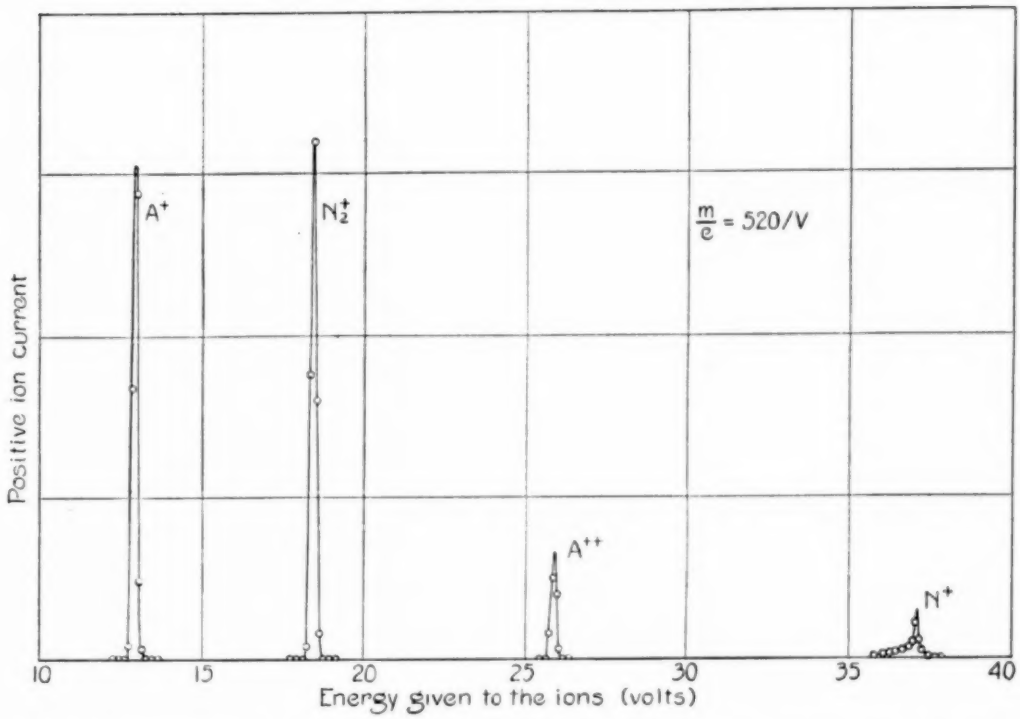

FIG. 3. Mass spectrum of the products of ionization in a mixture of argon and nitrogen. Electron energy $V_a = 100$ EV. $H = 900$ gauss.

tion of electrons. There remains only the uncertainty about the relative behavior of the ionization-probability curves for argon and nitrogen. It is probable that the onset of ionization in argon is somewhat sharper than in nitrogen.

The mass spectrum of an argon-nitrogen mixture is shown in Fig. 3. The heights of the A^+ and of the N_2^+ peaks are plotted against electron velocity in Fig. 4. It will be seen that the ionization potential of nitrogen is a little lower than that of argon. Twelve curves of the sort shown in Fig. 4 give for the difference in ionization potentials an average value of 0.04 volt. The mean deviation from this average was 0.04 volt. If we assume that the ionization-potential of argon is 15.69 volts, the apparent value for nitrogen is 15.65 volts. We believe that the true ionization potential is certainly not greater than this by more than 0.02 volt but may be less by perhaps 0.10 volt.

In Table I are given the values of previous measurements of the ionization potential of nitrogen. The fact that electron impact measurements lead to upper limits is indicated by the

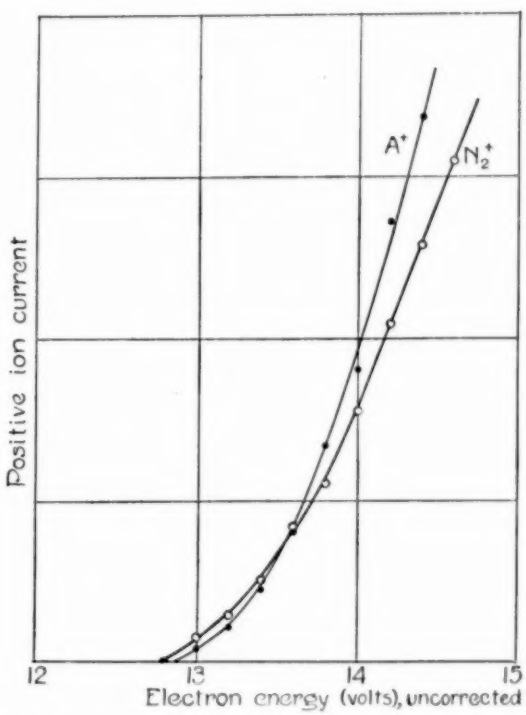

FIG. 4. Typical ionization curves showing positive ion current as a function of the electron energy (uncorrected).

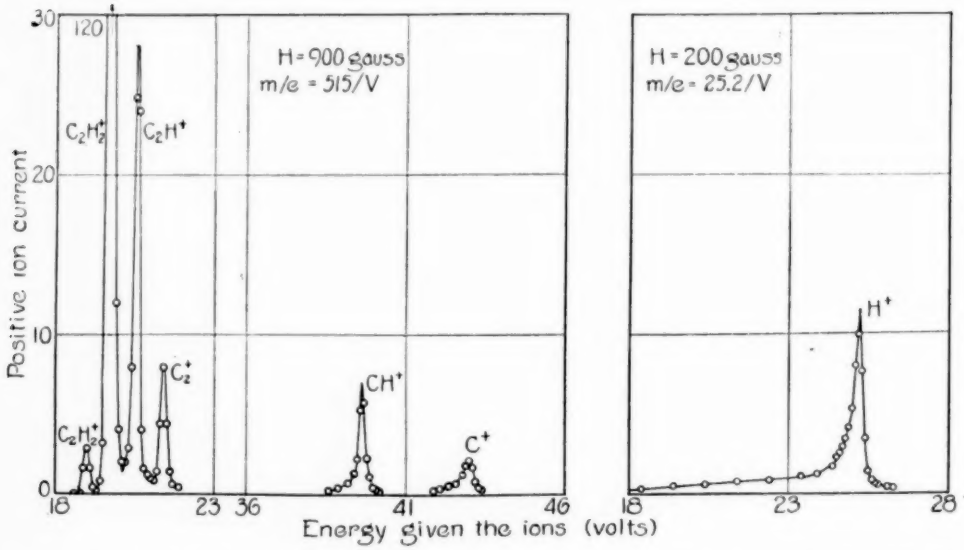

FIG. 5. Mass spectrum of the products of ionization in acetylene. Electron energy $V_a = 100$ EV.

way in which, as the experimental technique is refined the values given become lower and lower.

TABLE I. *Observed ionization potential for molecular nitrogen.*

I.P. (volts)	OBSERVER	REFERENCE
18	Davis and Goucher	Phys. Rev. **13**, 1 (1919)
18	Smyth	Phys. Rev. **14**, 409 (1919)
16.9	Mohler and Foote	Phys. Rev. **15**, 555 (1920)
17.2	Stead and Gosling	Phil. Mag. **40**, 413 (1920)
15.8	Found	Phys. Rev. **16**, 41 (1920)
16.95	Brandt	Zeits. f. Physik **8**, 32 (1921)
15.8	Boucher	Phys. Rev. **19**, 189 (1922)
16.2	Duffendack	Phys. Rev. **20**, 665 (1922)
16.3	Mackay	Phys. Rev. **24**, 319 (1924)
15.8	Turner and Samson	Phys. Rev. **34**, 747 (1929)
15.8	Vaughan	Phys. Rev. **38**, 1687 (1931)
15.7	Tate and Smith	Phys. Rev. **39**, 270 (1932)
15.65	Tate, Smith and Vaughan	This paper.

Recently Mulliken[2] concludes from Hopfield's[3] study of a Rydberg series of absorption bands that 15.51 volts is a minimum value for the ionization potential of nitrogen. We can therefore assert with some confidence that the ionization potential lies somewhere between 15.51 and 15.65 volts.

As a matter of general interest we looked for negative ions of nitrogen but found none at any velocity of impact.

[2] R. S. Mulliken, Phys. Rev. **46**, 144 (1934).
[3] J. J. Hopfield, Phys. Rev. **36**, 789 (1930).

III. PRODUCTS OF IONIZATION AND DISSOCIATION PRODUCED BY ELECTRON IMPACT IN ACETYLENE, NITRIC OXIDE, CYANOGEN AND CARBON MONOXIDE

A. Acetylene

The gas was prepared by repeated fractional distillation of the commercial product. The measurements were made with the acetylene at a pressure of about 10^{-5} mm Hg. The mass spectrum of the products of ionization and dissociation are shown in Fig. 5. Eisenhut and Conrad[4] found the same primary ions. The appearance potentials and estimated accuracy are obtained from curves of the type shown in Fig. 6 and are as follows:

Ion	$C_2H_2^+$	C_2H^+	C_2^+	CH^+	C^+		H^+
App. pot. (volts)	11.2	17.8	23.8	22.2	24.5	21.7	25.6
Est. error	±0.1	±0.2	±0.3	±0.5	±1.0	±1.0	±1.0

It will be noted that the peaks for the C^+, CH^+ and H^+ ions trail out to the left. This is due to the fact that in the dissociation process the ions pick up kinetic energy. The energy lost by the electron at impact is greater by several electron volts than the sum of the ionization potential and the heat of dissociation and the difference appears as kinetic energy of the dissociation products. This

[4] O. Eisenhut and R. Conrad, Zeits. f. Elektrochemie **36**, 654 (1930).

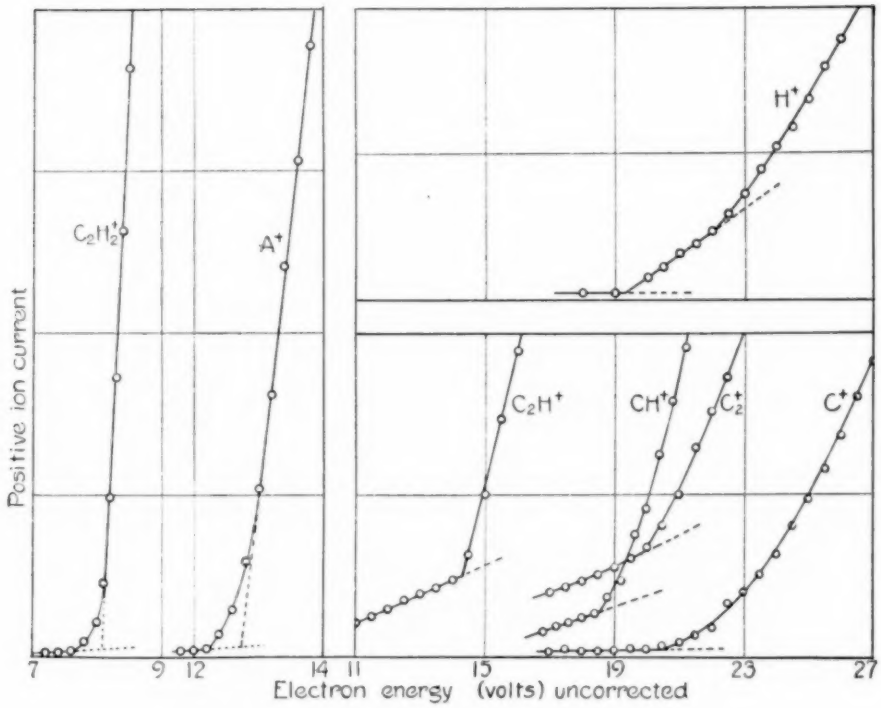

FIG. 6. Typical ionization potential curves in acetylene.

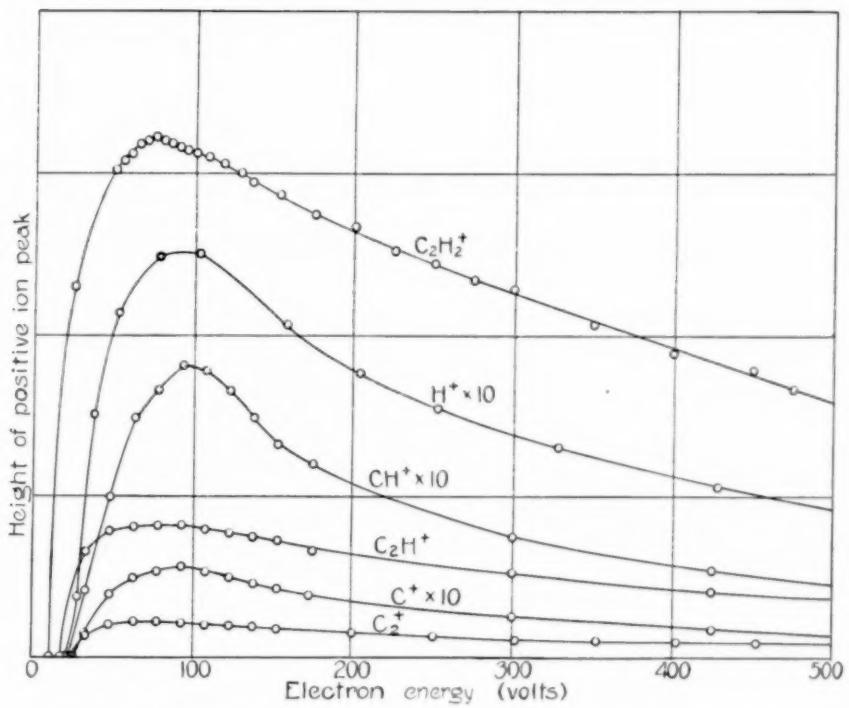

FIG. 7. Heights of ion peaks as a function of the electron energy in acetylene.

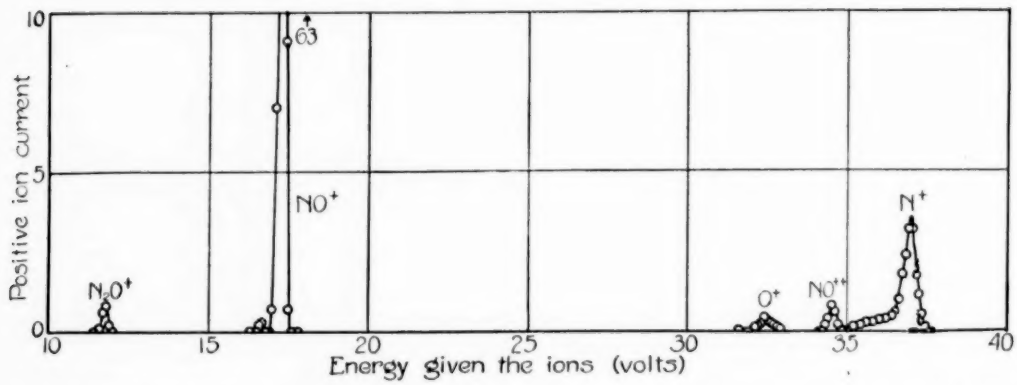

FIG. 8. Mass spectrum of the products of ionization in nitric oxide. Electron energy $V_a = 100$ EV.

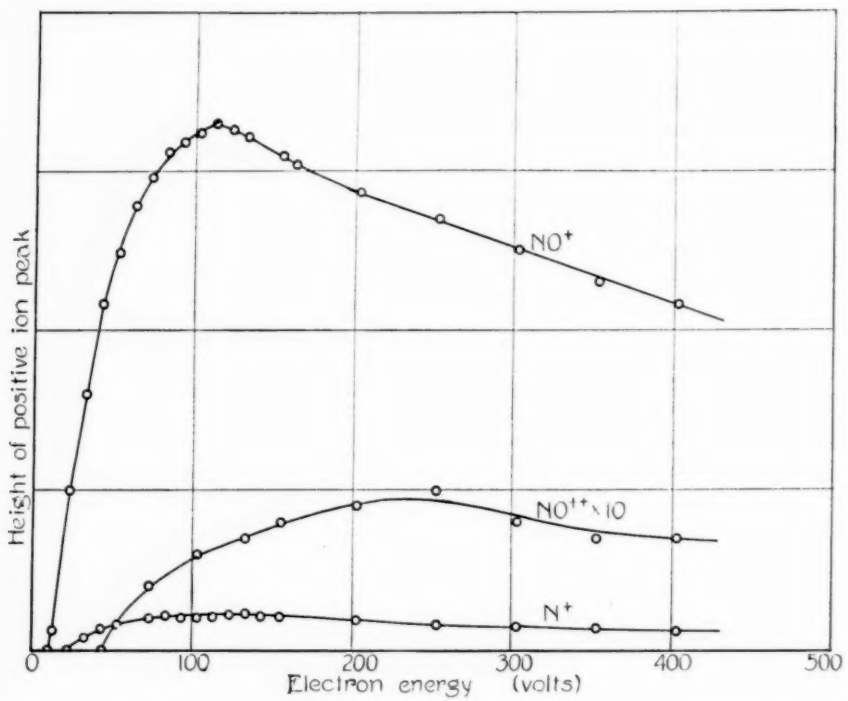

FIG. 9. Heights of the ion peaks as a function of the electron energy in nitric oxide.

effect will be the more marked the smaller the mass of the ion relative to the molecule. The C^+ and CH^+ ions have as much as 1.5 EV kinetic energy while the H^+ ion has up to 6 EV. Fig. 7 shows the heights of the various peaks (probability of formation) as functions of the electron energy in volts. No negative ions were observed.

There are two peaks labeled $C_2H_2^+$. The one on the left ($m/e = 27$) is presumably $(C^{12}C^{13}H_2)^+$. This ion appears at the same electron velocity as the ion of mass 26 and the relative heights of the two peaks remain the same as the electron velocity is varied. The relative abundance of C^{13} to C^{12} is approximately 1 part in 100. Jenkins and Ornstein[5] have reported a value of 1 part in 106. A more recent and refined determination[6] gives 1 part in 91.6. Aston[7] has found a ratio of 1 part in 140.

[5] F. A. Jenkins and S. S. Ornstein, Proc. Acad. Sci. Amsterdam **35**, 1212 (1932).
[6] A. L. Vaughan, J. H. Williams and J. T. Tate, Phys. Rev. **46**, 327 (1934).
[7] F. W. Aston, Proc. Roy. Soc. **A149**, 396 (1935).

B. Nitric oxide

The sample was prepared by the action of HNO_3 on Cu. The NO was passed through water to remove any NO_2, dried over solid NaOH, collected over liquid air, and purified by repeated fractional distillation. After all these precautions there still remained approximately one percent of N_2O as determined by the mass spectrograph. Fig. 8 shows the mass spectrum. Fig. 9 is the height of the peaks plotted as a function of the electron energy in volts. The negative ions found by Tate and Smith[8] showed up strongly and were identified as O^- ions. The results are given in the following table.

Ion	NO^+	N^+	NO^{++}
App. pot. (volts)	9.5	22.0	44
Error (volts)	±0.1	±0.5	±0.1

A very faint trace of O^+ ions appeared at 21 volts. The ionization potential of NO is taken as 9.5 volts from the work of Tate and Smith[8] and this value was used to calibrate the scale.

In Fig. 8 there is an ion having an m/e value of 31. This peak seems to bear a constant relation to the NO^+ peak of about 1/2 to 1/3 percent independent of electron velocity and is probably due to the N^{15} isotope. A more careful study[6] of this has given a ratio of N^{14}/N^{15} of 265.

C. Cyanogen

The sample of C_2N_2 was obtained from the Department of Chemistry. The results may be compared to those of Dorsch and Kallman.[9]

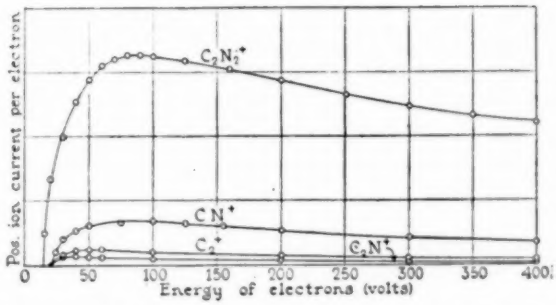

FIG. 10. Heights of the ion peaks as a function of the electron energy in cyanogen.

Ion		$C_2N_2^+$	CN^+	C_2^+	C^+	C_2N^+
App. pot. (volts)	Authors	14.1	21.3	18.6		19.8
	Dorsch and Kallman	13.5	18	17	22.5	

Fig. 10 shows the heights of the peaks as a function of the electron velocity in volts. C^+ and N^+ peaks were found, but their origin was uncertain since the sample of cyanogen contained small amounts of CO and N_2 as impurities.

D. Carbon monoxide

The work on carbon monoxide agrees with that published by Vaughan.[10] The O^+ ion which was masked by H_2O^+ in that work appears here but is very small. It appears at 27±1 volts and is only about 10 percent as plentiful as the C^+ ion at 100 volts electron velocity.

The authors are very grateful to C. H. Dane, E. F. Greinke and William B. Haliday for their help and cooperation. The senior author wishes to express his appreciation to the Graduate School of the University for a grant from the Fluid Research Funds.

[8] J. T. Tate and P. T. Smith, Phys. Rev. **39**, 270 (1932).
[9] K. E. Dorsch and H. Kallman, Zeits. f. Physik **60**, 376 (1930).
[10] A. L. Vaughan, Phys. Rev. **38**, 1687 (1931).

Effect of a Magnetic Field Upon the Polarization of Impact Radiation

W. H. McCorkle,* *Physical Laboratory, University of Iowa*

(Received July 8, 1935)

Sodium D line radiation excited by electrons moving parallel to a magnetic field of 300 gauss or more shows about 16 percent polarization, the major electric vibration being parallel to the direction of the exciting electron beam. In fields below 300 gauss the polarization is less, decreasing to zero in the absence of a field. That the polarization changes in a magnetic field must be due to the fact that the $3^2P_{3/2}$ level is a hyperfine multiplet which undergoes a Paschen-Back effect.

Introduction

IN most cases the application of the principle of conservation of angular momentum to the excitation of radiation by electron impact leads to results which are at least in qualitative agreement with experiment. The failure of sodium D line impact radiation to show polarization[1, 2] might be due to exchange, operating in such a way that the upper magnetic levels are always equally populated. However, it may be doubted that the probability of exchange should vary with velocity in such a way that this should be true over a considerable velocity range. Another possible explanation of the low polarization is that it results from the hyperfine structure of the levels involved. It is known that this is responsible for greatly lowering[3] the polarization of resonance radiation. Any effect of the hyperfine structure should however, disappear for the impact radiation just as for the resonance radiation[4] in a magnetic field strong enough to produce a complete Paschen-Back effect of the upper hyperfine multiplet.

With this in mind the writer has looked for polarization in the D line impact radiation excited in a magnetic field parallel to the direction of motion of the exciting electrons.

Apparatus and Procedure

The impact radiation was excited in a tube 2 cm in diameter which had on one side a window blown and flattened and on the opposite side a light trap in the form of a horn. A cylinder of sheet molybdenum with two rectangular apertures was inserted in the tube so that the apertures came opposite the window and light trap, respectively. The molybdenum cylinder contained the electron gun, which consisted of an oxide-coated platinum filament placed about 2 mm from a pair of 3-mm diaphragms arranged to project the electron beam into the space between the window and the light trap. The molybdenum cylinder and diaphragms were placed at the same electrical potential with the idea of providing a field-free space into which the electron beam should be projected. However at low electron velocities the potential difference due to space charge became troublesome, and in order to compensate this to some extent a third independent electrode was introduced, see Fig. 1. The entire electron gun except the filament was constructed of sheet molybdenum and arranged as shown in Fig. 1.

The oxide coating of strontium, barium and calcium oxides was applied by the method

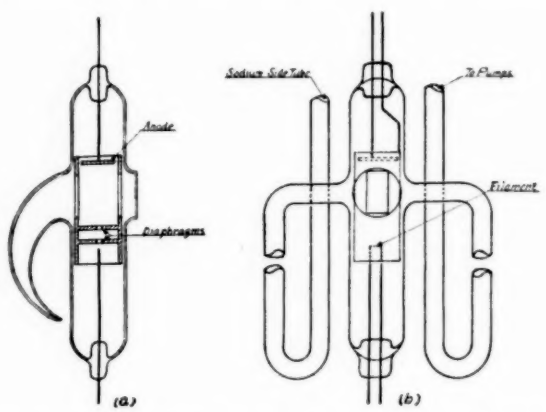

FIG. 1. Tube used for the excitation of impact radiation. (a) Sectional side view of tube. (b) Front view of tube.

* Now at Agricultural and Mechanical College, College Station, Texas.

[1] Kossel and Gerthsen, Ann. d. Physik **77**, 273 (1925).
[2] Ellett, Foote and Mohler, Phys. Rev. **27**, 31 (1926).
[3] A. Ellett, Phys. Rev. **35**, 588 (1930).
[4] L. Larrick, Phys. Rev. **46**, 581 (1934).

described by Arnold.[5] The filament used would yield a maximum current of 1 to 1.5 milliamperes in the electron beam with the accelerating potentials employed.

The heating chamber which was an asbestos cylinder painted on the inside with lampblack and shellac having a rectangular opening in one side to permit observation of the radiation excited by the electron impacts, extended to a gas burner 3 feet below. A water-cooled Helmholtz coil of copper tubing placed with its axis vertical and coincident with the direction given by a line drawn through the center of the filament and the defining diaphragms surrounded the heating chamber and provided the variable magnetic field to which the impact radiation was subjected. The entire assembly was mounted within a large Helmholtz coil adjusted to neutralize the earth's magnetic field.

The sodium which had been distilled in a vacuum and collected in small glass tubes was placed in one of the side tubes of the observation chamber and when the system had been sufficiently evacuated was redistilled into the observation chamber until a light coat of pure metallic sodium became deposited on the top and sides of the main tube.

A "sticking" vacuum, as indicated by the McLeod gauge, was maintained by means of a Cenco Hyvac and a mercury diffusion pump.

With the heating chamber adjusted for any desired temperature, observations were made of the impact radiation. The observations were made perpendicular to the electron beam and magnetic field, first, visually by means of a quartz wedge[6] and Ahrens prism, and later, photographically by the same method, and also photographically by the Cornu method employing a Wollaston double image prism and an Ahrens prism. The position of the Ahrens prism which gave equal intensity of the two images was determined by microphotometer measurements of the two images obtained for various settings of the prism. The angular position of the Ahrens prism was read from a vernier scale arranged to read to tenths of a degree of arc.

[5] H. D. Arnold, Phys. Rev. **16**, 70 (1920).
[6] R. W. Wood, *Physical Optics*, third edition, pp. 339–340.

Results

From the work of Larrick[4] it is known that a magnetic field of 300 gauss is sufficient to complete the Paschen-Back effect of the hyperfine structure for the sodium $3^2P_{3/2}$ hyperfine multiplet and produce the maximum polarization of resonance radiation. Hence observations of the impact radiation of sodium were first made in a magnetic field of 300 gauss. Preliminary observations showed that below sodium vapor pressures of 2×10^{-7} mm of Hg, absorption and secondary resonance radiation did not influence the polarization of the impact radiation.

When the electrons in the incident beam had very nearly the critical velocity corresponding to the excitation potential the polarization of the impact radiation was found to increase with the applied magnetic field to a value slightly above 16 percent, with the maximum polarization approximately realized at 200 gauss and remaining nearly constant for higher fields as Fig. 2 shows.

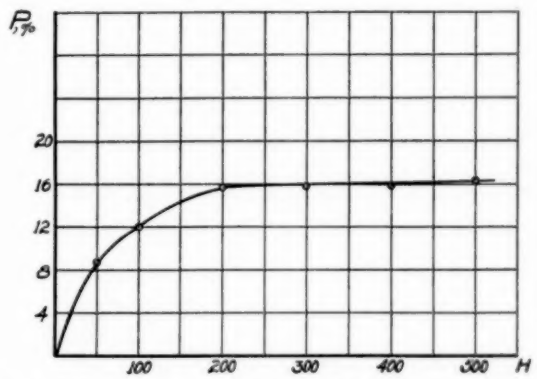

FIG. 2. Polarization *vs.* magnetic field for electrons having energy within one volt of the resonance potential.

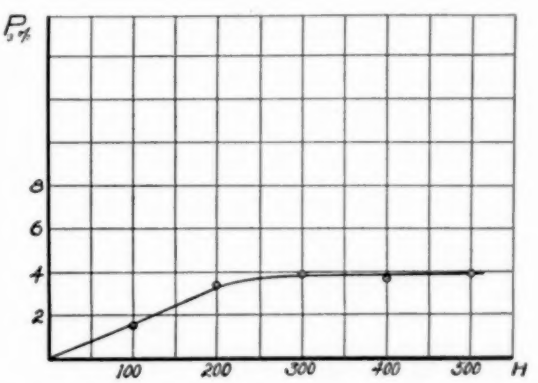

FIG. 3. Polarization *vs.* magnetic field for electrons with energy 3–5 volts above the ionization potential.

As one might expect the speed of the incident electron was an important factor in determining the magnitude of the polarization. The speed of the incident electron was controlled by the applied accelerating potential and the space charge effect in the electron beam. For accelerating potentials in excess of the ionization potential the space charge disappeared and there was a decrease of the polarization for all magnetic fields as indicated by Fig. 3. If the accelerating potential and electron current were fixed to give the space charge effect for higher fields but not adjusted for the lower fields there was a decrease of the value of the lower field polarization caused by the change of space charge with magnetic field. This is shown by comparison of Fig. 4 and Fig. 2.

At a temperature of 130°C the impact radiation was apparently limited to a well-defined beam, while at higher temperatures a nebulous glow of secondary radiation could be seen to surround this beam. Observations made by means of the quartz wedge and Ahrens prism above 130°C showed polarization of the secondary radiation as may be seen in Fig. 5. Observations of the main beam by this method failed to show definite evidence of polarization either in the field of 300 gauss or in the absence of a magnetic field. However, when the Cornu method was employed at a somewhat lower temperature, polarization of the impact radiation was clearly indicated. The degree of polarization was still very small even in the field of 300 gauss. It was observed, however, that when large electron currents were used there occurred a break in the beam of impact radiation (see Fig. 6) and at the same time the polarization increased.

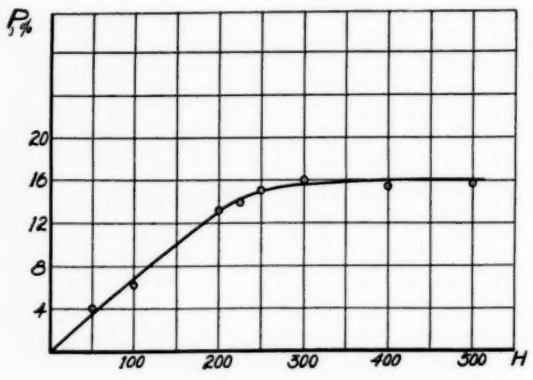

FIG. 4. Polarization vs. magnetic field showing decrease of low field polarization due to modification of the space charge by the magnetic field.

FIG. 5. Photograph of impact radiation using a quartz wedge and Ahrens prism. (a) Fringe system with slightly convergent light incident on the quartz wedge, with the sodium vapor at 160°C in a magnetic field of 400 gauss. (b) Fringe system in secondary radiation when the image of the main beam coincides with the plane of the wedge and the sodium vapor is at 150°C in a magnetic field of 400 gauss. (c) Same as (b) above with the sodium vapor at 130°C.

FIG. 6. Beam of radiation excited by electron impact. (a) Effect of space charge in the electron beam. (b) Space charge removed by higher accelerating potential.

For magnetic fields of various intensities with the sodium vapor at 110°C it was found that the polarization in any given field was a maximum when the space charge in the electron beam was sufficient to render a portion of the beam nonluminous. The radiation excited by the electrons on either side of the nonluminous portion of the beam is attributed to electrons with energy close to the resonance potential, since in the nonluminous part of the beam their energy must be insufficient to produce excitation. To verify this the polarization of the impact radiation was determined in magnetic fields of 400 and 500 gauss for accelerating potentials less than one volt above the resonance potential. The same strong field polarization was observed under these conditions. The exposure time required for a picture used in the microphotometer measurements was however increased from a few minutes to 8 or 9 hours with this adjustment of accelerating potential and necessarily smaller electron current, consequently the observations with the low accelerating potential were not applied to other points of the curves.

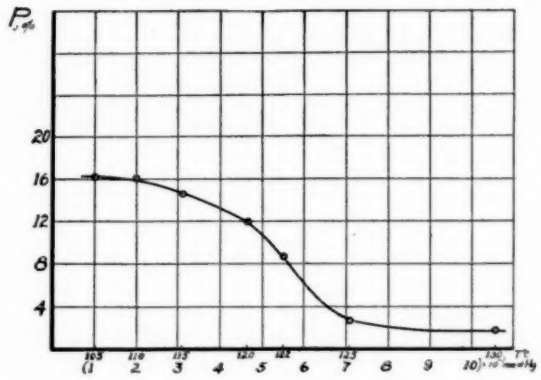

FIG. 7. Polarization *vs.* vapor pressure for sodium vapor in a magnetic field of 300 gauss.

From consideration of the principle of conservation of angular momentum the polarization should be expected to be greatest when the energy of the exciting electron is equal to or just exceeds that necessary for excitation. This is confirmed by the above observations of increased polarization in the region where the electron beam was retarded by space charge. The effect of the space charge on the electron beam was decreased by increasing the vapor pressure of the sodium since more ionizing collisions occurred. In addition to the decrease of space charge with increase of vapor pressure there was an increase of the depolarizing effect of the secondary radiation. The result of these combined effects caused the polarization to decrease from about 16 percent at 105–110°C to nearly zero at 130°C as shown by Fig. 7.

DISCUSSION

It is evident that measurements of the polarization of the radiation excited by electron impact on sodium vapor in a magnetic field must be made below 130°C to escape the effect of the polarized secondary radiation. There is a depolarizing effect due to the secondary radiation appreciable at temperatures as low as 115°C but the effect is exaggerated by Fig. 7 which must be to a considerable extent characteristic of the apparatus, since space charge is affected by the vapor pressure of the sodium due to increase in the number of positive ions with increase of vapor pressure.

There is qualitative agreement between the polarization of impact radiation from sodium observed perpendicular to the applied magnetic field and electron stream, and the polarization of the resonance radiation excited by the sodium D lines polarized with $E||H$. The separation of the hyperfine levels appears to be completed at about the same value of the magnetic field for the impact radiation as for the resonance radiation with $E||H$ but the value of the polarization reaches a maximum of only 16 percent for the impact radiation compared with about 50 percent for the resonance radiation.

If the electron beam consisted only of electrons having energy equal to the resonance potential and moving accurately parallel to the magnetic field, it would seem upon the basis of a simple theory that no angular momentum parallel to the magnetic field could be imparted to the excited sodium atom. The excited atom should then be raised to the same state as when excited by light polarized with its electric vector parallel to the magnetic field. That is, in strong fields only the $M_j = \pm\frac{1}{2}$ levels of the $3^2P_{3/2}$ state should be populated, and the light emitted by the transitions from the $3^2P_{3/2}$ should be 60 percent polarized. The polarization observed should be less than this because of unpolarized emission from $3^2P_{\frac{1}{2}}$, but probably not less than 33 percent, corresponding to equal excitation of the $M_j = \pm\frac{1}{2}$ levels of $^2P_{3/2}$ and $^2P_{\frac{1}{2}}$.

The low (16 percent) strong field polarization observed shows that the $M_j = \pm 3/2$ levels of $^2P_{3/2}$ are excited, and this requires the communication of angular momentum parallel to the magnetic field. The writer was not able to work with accelerating potentials less than one-half volt above the excitation potential, for as the excitation potential is approached more closely the intensity drops to so low a value that polarization measurements are not feasible.

In conclusion the author wishes to take this opportunity to thank Professor A. Ellett for his assistance and suggestions during the course of this research.

Atomic Energy States for Excited Helium

WM. S. WILSON, *Sterling Chemistry Laboratory, Yale University*

(Received July 8, 1935)

By means of Slater's method the total atomic energies for the excited states, $1s^2$, $1s2s$, $1s2p$, $2s^2$, $2s2p$ and $2p^2$ of helium have been calculated with the use of Hartree functions previously published.

INTRODUCTION

SLATER'S method[1] of calculating total atomic energies has been applied to several atoms.[2] The success of these calculations suggested the desirability of determining theoretically the more important term values of the unobserved states of doubly excited helium, by using the results of self-consistent field calculations previously published.[3] The results are compared with experimental data as far as possible.

METHOD OF CALCULATIONS

The method used in the present calculations was to consider the two-electron problem as a special case of the n-electron problem described by Slater, the procedure being similar to that used by Hartree and Black. Since no essentially new features were developed for this work, any description of the method will be omitted because the method is amply described in the two references given. However, there is one point to be noted; that is, if we omit the Hartree energy parameter from the definition of $I(\alpha)$ as given by Hartree and Black, we can at once write the equality:

$$I(\alpha)=I(\beta)=F_0(\alpha\beta)=F_0(\beta\alpha)$$

for those states of two electron atoms or ions for which the Hartree functions are already orthogonal. In the present work this equality was used to check the numerical work by calculating a given quantity in two essentially different ways. Should the Hartree functions be changed by orthogonalization, it is necessary to use the method of treatment given by Hartree and Black. This was here necessary only for the $(1s)\ (2s)\ ^3S$ level.

In the actual calculations the full five place figures used in the Hartree calculations as well as the values at the intervals omitted in the tabulation of references were used. These extra intervals enabled all integrals to be evaluated conveniently by direct quadratures rather than with the more elaborate method described by Macdougall for large k. The energy values were obtained from the integrals by using Eq. (8) of Hartree and Black in the manner outlined by Slater in the latter part of his article.

RESULTS AND DISCUSSION

The results of these calculations are presented in Tables I and II. Table I gives the mean values of the various Slater integrals, Table II the energy values obtained from these, together with experimental values and the results of other computations where such are available. The fourth column of this table gives the values obtained if the smaller Hartree energy parameter is *assumed* to be equal to the first ionization potential of that state. The agreement of the calculated energy values with the experimental ones where such are available is satisfactory, there being a maximum deviation of 1.5 percent for $(1s)^2\ ^1S$ and a much smaller deviation for other levels. The agreement with calculations is very good, save for ^1S states. An exception to this last statement is the discrepancy of the $(2p)^2\ ^3P$ level when com-

TABLE I. *The Slater functions for the several excited states* (in units Rhc where $R=109{,}737$).

CONFIGURATION	ELECTRON	ϵ	$I(n,l)=I(n'l')=F_0(nl,n'l')$	$G(nl.\ n'l')$
$(1s)^2$	$1s$	1.836	2.051	
$(2s)^2$	$2s$	0.4606	0.5189	
$(1s)(2s)'S$	$1s$ $2s$	3.469 0.3068	0.5317	$G_0=0.0740$
$(1s)(2s)^3S$	$1s$	3.469	$I(1s)=0.5317$ $I(2s)=0.4911$ $F_0(1s2s)=0.4764$	$G_0=\ .0123$
	$2s$	0.3068		
$(1s)(2p)$	$1s$ $2p$	3.496 0.2522	0.5070	$G_1=\ .0261$
$(2s)(2p)$	$2s$ $2p$	0.4195 0.4443	0.5403	$G_1=\ .2942$
$(2p)^2$	$2p$	0.3861	0.5761 $F_2(2p,2p)=0.2675$	Same as $F_2(2p,2p)$
$Be^{++}(1s)^2$	$1s$	11.344	4.558	

[1] J. C. Slater, Phys. Rev. **34**, 1293 (1929).

[2] See, for example, D. R. Hartree and M. M. Black, Proc. Roy. Soc. **A139**, 311 (1933); J. Macdougall, ibid. **A138**, 550 (1932).

[3] W. S. Wilson and R. B. Lindsay, Phys. Rev. **47**, 681 (1935).

TABLE II. *The atomic energies* (units Rhc).

CONFIGURATION	MULTIPLET	ENERGY	HARTREE	EXPERIMENTAL[1]	OTHER METHODS
$(1s)^2$	^1S	−5.723	−5.836	−5.807	−5.809[2]
$(2s)^2$	^1S	−1.4400	−1.4605		−1.49[4]
$(1s)(2s)$	^1S	−4.232	−4.3062	−4.2919	−4.290[2] −4.289[3]
	^3S	−4.334		−4.3499	−4.334[5]
$(1s)(2p)$	^1P	−4.246+	−4.2517	−4.2473	−4.245[5]
	^3P	−4.264		−4.2660	−4.262[5]
$(2s)(2p)$	^1P	−1.3060	−1.4194		−1.301[4] −1.308[6]
	^3P	−1.5022			−1.498[4] −1.504[6]
$(2p)^2$	^3P	−1.4018	−1.3860		−1.662[6]
	^1D	−1.3376			−1.320[6]
	^1S	−1.2323			
$Be^{++}(1s)^2$	^1S	−27.246	−27.344	−27.312	−27.308[7]

[1] Bacher and Goudsmit, *Atomic Energy States*.
[2] E. A. Hylleraas, Zeits. f. Physik **65**, 209 (1930).
[3] J. P. Vinti, Phys. Rev. **37**, 448 (1931).
[4] F. G. Fender and J. P. Vinti, Phys. Rev. **46**, 78 (1934).
[5] C. Eckart, Phys. Rev. **36**, 878 (1930).
[6] Ta-You Wu, Phys. Rev. **46**, 239 (1934).
[7] E. A. Hylleraas, Zeits. f. Physik **83**, 739 (1933).

pared with Wu's value. The value listed by him gives too large a multiplet separation.[4] Further as we will see later the present value is in line with some experimental predictions. The simple Hartree values in most cases gave very closely the center of gravity of the multiplet system as calculated by the Slater method for states having but two levels. The values for $Be^{++}(1s)^2\,{}^1S$[5] are included to show the trend for the more closely bound beryllium charge. The fractional error is smaller than for normal helium. Whether this is generally true for other levels of Be^{++} cannot be stated at present.

The assignment of the newly calculated levels to experimental results is restricted because of the lack of data. If we calculate transitions from singly to doubly excited states using the known experimental values for the singly excited states, we may note the following results. Wilson and Lindsay's assignment of the transition $(1s)^2\,{}^1S - (2s)^2\,{}^1S$ to the energy lost observed by Whiddington and Priestley seems to be further verified. It might be that the line is due to transitions from $1s^2\,{}^1S$ to both $(2s)^2\,{}^1S$ and $(2p)^2\,{}^3P$ which lie very close together. This would also explain the indications of structure observed.

[4] If we apply the rule that the $^3P - {}^1D$ separation is three halves the $^1D - {}^1S$ separation we find, using Wu's value for this separation, the ^1S level to lie at −0.777 Rhc, which indeed is unlikely since this is greater than the ionization potential of the ion $He^+(2p)$.

[5] Based on the wave function recently published by D. R. Hartree, Proc. Roy. Soc. **A149**, 210 (1935).

TABLE III. *Observed lines from the helium spectrum.*

LINE	PREVIOUS ASSIGNMENT	PRESENT PAPER
357.507[1]A	$(1s)(2s)\,{}^1S - (2s)^2\,{}^1S$[1]	none
322.517[1]	$(1s)(2p)\,{}^1P - (2p)^2\,{}^1D$[1]	none
321.186[1]	$(1s)(2p)\,{}^1P - (2p)^2\,{}^1S$[1]	none
320.392[1]	$(1s)(2s)\,{}^3S - (2p)^2\,{}^3P$[1] $(1s)(2s)\,{}^3S - (2s)(2p)\,{}^3P$[2]	$(1s)(2s)\,{}^3S - (2s)(2p)\,{}^3P$
309.04[2]	$(1s)(2p)\,{}^1P - (2s)(2p)\,{}^1P$[3]	$(1s)(2s)\,{}^3S - (2p)^2\,{}^3P$

[1] P. G. Kruger, Phys. Rev. **36**, 855 (1930).
[2] K. T. Compton and J. C. Boyce, J. Frank. Inst. **205**, 497 (1928).
[3] F. G. Fender and J. P. Vinti, Phys. Rev. **46**, 78 (1934).

The results of a study of the observed lines in the helium spectrum and their previous assignments are given in Table III. In this respect the results of these calculations verify those given by Fender and Vinti with the one exception noted. Calculation of transitions between the doubly excited levels fail to fit any of the corona lines discussed by Rosenthal.[6] The values thus calculated might, however, be in error by an amount which would mask any agreement and too definite conclusions cannot be drawn from these transitions between doubly excited states.

It is believed that the error in the doubly excited states is much less than that in some of the singly excited states. This belief is founded on the excellent agreement of calculations for higher atoms by other workers with observed values which involve $2s$ and $2p$ electrons, as well as the agreement with other calculations noted in Table II. Further, should it prove that the absolute errors in these levels remain essentially the same for all levels of higher two electron ions as it does for $Be^{++}\ (1s)^2\,{}^1S$, this would introduce a great simplification in the calculation of the relative positions of many closely lying transitions for the helium atom. For in that case one need only compute the larger and more easily obtainable similar separations for higher ions and contract them suitably, thus rendering the error small. The Hartree-Slater method, though having the great drawback of involving considerable work seems on the whole to give quite tenable results for two electron atoms and ions.

It is a pleasure to thank Professor Henry Margenau of the Sloane Physics Laboratory for his many helpful discussions and suggestions.

[6] A. H. Rosenthal, Zeits. f. Astrophysik **1**, 115 (1930).

Dielectric Constant of Water Vapor

J. D. STRANATHAN, *Department of Physics, University of Kansas*

(Received June 27, 1935)

The frequently discussed deviations from linearity in the curves of $(K-1)/(K+2)$ *versus* pressure for water vapor have been investigated. It has been shown: (1) That with proper location of the insulators of the vapor condenser in weak fields, the dielectric constant curves for the vapor are linear until saturation is approached closely; they are linear over the entire range of pressures at which breaks have previously been reported; (2) that neither pronounced breaks similar to those reported by several workers, nor the small residual deviations always present near saturation are due to the conductivity effect as commonly supposed; (3) that these breaks are due wholly to the added polarization contributed by the film of water molecules adsorbed on the insulator surfaces. Accurate dielectric data have been obtained for water vapor at 14 temperatures ranging from 21.3°C to 197.9°C; they can be represented by the equation $[(K-1)/(K+2)]RT/p' = (4.03 \pm 0.39) + (20{,}710 \pm 140)/T$. These data fall accurately along a Debye line, yielding an electric moment of $(1.831 \pm 0.006) \times 10^{-18}$ e.s.u. for the water molecule.

ON THE DEVIATIONS FROM LINEARITY

EARLY dielectric data for water vapor obtained by Jona[1] did not conform to the theoretical Debye line at the lower temperatures; the deviations were attributed to association of vapor molecules. Zahn[2] obtained data which showed the measured polarization of water vapor not at all proportional to the pressure at temperatures of 40°C or less. Pronounced breaks occurred at a pressure of the order of 1 cm of Hg; the lower the temperature the more pronounced was the break. Zahn attributed these breaks to the probable existence of a film of adsorbed water on the surfaces of the condenser plates. He pointed out that if observations were confined to pressures below those at which the breaks occurred, the data, while not accurate, were not inconsistent with the Debye theory. Wolf[3] confirmed the general nature of the breaks reported by Zahn, but observed that they were entirely independent of plate spacing. He reported also that the magnitude of the break depended upon the insulating material used in the vapor condenser, being least for quartz; it appeared that even the slope of the line below the break was somewhat dependent upon the kind of insulator used. He further observed that the d.c. conductivity of the vapor condenser varied with the type of insulator used and with the pressure of the vapor in the condenser. The fact that the conductivity increased rapidly at approximately those pressures for which the breaks in the dielectric curves occurred for the several insulators, led him to attribute the existence of the breaks to the conductivity effect. Zahn[4] apparently confirmed these observations and was led to the same conclusion. Similar breaks, though occurring much nearer saturation, have since been observed for many materials. Maske[5] reported them for benzophenone vapor; Knowles[6] reported them for ethyl alcohol; and the author has found though not reported them for all vapors studied near saturation, including numerous alcohols, toluene and the nonpolar vapor benzene. Knowles studied variations in d.c. conductivity in the region of the breaks for ethyl alcohol vapor, and concluded that both experimentally and theoretically the breaks could not be caused by a conductivity effect; the conductivity effect was neither of the proper magnitude nor, for his experimental arrangement, in the proper direction.

Since there appears some evidence conflicting with each of the three suggested interpretations of the breaks (association, the added polarization due to adsorption on the condenser plates, and conductivity across the insulator surface), the author has undertaken to get at the real cause. He has chosen to study water vapor, that material yielding the most pronounced breaks. By use of an unusually stable heterodyne beat apparatus[7] operating entirely on alternating current, along with a carefully calibrated variable

[1] Jona, Physik. Zeits. **20**, 14 (1919).
[2] Zahn, Phys. Rev. **27**, 329 (1926).
[3] Wolf, Ann. d. Physik **83**, 884 (1927).
[4] Zahn, Phys. Rev. **35**, 1047 (1930).
[5] Maske, Physik. Zeits. **28**, 533 (1927).
[6] Knowles, J. Phys. Chem. **36**, 2554 (1932).
[7] Stranathan, Rev. Sci. Inst. **5**, 334 (1934).

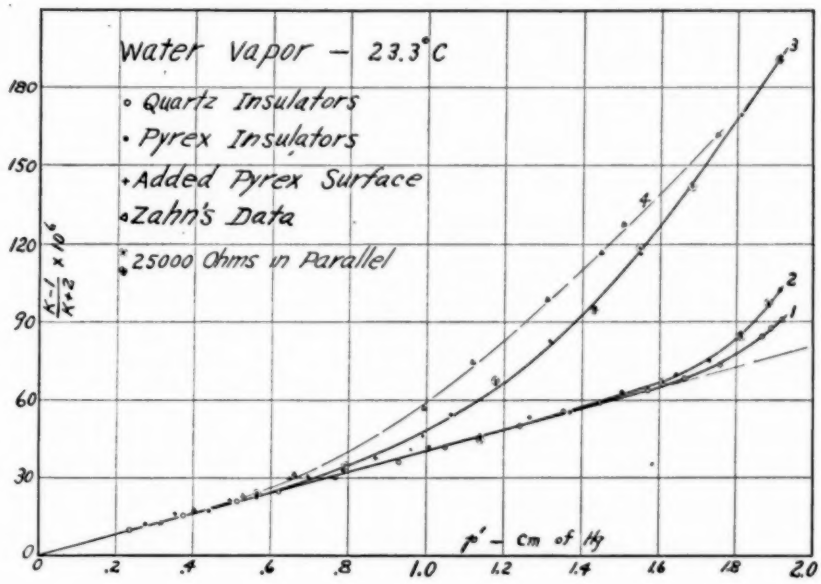

FIG. 1.

capacity standard,[8] both previously described by the author, capacity changes as small as a few thousandths of a $\mu\mu$f due to the vapor could be observed accurately. It was found[9] immediately that by using a vapor condenser similar to that described by Knowles,[6] in which care is taken to locate the insulators in weak fields, the dielectric polarization of water vapor varies linearly with pressure up to pressures far higher than those at which pronounced breaks have previously been reported. Large deviations could be observed only if the vapor were allowed to enter the condenser too rapidly; these could not be repeated and were probably due to local condensation. The addition of a tightly packed glass wool plug through which the vapor must pass in going from the vapor system (which was that used by Knowles[6]) to the condenser, completely eliminated any such possibility of error. Curve 1, Fig. 1 shows the results at 23.3°, using quartz insulators. Plotted in the same figure, curve 4, is the pronounced break reported by Zahn[2] for the same temperature, and confirmed approximately by Wolf.[3] It is apparent that the present curve (1) is essentially linear up to the highest pressures for which observations were heretofore reported. Curve 2 represents data obtained using Pyrex insulators. The break from linearity is somewhat larger and occurs at a somewhat lower pressure than for quartz, though it is even here not comparable with previously reported breaks. The slope of the line below the break is independent of the kind of insulator used. Fig. 2 shows similar data taken at 29.6°, curve 2 being the author's data obtained with Pyrex insulators, and curve 4 observations reported by Zahn. Even using Pyrex insulators, the curve is accurately linear up to pressures higher than the highest for which observations have been reported previously. While data using quartz insulators were not actually taken at this temperature, they have been taken for various nearby temperatures, and the results leave no doubt but that such a curve would be linear up to a still higher pressure, and the extent of the break less.

In spite of the fact that several observers who have measured the conductivity of the vapor condenser have attributed the nonlinearity of the dielectric curves to the conductivity effect, it has always appeared impossible to the author to reconcile the magnitude of the break with the measured conductivities. The author has therefore made three tests to show that the conductivity is not the cause of even the small residual breaks found here. First, since all previous workers seem to have measured d.c. conductivities, and since it is now recognized

[8] Stranathan, Rev. Sci. Inst. **5**, 315 (1934).
[9] Reported at the Washington meeting of the Am. Phys. Soc., 1934.

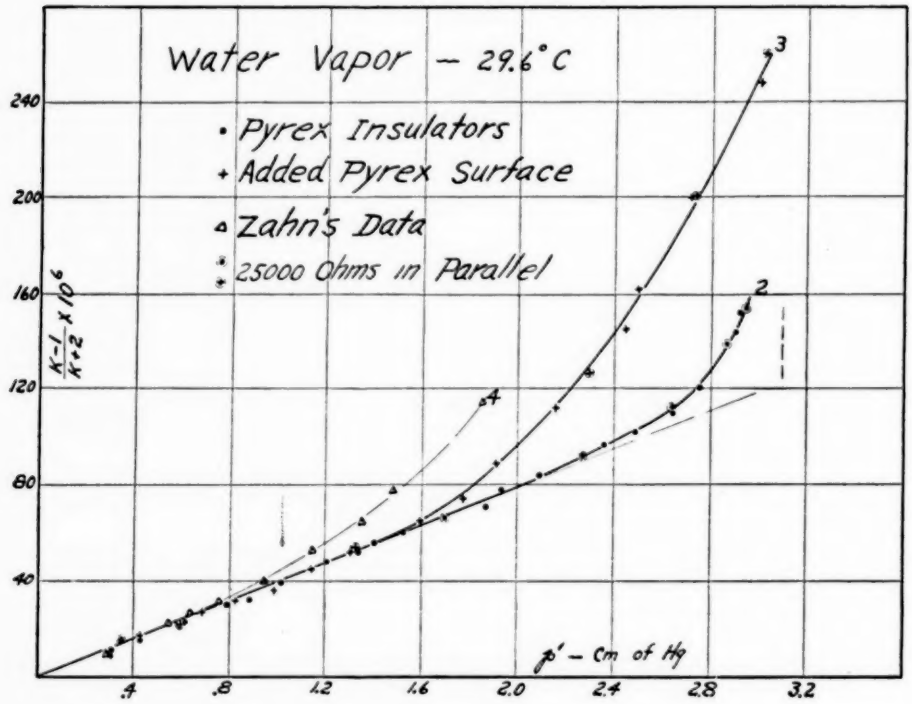

FIG. 2.

from the works of Yeager and Morgan[10] and of Roberds[11] that the high frequency conductivity is larger than the d.c. conductivity, it seemed advisable to measure the conductivity of the vapor condenser at the same frequency as was used in making dielectric constant measurements. The author has made such measurements (at 545 kilocycles), by a method since described and used extensively by Roberds.[11] Since the large condenser (840 $\mu\mu$f) used in dielectric measurements is not conducive to accurate measurement of high leakage resistances at this frequency, no claim is made of accuracy other than as to order of magnitude. It can be stated definitely that the high frequency leakage resistance of the condenser was never less than 5 megohms at any vapor pressure of water less than saturation; except at pressures barely below saturation, it was very much higher. This value agrees with calculations from the specific conductivities quoted by Yeager and Morgan and by Roberds. Theoretically it appears that the magnitude of the break is entirely inconsistent with this high a leakage resistance.

[10] Yeager and Morgan, J. Phys. Chem. **35**, 2026 (1931).
[11] Roberds, Physics **6**, 227 (1935).

Second, the author has made several experimental measurements of the effect of conductivity, measurements similar to those reported by Knowles.[6] While it is impossible to introduce an artificial leakage resistance in parallel with the test condenser without introducing at the same time an appreciable capacity, it is possible by choice of appropiate resistors to introduce various leakage resistances all with essentially the same capacity; thence the effect of conductivity can be deduced. This has been done, using artificial leaks varying from 10^8 down to 10^4 ohms. Groups of such artificial leaks of several different types have been used, and the results obtained have been consistent as regards the magnitude of the conductivity effect. Experimentally the effect of conductivity is here in the proper direction but of entirely too small a magnitude to cause even the small residual breaks observed by the author. The leakage of the vapor condenser would apparently have to be at least 200 times as great as the actually measured value in order that the conductivity might produce breaks comparable with those observed.

Third, a test was made by placing an artificial leak directly in parallel with the vapor condenser

and leaving it there throughout the determination of the dielectric constant curve. Thus the vapor condenser was always of quite high leakage regardless of the pressure of the vapor within. It can easily be shown that, under such conditions, any change in leakage accompanying increases in vapor pressure would produce an entirely different effect upon the measured capacity than would be the case were the low resistance leak not permanently in parallel. As shown in both Figs. 1 and 2, dielectric observations, including the residual breaks near saturation, were identical with and without a permanent parallel leak of 25,000 ohms. Thus all three pieces of evidence here cited seem to show definitely that even the small residual breaks in the dielectric curves just below saturation cannot be caused by the conductivity effect.

In the test cited just above, one in effect changes the conductivity of the vapor condenser without changing the nature or extent of the insulator surfaces on which water molecules might be adsorbed. A test was next made under such conditions as would change markedly the extent of the adsorbing surface within the condenser without changing the leakage resistance. This was done in the following way: In the condenser used (see work of Knowles[6] for diagram), the two sets of plates were built as two rigid metallic units. The one unit is then supported by four cylindrical compression insulators, 1.2 cm diameter, and 1.6 cm long. Three of these support the insulated unit on the bottom of the condenser housing, while the fourth is placed on top of the unit and has applied to it the compressional force which clamps the unit into place. While the normal plate spacing is approximately 1.5 mm, the insulators are all mounted between plates whose spacing is at least 10 times as large, thus placing them in a relatively weak field. Into the upper side of the lower of the two top plates (those between which the upper insulator was located) there were drilled 47 holes passing only part way through the plate. Into each of these was wedged in an upright position a piece of 8 mm Pyrex tubing carefully cut to such a length that it failed by approximately 2 mm to touch the adjacent plate. In this manner the effective insulator surface area which may adsorb water was increased by a factor approximately 6 but, since the new insulator material touches only one plate, the leakage resistance of the condenser remains unchanged. Dielectric data[12] taken under these conditions are shown by curves 3 of Figs. 1 and 2. Again the same curve is obtained with or without the use of a permanent parallel leak of 25,000 ohms. The presence of additional adsorbing insulator surface thus emphasizes the break; the break is of much greater magnitude, the ratio of magnitudes being roughly the ratio of effective adsorbing surfaces, and it occurs in measurable magnitude at a lower pressure. Dielectric curves obtained under these conditions show breaks quite similar to those reported by Zahn and Wolf. One can scarcely escape the conclusion that all breaks obtained here are caused almost wholly by the added polarization contributed by the presence of a water film adsorbed on the surfaces of the insulators. While one cannot say definitely that previously reported breaks have not been due to conductivity, for it is always possible that an oscillator whose frequency is unusually dependent upon leakage has been used, still it appears unlikely indeed. It is far more probable that all such breaks have been caused by the added polarization contributed by the water film adsorbed on the insulators.

Two further experiments have been carried out to see whether the presence of such an adsorbed film of reasonable thickness would produce an added capacity of the proper magnitude to account for the observed break. An effort was first made to calculate by rough approximation the capacity contributed by a film of given thickness, taking into account the fringing of the electric flux caused by the insulator and by the long thin adsorbed film of dielectric constant 80. Actual measurements of the capacity increases caused by similar though much thicker films (a few tenths of a mm thick) confined between two closely fitting pieces of glass tubing placed in a position between plates similar to that of the insulator, though touching only one of the plates, showed that the crude method of calculating the capacity contributed by the thin film gave surprisingly the right magnitude. Such experiments and calculations indicate that an adsorbed

[12] Reported at the Washington meeting of the Am. Phys. Soc., 1935. J. D. Stranathan, Phys. Rev. **47**, 794A (1935).

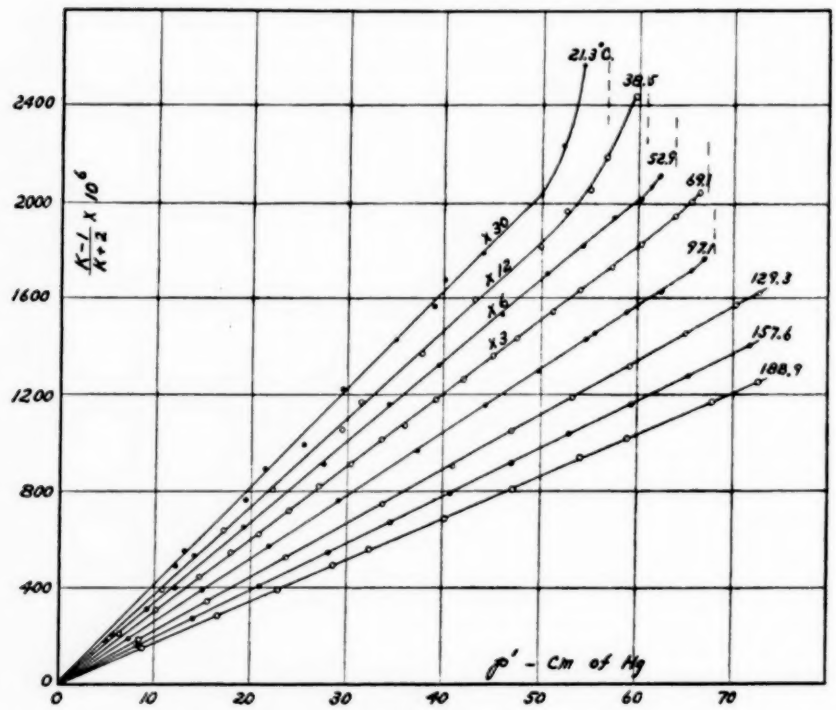

FIG. 3. For the lower temperature curves both ordinate and abscissa have been multiplied by the factor indicated.

water film a few hundred molecules thick would contribute a capacity increase sufficient to cause the deviation from linearity of the dielectric curve just below saturation. This requirement is quite consistent with the thickness of adsorbed films reported by various workers, McHaffie and Lehner[13] for example, for glass near room temperature.

The second experiment was carried out with a "condenser" designed to emphasize any effect, either conductivity or capacity, of an adsorbed film. The actual piece used has been described by Roberds,[11] and consists of a series of conducting rings fitted tightly around a large Pyrex tube, alternate rings being connected together. The total capacity of this element, including that due to solid dielectric, was approximately 60 $\mu\mu$f. Calculations involving the number, length, and spacing of these rings show that for a given thickness of adsorbed film this element should show an increase in capacity 324 times the increase which would be caused by the same thickness of film on the Pyrex insulators of the condenser used for dielectric measurements. Incidentally, it would also have 324 times the leakage. The increase in capacity of this element due to the presence of water vapor at 23.3°C was measured for a great number of pressures ranging up close to saturation. Measurements were made both with and without the permanent artificial leak of 25,000 previously referred to, and the results were entirely independent of its presence, indicating that even here the change in capacity observed was affected scarcely at all by any effect of conductivity. It is interesting that the resultant curve of capacity increase *versus* pressure of water vapor was quite similar to the curves obtained by plotting the number of molecular layers of water adsorbed *versus* the pressure from McHaffie and Lehner's[13] data. As a specific example, the increase in capacity was 11.0 $\mu\mu$f for a water vapor pressure of 1.8 cm of Hg. This increase may rightfully all be attributed to the film, for calculation shows that the vapor, with its observed dielectric constant, could account for less than 0.02 $\mu\mu$f of the increase. If the capacity due to the film here is divided by 324, it appears that the same film present on the Pyrex

[13] McHaffie and Lehner, J. Chem. Soc. London **127**, 1559 (1925).

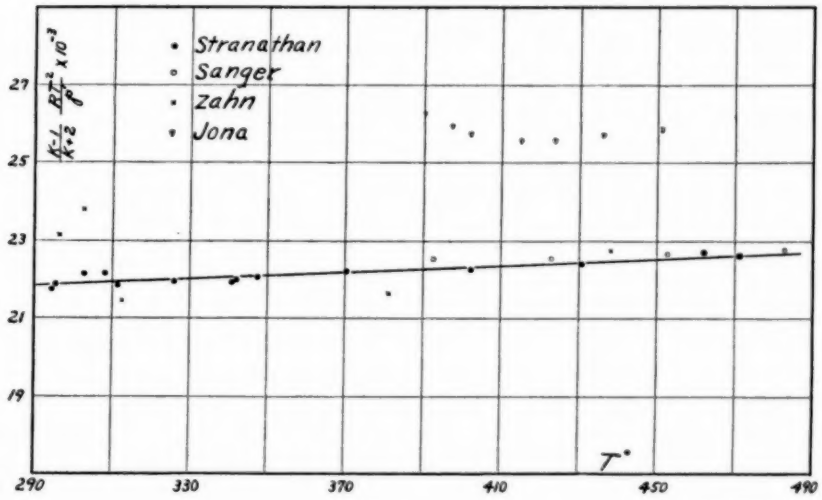

FIG. 4.

insulators of the condenser used for dielectric measurements should cause a capacity increase of 0.034 $\mu\mu$f. The actual deviation from linearity of the dielectric curve at 23.3°C and 1.8 cm of Hg pressure, under which conditions this identical film exists, represents (from curve 2 of Fig. 1) a capacity increase of 0.030 $\mu\mu$f. There can be no doubt that the added polarization due to the actual film of water adsorbed on the insulator surfaces will account quantitatively for the breaks observed in the dielectric curves for water vapor. The author suggests that probably all such breaks observed for various vapors are due mainly to this same effect. He has actually found that the addition of adsorbing insulator surface as mentioned above emphasizes the breaks for ethyl alcohol and for toluene, though no quantitative calculations have been attempted.

ON THE MOMENT OF THE WATER MOLECULE

Dielectric data have been taken at 14 different temperatures from 21.3° to 197.9°C, using quartz insulators. For the sake of clarity only half of these have been shown in Fig. 3. p' represents the pressure the vapor would exert were it an ideal gas; it is obtained from the observed pressure p and the van der Waals constants a and b, thus

$$p'=p\{1+(p/RT)(a/RT-b)\}.$$

The molecular polarization is then given by

$$(K-1)M/(K+2)d=(K-1)RT/(K+2)p' \\ =A+B/T,$$

the last equality being a result of the Debye theory. The constant A should be equal to the molecular refraction at infinite wave-length, and B is related to the permanent electric moment μ of the molecule by

$$\mu=1.272\times10^{-20}\sqrt{B}.$$

The molecular polarization at any temperature can be determined from the slope of the curve in Fig. 3. The best slopes of these lines were obtained by least squares, using all experimental points below the breaks.

Fig. 4 shows the product of molecular polarization and absolute temperature plotted against T. Previous data by Jona,[1] Zahn[2] and Sanger[14] are indicated. The present data, including that at low temperatures, fall accurately on a straight line as demanded by theory; no point deviates by more than one percent. Sanger's data, though confined to the upper half of the temperature range here investigated, fall quite close to the present curve. Zahn's data, for which he makes no claim of accuracy, are not inconsistent with the present unless it be at the lower temperatures. A least-squares solution for the best straight line through the author's data gives

$$(K-1)RT/(K+2)p'=(4.03\pm0.39) \\ +(20{,}710\pm140)/T.$$

[14] Sanger, Physik. Zeits. **31**, 306 (1930); Helv. Phys. Acta. **5**, 200 (1932).

The least-squares value for the electric moment of the water molecule is $(1.831\pm0.006)\times10^{-18}$ e.s.u. The polarization 4.0 contributed by other than the permanent moment agrees within the probable error with the molecular refraction 3.7. In view of the range of temperature over which measurements were made, and in view of the fact that not one of the 14 points deviates by more than one percent from the Debye line, the moment here found should be quite reliable. Previously reported values have varied considerably. Jona[1] reported 1.87×10^{-18}, from early vapor data. Stuart[15] reported 1.79×10^{-18}. Williams[16] obtained $(1.70\pm0.06)\times10^{-18}$ by dissolving water in benzene. Sanger[14] obtained $(1.842\pm0.008)\times10^{-18}$ from vapor data. Sanger's value appears the most reliable of the group, though it was calculated using only three points all within a temperature range of 60°. Sanger's value and the present value, obtained from 14 points covering a temperature range of 177°, agree well within the sum of the probable errors.

[15] Stuart, Zeits. f. Physik **51**, 490 (1928).
[16] Williams, Physik. Zeits. **29**, 204 (1928).

SEPTEMBER 15, 1935 PHYSICAL REVIEW VOLUME 48

The Rate of Change of Electron Temperature in the Mercury Afterglow

ROBERT H. RANDALL, *College of the City of New York*
AND
HAROLD W. WEBB, *Columbia University*

(Received July 8, 1935)

A study has been made of the behavior of a plasma in which no new ions are found, as regards electron temperature and concentration, to determine the sources of the electron energy. Measurements were made with a movable probe in a stream of ionized mercury vapor passing out from an arc discharge. The velocity and vapor concentration were determined by stroboscopic measurements on moving striations produced by an impressed alternating voltage. The vapor concentration, expressed in pressure reduced to 0°C, varied between 0.05 and 1.5 mm of mercury. The rate of cooling of the electrons was very rapid at first, but below 2500°K this rate decreased rapidly. Finally the electron temperature reached a constant value which was several hundred degrees above that of the vapor, the difference being proportional to the vapor concentration. The most reasonable source of energy necessary to keep up the electron temperature seems to be either the local recombination process, directly or through the metastable atoms formed, or the metastable atoms brought down the tube by the vapor stream.

INTRODUCTION

INVESTIGATIONS of the velocity distribution of free electrons in the plasma of an arc discharge[1] and in the plasma which diffuses out of the direct discharge as the afterglow, show that the Maxwellian law is followed, so that the distribution may be stated in terms of temperature. The conditions in the afterglow have been studied by a number of investigators[2] and the rate of recombination has been found to be closely connected with the electron temperature. The variation of the electron temperature in the afterglow indicated that the electron energy was markedly affected by the various conditions in a plasma in which there was present no new excitation or ionization. The purpose of the present investigation was to study the important factors in more detail by observing under varying conditions the time-rate of decrease of the electron temperature and concentration in the afterglow.

[1] I. Langmuir and H. M. Mott-Smith, Gen. Elect. Rev. **27**, 449, 538, 616, 762, 810 (1924); I. Langmuir, Phys. Rev. **26**, 585 (1925); H. M. Mott-Smith and I. Langmuir, Phys. Rev. **28**, 727 (1926); T. I. Killian, Phys. Rev. **35**, 1238 (1930); R. Seeliger and R. Hirchert, Ann. d. Physik **11**, 7, 817 (1931).
[2] F. L. Mohler, Phys. Rev. **31**, 187 (1928); Mohler and Boeckner, Bur. Standards J. Research **2**, 489; **3**, 303 (1929); H. W. Webb and S. C. Wang, Phys. Rev. **33**, 329 (1929); H. W. Webb and D. Sinclair, Phys. Rev. **37**, 182 (1931).

EXPERIMENTAL

The discharge tube used is shown in Fig. 1. Between the hot cathode[3] C and the anode Q

[3] For this we are indebted to the General Electric Vapor Lamp Co.

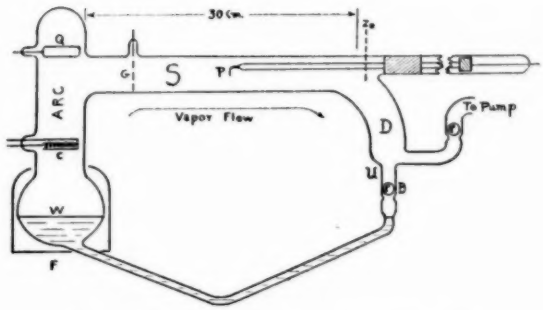

FIG. 1. Diagram of the experimental tube.

was an arc discharge of 5 to 10 amperes. Mercury evaporating from the well W, heated by the furnace F, caused a rapid flow through the arc and down the side tube S (about 30 cm long) to the condenser D, where a reflux tube brought the mercury back to the well. The streaming mercury carried with it a large quantity of electrons and positive ions, filling the side tube with a moving plasma. S was super-heated so as to prevent condensation of mercury except at the condenser D.

The probe P was of tungsten wire, 0.0025 cm in diameter and 4 mm long, mounted at right angles to the axis of the tube. It could be slid along the axis by means of an external electromagnet, and was mounted eccentrically so that by rotating it, it could be moved at right angles to the axis of S.

A nickel mesh G was mounted in S, several centimeters from the edge of the arc discharge. A magnetically controlled gate in G made it possible to move the probe into the arc.

To measure the quantity of mercury passing through S in a given time, a movable steel ball B, controlled magnetically, was used to cut off the reflux tube, so that the condensed mercury was collected in the small tube U, of known volume.

During the measurements the tube was connected to a mercury diffusion pump to prevent accumulation of gas.

The vapor velocity and concentration in S were measured, using the method designed by Ricker.[4] An alternating potential of 25 to 50 volts, supplied by a vacuum tube oscillator, was impressed between the anode Q and the mesh G, which was biased so that it was always slightly negative with respect to Q. As G was made more negative to Q, the concentration of the electrons and positive ions in its vicinity was diminished, accompanied by a decrease in the afterglow in

[4] N. H. Ricker, Phys. Rev. **17**, 195 (1921).

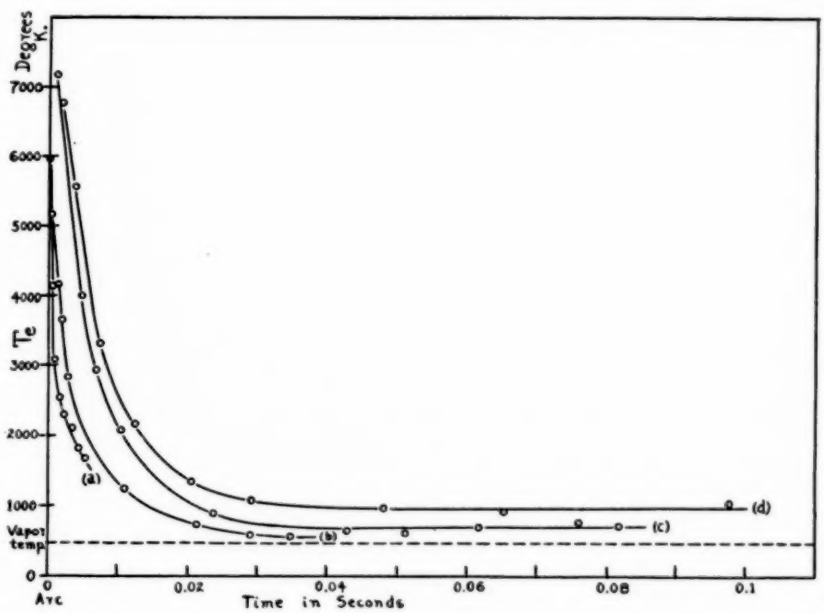

FIG. 2. Electron temperature plotted against time, as measured from the arc. Vapor concentrations in atoms/cm³: curve (a) 0.79×10^{16}; curve (b) 1.92×10^{16}; curve (c) 4.91×10^{16}; curve (d) 7.88×10^{16}. Vapor velocities in cm/sec.: curve (a) 5200; curve (b) 1300; curve (c) 464; curve (d) 300.

the vapor flowing through the mesh. As a consequence, with the alternating potential, the afterglow was broken up into moving striations, the spacing of which was measured with a stroboscopic wheel. From the frequency of the alternating voltage the velocity of the vapor was determined. From the measurement of mass flow already described the concentration of the vapor in the tube was then calculated. The striations were fairly plane and evenly spaced, showing that for any given conditions the vapor concentration and velocity were uniform throughout S.

By controlling the difference in temperature between the well and the condenser, vapor velocities between 300 and 7000 cm/sec. were obtained. By raising or lowering both well and condenser temperatures, vapor concentrations in S were obtained corresponding to pressures, reduced to 0°C, of 0.05 to 1.5 mm. The electron concentration was controlled independently of pressure and velocity conditions and of the distribution of electron temperature by varying the arc current.

The electron temperatures were measured by using the probe current-voltage characteristics, according to the methods of Langmuir and Mott-Smith. The electron concentrations were obtained from the probe currents at the "break-points."

Results

The percentage variation of the electron temperature over any one cross section of the tube S was found to be small. Therefore the results given are temperatures taken on the axis. In Fig. 2 are shown four typical electron temperature-time curves for four different vapor concentrations. The electron temperature T_e is plotted against elapsed time t, as measured from the edge of the arc discharge. The corresponding vapor concentrations and velocities are given below the graph. Since the vapor concentration could not be increased without decreasing the vapor velocity, the total time covered by each curve is different. Each curve includes data taken over the full length of the straight portion of the tube, S.

In the early part of the curves T_e falls rapidly. In the later portions, T_e reaches a constant value T_f, considerably higher than the temperature of the vapor T_g. For all these curves $T_g = 480°\text{K}$; while in curve b, $T_f = 550°\text{K}$, in curve c, 700°K and in curve d, 975°K.

The vapor velocity was not always slow enough to show the final flattening out of the $T_e - t$ curves. Fig. 3 shows the final electron temperature level T_f, where it was clearly reached, plotted against vapor concentration C. The relation between C and T_f is approximately linear, the scattering of the points being accounted for by the small range of temperatures involved and the difficulty of making precise temperature measurements. For zero concentration $T_f = 470°\text{K}$, which was very closely the temperature of the vapor T_g.

The value of T_g, i.e., 480°K, in the region where $T_e = T_f$, was taken as the wall temperature. This was checked in the following manner. Because of the low heat capacity of the gas and the streaming of the vapor, the temperature within the vapor could not be measured directly. A thermocouple was therefore placed on the outside of the wall of tube S in this region, and that portion of the tube lagged. No rise in temperature, such as would be expected if the vapor were hotter than the wall, was obtained. A computation of the rate of cooling of the vapor as it flowed down the tube showed that at this point of the tube the difference between T_g and the wall temperature was less than the experimental error of measuring T_f.

The measurements of the electron concentration were the most uncertain. Over the length of S the change of concentration varied between 100 and 10,000-fold, according to conditions. As the vapor moved down the tube, the electron concentration on the axis, n_0, fell off rapidly at

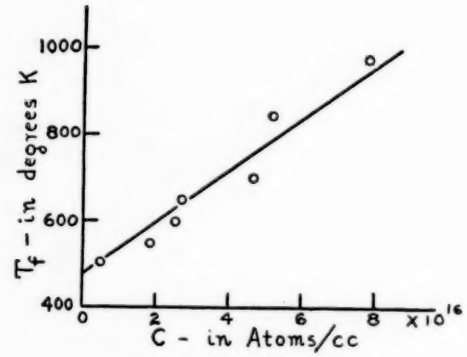

FIG. 3. Final electron temperature level T_f plotted against vapor concentration in atoms/cm³.

first; near the arc there was, in many cases, a 1000-fold change within a few centimeters. The decrease in n_0 continued throughout the whole length of S, but at a continuously decreasing rate. The electron concentration was nearly uniform over any one cross section of S. Half-way between the axis and the wall the electron concentration had fallen off less than 20 percent. This is of importance in the later discussion.

Discussion

The most interesting characteristic of the results is that T_e drops to a constant value T_f which is above the gas temperature. Since the factors determining the cooling of the electrons which are effective in the falling part of the $T_e - t$ curves must still be operative in this region, there is evidently an important mechanism in the plasma tending to raise the temperature of the electrons. The complete solution of the problem presented here is difficult because of the variation of the electron temperature along the axis and because the mechanism of the energy transfer by the electrons and of the maintenance of the Maxwellian distribution is not understood. However, the measurements give the distribution of electron temperature and concentration over the greater part of the tube S, so that the distribution of space potential, wall potential and current to the wall can be approximately computed.

In making these computations use was made of the theory worked out for the plasma by Tonks and Langmuir.[5] Let r and z be the radial and axial coordinates and let R be the radius of the wall. The space potential in each cross-sectional element is taken as zero on the axis. Let $\eta = eV/kT_e = 11{,}600\ V/T_e$, where e is the electronic charge, V the space potential in volts for any value of r, and k the Boltzmann constant. For any value of r, the concentration of electrons or ions is $n = n_0\epsilon^{-\eta}$, where n_0 is the concentration on the axis.

From kinetic theory the electron current density to the wall is

$$I_n = en_0\epsilon^{-\eta_w}(kT_e/2\pi m_e)^{\frac{1}{2}},$$

where η_w is the value of η at the wall and m_e is the electronic mass. If it is assumed that the loss of number by recombination is negligible,[6]

$$I_n(2\pi R) = ev\frac{\partial}{\partial z}\int_0^R n_0\epsilon^{-\eta}2\pi r dr = ev\frac{\partial}{\partial z}(An_0)\pi R^2,$$

where v is the vapor velocity, and An_0 is the average electron concentration in any one section.

To determine the value of η_w (and hence the wall potential) from the above equations, it is necessary to determine A. Since the electron concentration was found to be nearly uniform across the tube for all values of z, A certainly lies between 1.0 and 0.5. If $A = 1$, the maximum possible value, η_w is 12.1, 12.5, 15.8, and 11.6 for curves a, b, c, and d, respectively, in Fig. 2, while for $A = 0.5$, η_w has values smaller by 0.6. This variation in η_w is negligible for the purposes of these computations.

The variation of η_w with z was found to be very small. This, together with the fact that $\epsilon^{-\eta}$ varies only slowly with r, until near the wall, justifies for a first approximation the assumption that $\epsilon^{-\eta}$ is independent of z. This gives a condition similar to case 4 on page 889 of the paper by Tonks and Langmuir. In this the potential distribution was determined in a plasma, with short ionic mean free path and ion generation proportional to electron density. The generation of new ions is replaced here by the net flow in the z direction of electrons and ions, $v\partial n/\partial z$, into any element, since if $\epsilon^{-\eta}$ is a function of r only,

$$v\frac{\partial n}{\partial z} = v\frac{\partial}{\partial z}(n_0\epsilon^{-\eta}) = v\frac{1}{n_0}\frac{dn_0}{dz}n = \text{constant } n.$$

The solution* is

$$\epsilon^{-\eta} = J_0\left[\left\{v\left(\frac{1}{n_0}\frac{dn_0}{dz}\right)\Big/(qkT_e)\right\}^{\frac{1}{2}} r\right],$$

where $q = 0.895\ l_g/(kT_g m_p)^{\frac{1}{2}}$, l_g being the molecular mean free path and m_p the mass of the positive ion.

As a check on the accuracy of this expression, the value of $\epsilon^{-\eta_w}$ determined above and experimentally determined values for the variables in the argument of J_0 were substituted, and the equations solved for R. The average value found

[5] L. Tonks and I. Langmuir, Phys. Rev. **34**, 876 (1929).

[6] K. T. Compton and I. Langmuir, Rev. Mod. Phys. **2**, 197 (1930).

* Reference 5, cf. equation at bottom of p. 889.

was approximately 2 cm, the discrepancy between this and the actual value, 1.77 cm, being accounted for by the precision in the measurement of $(1/n_0)dn_0/dz$. Using the expression for $\epsilon^{-\eta}$, the value of A was found to be 0.95.

It must be emphasized that all the above results are based on the assumption that a Maxwellian distribution is always maintained throughout the space in question. The probe current-voltage curves taken here give the energy distribution of the electrons only up to a few tenths of a volt and any departure from the assumed distribution for higher energies could not be detected.

The nature of the mechanism of the cooling of the electrons as they pass down the tube can be best discussed by considering the total changes in energy in any fixed volume. Calculations were made of the energy gained and lost in the whole of a cylinder formed by that part of the tube S lying between a transverse section at z and a second section at z_e, at the lower end of S (see Fig. 1). The net energy brought into such a cylinder by convection is $E_c=(3/2)kT_evA[n_0-(n_0)_e]\pi R^2$ ergs/sec., where n_0 and $(n_0)_e$ are the electron concentrations on the axis at z and z_e, respectively. The energy carried out per second by the electrons escaping to the wall is

$$E_w=\int_z^{z_e}\left[T_ev\frac{dn_0}{dz}\left\{\int_o^R\frac{e10^7}{11{,}600}(\epsilon^{-\eta})(\eta_w-\eta)2\pi rdr\right\}\right]dz+\int_z^{z_e}\left[\frac{3}{2}kT_ev\frac{dn_0}{dz}\left(\int_o^R\epsilon^{-\eta}2\pi rdr\right)\right]dz.$$

The first part of E_w is the work done by the electrons in reaching the wall against the retarding potential; the second part, which is small in comparison (about 10 percent of the whole), is the energy carried out by the electrons as kinetic energy. Neglecting η with respect to η_w, since η is nearly zero except near the wall, this equation becomes

$$E_w=A\pi R^2v\left(\frac{e10^7}{11{,}600}\eta_w+\frac{3}{2}k\right)\int_{n_0}^{(n_0)_e}T_edn_0.$$

By substituting experimental values in the equations for E_c and E_w, it was found that in all cases the loss to the wall was much greater than the energy brought in by convection. For the data of curve a, Fig. 2, $E_c=435$ ergs/sec. and $E_w=1500$ ergs/sec. for a point z near the arc. For a point near the condenser, $E_c=7$ ergs/sec. and $E_w=38$ ergs/sec. For the data of curve c, where the vapor velocity was only 0.1 as great, near the arc $E_c=0.25$ ergs/sec. and $E_w=1.0$ ergs/sec.; near the condenser $E_c=9.1\times10^{-5}$ ergs/sec. and $E_w=73\times10^{-5}$ ergs/sec.

To account for this difference in energy ΔE, several sources must be considered. The more obvious are the transfer of energy to electrons by metastable atoms swept down the tube S or produced throughout S by the recombination process, the recombination process itself, and the transfer of energy in the z direction between the electrons.

The magnitude of this last process, which by analogy can be referred to as conduction, is difficult to estimate, since it involves the mechanism of the reestablishment of the Maxwellian distribution, which is not clearly understood. When the electron temperature is falling rapidly, as in the early part of the flow, conduction is probably important. If it is assumed that all of ΔE is due to this factor and if the small quantity of energy leaving the cylinder zz_e at the lower end is neglected, since any process of this type must depend upon the concentration at the section across which the energy transfer is taking place, it is convenient to compute $\Delta E/An_0$. Starting at the edge of the arc discharge, the value of the quotient falls rapidly with the temperature, decreasing to approximately one-fourth its initial value when the final temperature level T_f is attained. The fact that this quotient decreases with the electron temperature and with the temperature gradient is consistent with the assumption that such a process is important in the region of falling temperature. In the region in which the electron temperature is constant, however, there should be no energy transfer of this type, since the electrons are all at the same temperature. Here ΔE must be due to other sources of electron energy.

The probability of the transfer of energy by metastable atoms to electrons on impact is high. No estimate of the concentration of metastable atoms or of the energy which they might give to

the electrons has been attempted, since no data are available for such a computation. Furthermore it is not known to what extent these metastable atoms are produced locally by recombination and to what extent they are swept down by the vapor from the region of the arc. Webb and Wang[2] found that both factors are important. They further showed that if into a moving plasma similar to that studied here, they introduced sodium vapor, a marked drop in electron temperature immediately resulted; in the case cited from 2300° to 800°K. The most important action of the sodium on the flowing vapor was to eliminate the metastable atoms by excitation of the sodium, and the most probable explanation of the temperature drop is that the elimination of the metastable atoms removed a source of electron energy, resulting in lowered electron temperature.

Webb and Sinclair[2] found that the rate of recombination depended to a large extent on the electron temperature, and came to the conclusion that a somewhat complex interaction between ions and fast and slow electrons was involved in the recombination process. Furthermore, a study of the intensity distribution in the afterglow spectrum leads to the conclusion that considerable kinetic energy may be freed by the process. It therefore seems probable that the recombination process is largely responsible for the energy supply which tends to hold up the electron temperature, either through some process involving many-body collisions, or by the metastable atoms which constitute a large part of the atoms formed by recombination. It may be noted that the recombination has been found by Webb and Sinclair and by Mohler and Boeckner[7] to increase with the pressure, which corresponds to the increase in the final electron temperature level with increase in pressure found here. On the other hand, for a given rate of production, the concentration of metastable atoms also tends to increase with increased pressure, as under these conditions the life of these atoms is practically determined by the diffusion to the wall.

The authors wish to express their appreciation to Mr. T. C. Hardy for his assistance in the taking of the measurements.

[7] Mohler and Boeckner, Bur. Standards J. Research **2**, 489 (1929).

SEPTEMBER 15, 1935 PHYSICAL REVIEW VOLUME 48

A Contribution to the Theory of the B. W. K. Method

EDWIN C. KEMBLE, *Research Laboratory of Physics, Harvard University*

(Received April 16, 1935)

In order to put Zwaan's scheme for deriving the Kramers connection formulas on a rigorous basis, differential equations are set up governing the variation in the coefficients used to fit a linear combination of the B. W. K. type approximation functions to an exact solution of Schrödinger's equation in one dimension. Approximate solutions of the differential equations are worked out which lend themselves to the setting up of the connection formulas and give definite upper bounds to the errors involved in their use. The method is also used to set up the Sommerfeld phase integral quantum condition independently of the connection formulas. An upper limit to the error in the energy is worked out. A similar treatment of the problem of the transmission of matter waves through rounded potential barriers is formulated.

1. INTRODUCTION

Zwaan's[1] scheme for deriving the Kramers connection formulas[2] used in the Brillouin-Wentzel-Kramers (B. W. K.) method is simple and illuminating, but not entirely rigorous. In the attempt to put Zwaan's argument on a rigorous basis the author has developed a new way of studying the relation of the Stokes phenomenon to the B. W. K. method whose value extends beyond the scope of the connection formulas themselves.

Consider a one-dimensional problem in wave mechanics with the potential energy $V(z)$ and the classical local momentum

[1] A. Zwaan, *Intensitaten im Ca-Funkenspektrum*, Dissertation, Utrecht, 1929.

[2] H. A. Kramers, Zeits. f. Physik **39**, 828 (1926); H. A. Kramers and G. P. Ittman, Zeits. f. Physik **58**, 217 (1929).

$$p(z, E) = \{2\mu[E - V(z)]\}^{\frac{1}{2}}.$$

The Schrödinger equation takes the form

$$\psi'' + \lambda^2 p^2 \psi = 0 \tag{1}$$

with λ set equal to $2\pi/h$. The basic approximation functions of the B. W. K. method are

$$\begin{aligned} f_i(z, E) &= p(z, E)^{-\frac{1}{2}} e^{\imath w(z, E)}; \\ f_v(z, E) &= p(z, E)^{-\frac{1}{2}} e^{-\imath w(z, E)}; \end{aligned} \tag{2}$$

$$w(z, E) = \lambda \int_{z_0}^{z} p(\zeta, E) d\zeta. \tag{3}$$

Here $\imath$ denotes $\sqrt{-1}$. The point z_0 can be chosen at pleasure but is ordinarily placed on the axis of reals. f_i and f_v are readily shown to be solutions of the differential equation

$$f'' + [\lambda^2 p^2 - Q] f = 0, \tag{4}$$

where Q denotes the function

$$Q = \frac{3}{4}\left(\frac{p'}{p}\right)^2 - \frac{p''}{2p} \equiv \frac{1}{4}\left[\frac{5}{4}\left(\frac{V'}{E-V}\right)^2 + \frac{V''}{E-V}\right]. \tag{5}$$

Wherever $|Q| \ll \lambda^2 p^2$, Eq. (4) is very nearly the same as (1) and f_i, f_v may be said to be good approximate solutions of (1).

Let z' denote a simple real zero point of the function $E - V(z)$ (primes and double primes denote differentiation *except* when applied to the symbol z itself). For definiteness, we assume that $E - V$ is negative to the left of z' and positive to the right (cf. Fig. 1). At z', f_i, f_v and Q all become infinite. Hence f_i, f_v have no value as approximate solutions of (1) in the neighborhood of z'. We shall suppose, however, that there exist regions I and II to the left and right of z', respectively, where $|Q| \ll \lambda^2 p^2$ and where the f's are good approximate solutions. Then if $\psi(z)$ is an exact solution of (1), we may reasonably assume that in any not too large portion of I, $\psi(z)$ is approximately equal to some suitable linear combination of f_i and f_v. Thus, if α_i and α_v are suitably chosen constants,

$$\alpha_i f_i + \alpha_v f_v = \psi(z) \qquad \textit{in region I.}$$

Similarly

$$\beta_i f_i + \beta_v f_v = \psi(z) \qquad \textit{in region II.}$$

It is well known that the coefficients β_i, β_v are not equal to α_i, α_v, respectively. The shift in the values of the coefficients is called the Stokes phenomenon and the problem is to determine the magnitude of this shift in terms of the values on one side of z', say in I.

Kramers method of attack is based on the assumption that $V(z)$ is sensibly linear in the interval between I and II. Under these circumstances $\psi(z)$ can be approximated by a suitable Bessel's function over the interval in question and this function constitutes a bridge between the B. W. K. approximations in I and II. Langer[3] has introduced a different type of approximation function involving a Bessel's function of the argument $w(x)$ defined in Eq. (3). The Langer approximation function degenerates into the B. W. K. type in I and II, but does not go to pieces near z'. This method is very powerful, but has some disadvantages with respect to that developed in the present article.

Zwaan's derivation of the connection formulas follows closely a line of thought previously developed by Stokes.[4] It is based on the introduction of complex values of the independent variable and the existence of a path Γ joining I and II, but passing around z' in the complex plane so that the inequality $|Q| \ll \lambda^2 p^2$ is good along its entire length. If $V(z)$ is analytic on the axis of reals between I and II, and if its analytic extension into the upper half plane yields no roots of $V(z) - E$ near z', we may assume that such a path can be found.[5]

The essential feature of the situation to which Zwaan calls attention is that along a portion of any such path Γ the approximation f_i becomes

[3] R. E. Langer, Trans. Am. Math. Soc. **33**, 23 (1931); **34**, 447 (1932); Bull. Am. Math. Soc. **40**, 545 (1934).

[4] Sir George Gabriel Stokes, *Math. and Phys. Papers*, Vol. 4, pp. 77–109 and 283–298.

[5] Let us assume that $V(z) - E$ is a polynomial of degree n, or can be accurately represented by such a polynomial in the interval between I and II. Then, if z_k denotes the kth root, $E - V = C \prod_{k=1}^{n} (z - z_k)$. It follows that

$$(E-V)'/(E-V) = \sum_{k=1}^{n} \frac{1}{z - z_k};$$

$$(E-V)''/(E-V) = \left(\frac{E-V'}{E-V}\right)^2 - \sum_{k=1}^{n} \frac{1}{(z-z_k)^2}.$$

Hence

$$\frac{Q}{p^2} = \frac{1}{8\mu C \Pi_k (z - z_k)} \left[\frac{1}{4}\left(\sum_{k=1}^{n} \frac{1}{z - z_k}\right)^2 + \sum_k \frac{1}{(z-z_k)^2}\right].$$

Inspection of this expression for Q/p^2 proves the above statement for the case that n is small.

very small, while f_v becomes very large. Hence f_v and f_i are said to be *dominant* and *subdominant*, respectively, in the region in question. Where this is true changes in the subdominant coefficient can take place even when $|Q| \ll \lambda^2 p^2$. On the other hand the coefficient of the dominant approximation function cannot change much, since a small change in this coefficient makes a very large difference in the function. Zwaan assumes that the latter coefficient is constant.

2. The Differential Equations for the Coefficients

Granted that the changes do take place, we propose here to investigate them by setting up explicit differential equations for the variation in the coefficients. The formulation of these equations, which forms the essential contribution of the present paper, is reminiscent of a method of attack on one-dimensional problems in quantum mechanics due to Hill.[6]

Let $\psi(z)$ be an exact solution of (1). Let $u = a_i f_i + a_v f_v$ be a linear combination of f_i and f_v which is fitted to ψ at the arbitrary point $z = z_1$. The best fit will evidently be obtained if u and du/dz are made equal to ψ and $d\psi/dz$, respectively, at the point z_1. In that case

$$a_i f_i(z_1) + a_v f_v(z_1) = \psi(z_1); \tag{6}$$

$$a_i f_i'(z_1) + a_v f_v'(z_1) = \psi'(z_1). \tag{7}$$

As the Wronskian determinant $f_i f_v' - f_v f_i'$ does not vanish (it has the constant value $-4\pi\iota/h = -2\lambda\iota$) it is possible to choose a_i and a_v so as to satisfy these equations at an arbitrary point z_1 where f_i and f_v are uniquely defined. The coefficients so obtained will then vary *continuously* as z_1 moves around the path Γ, reducing to α_i and α_v where Γ meets the axis of reals in I and to β_i, β_v where Γ meets the axis of reals in II.

Dropping the subscript 1 in Eqs. (6) and (7), solving for a_i, and differentiating with respect to z, we obtain

$$\frac{da_i}{dz} = (\iota/2\lambda)(f_v''\psi - f_v\psi''). \tag{8}$$

On reduction with the aid of Eqs. (1) and (4)

$$\frac{da_i}{dz} = \frac{\iota}{2\lambda} Q f_v \psi = \frac{\iota}{2\lambda}\frac{Q}{p}[a_i + e^{-2\iota w} a_v]. \tag{9}$$

Similarly

$$\frac{da_v}{dz} = -\frac{\iota}{2\lambda} Q f_i \psi = -\frac{\iota}{2\lambda}\frac{Q}{p}[a_v + e^{2\iota w} a_i]. \tag{10}$$

These differential equations are *exact*. Their integration is equivalent to the integration of Eq. (1), although they blow up at the zeros of $p(z, E)$. If an exact integration were possible, it would be a simple matter to work out the exact eigenfunctions and eigenvalues of (1). The primary usefulness of Eqs. (9) and (10), however, lies in the possibility of deriving useful approximations from them.

3. The Approximate Integration of Eqs. (9) and (10)

Introducing a fixed point ξ, let us make the transformation

$$\begin{aligned} b_i(z, \xi) &= a_i(z) e^{-\iota F(z, \xi)}; \\ b_v(z, \xi) &= a_v(z) e^{+\iota F(z, \xi)}, \end{aligned} \tag{11}$$

where

$$F(z, \xi) = \frac{1}{2\lambda}\int_\xi^z \frac{Q}{p} dz. \tag{11a}$$

This change of variables leads to the following simpler system of differential equations:

$$\begin{aligned} \frac{db_i}{dz} &= \frac{\iota}{2\lambda}\frac{Q}{p} e^{-2\iota(F+w)} b_v; \\ \frac{db_v}{dz} &= -\frac{\iota}{2\lambda}\frac{Q}{p} e^{2\iota(F+w)} b_i. \end{aligned} \tag{12}$$

Clearly b_i and b_v will be sensibly equal to a_i and a_v, respectively, at any point z which can be connected with ξ by a path along which $|Q/p|$ is small enough. It is convenient to define an index of quality μ_Λ for a path Λ in the complex plane by the equation

$$\mu_\Lambda = \frac{1}{\lambda}\int_\Lambda \left|\frac{Q}{p}\right| ds = \frac{1}{\lambda^2}\int_\Lambda \left|\frac{Q}{p^2}\right| |dw|. \tag{13}$$

We shall hereafter refer to a path as good, provided that its index of quality is much less than unity. Any short path which gives a wide berth to the

[6] E. L. Hill, Phys. Rev. **38**, 1258 (1931).

zeros of $p(z, E)$ can ordinarily be assumed to be "good" in this sense. Since

$$\left|\frac{1}{\lambda}\int_{\Lambda}\frac{Q}{p}dz\right| \leqslant \mu_{\Lambda},$$

it follows that $|F(z, \xi)| \leqslant \frac{1}{2}\mu_{\Lambda}$ if z and ξ are any two points on Λ. b_i and b_v are thus sensibly equal to a_i and a_v at any point z which can be connected with ξ by a good path.

It will simplify the discussion of the integration of Eqs. (12) if we assume at first a definite path of integration Λ, of total length l, leading from an initial point Z_0 to a final point Z_1, and having the property that the imaginary part of w is a monotonically decreasing function of the path length s measured from Z_0. In other words, we assume that $|e^{iw}|$ increases monotonically as we move from Z_0 to Z_1 along Λ. With these restrictions we introduce the real variable of integration s and the notation

$$\begin{aligned} w(z) &= \omega(s), \quad iQ(z)/2\lambda p(z) = \Sigma(s), \\ dz/ds &= \varphi(s), \quad F(z, \xi) = \theta(s, \xi). \end{aligned} \tag{14}$$

Eqs. (12) take the form

$$db_i/ds = \Sigma(s)\varphi(s)e^{-2i(\theta+\omega)}b_v, \tag{15}$$

$$db_v/ds = -\Sigma(s)\varphi(s)e^{2i(\theta+\omega)}b_i. \tag{16}$$

Under favorable circumstances b_i can be computed approximately for points on Λ by replacing b_v in (15) by its initial value $b_v^0 \equiv b_v(Z_0)$. Let $\tilde{b}_i(z)$ denote the corresponding approximation for $b_i(z)$. Then

$$\tilde{b}_i(s) = b_i^0 + b_v^0 \int_0^s \Sigma(s_1)\varphi(s_1)e^{-2i[\theta(s_1)+\omega(s_1)]}ds_1. \tag{17}$$

This approximation can be tested by computing an upper bound on $|b_i(Z_1) - \tilde{b}_i(Z_1)|$. We have

$$b_i(Z_1) - \tilde{b}_i(Z_1) = \int_0^l [b_v(s) - b_v^0]\Sigma(s)\varphi(s)e^{-2i(\theta+\omega)}ds. \tag{18}$$

But from (16)

$$b_v(s) - b_v^0 = -\int_0^s b_i(s_1)\Sigma(s_1)\varphi(s_1)e^{2i[\theta(s_1)+\omega(s_1)]}ds_1. \tag{19}$$

Hence

$$\begin{aligned} b_i(Z_1) - \tilde{b}_i(Z_1) &= -\int_0^l ds\,\{\Sigma(s)\varphi(s)e^{-2i[\theta(s)+\omega(s)]}\int_0^s b_i(s_1)\Sigma(s_1)\varphi(s_1)e^{-2i[\theta(s_1)+\omega(s_1)]}ds_1\} \\ &= -\iint_T b_i(s_1)\Sigma(s_1)\Sigma(s)\varphi(s_1)\varphi(s)e^{-2i[\theta(s)-\theta(s_1)+\omega(s)-\omega(s_1)]}ds_1 ds, \end{aligned} \tag{20}$$

where T is a triangle in the s, s_1 plane defined by the inequalities $0 \leqslant s_1 \leqslant s$; $0 \leqslant s \leqslant 1$. Since $|e^{iw}|$ increases monotonically along Λ, $|e^{-2i[\omega(s)-\omega(s_1)]}| \leqslant 1$ at every point in T. $\varphi(s)$ is of unit absolute value and

$$|e^{-2i[\theta(s)-\theta(s_1)]}| = |e^{-(i/\lambda)\int_{s_1}^{s}[Q(s')/p(s')]\varphi(s')ds'}| \leqslant e^{\mu_{\Lambda}}.$$

Introducing the symbol M_i for the maximum value of $|b_i|$ on Λ, we readily derive the inequality

$$|b_i(Z_1) - \tilde{b}_i(Z_1)| < M_i e^{\mu_{\Lambda}} \iint_T |\Sigma(s_1)|\,|\Sigma(s)|\,ds_1 ds. \tag{21}$$

The function $|\Sigma(s)|\,|\Sigma(s_1)|$ being symmetrical with respect to its arguments, the above integral over T is half the corresponding integral over the complete square $0 \leqslant s \leqslant 1$; $0 \leqslant s_1 \leqslant 1$. Thus

$$|b_i(Z_1) - \tilde{b}_i(Z_1)| < \tfrac{1}{2}M_i e^{\mu_{\Lambda}}\{\int_0^l |\Sigma(s)|\,ds\}^2 = \mu_{\Lambda}^2 e^{\mu_{\Lambda}}(M_i/8). \tag{22}$$

We conclude that in the case of a good path leading uphill with respect to $|e^{iw}|$ the approximation (17) will lead to an error which is small in comparison with the maximum value of $|b_i|$ on the path.

Let w_0 denote the value of w at the point Z_0. The maximum absolute value of the factor $e^{-2i\omega(s_1)}$ of the integrand of Eq. (17) is $|e^{-2iw_0}|$. Furthermore on the path $\Lambda\,|e^{-2i\theta}| \leqslant e^{2|\theta|} < e^{\mu_0+\mu_{\Lambda}}$ where μ_0 denotes the index of quality of the best path leading from ξ to Z_0. We assume that μ_0 is a small quantity of the order of μ_{Λ}. Eq. (17) yields

$$|\tilde{b}_i(Z_1) - b_i^0| < \tfrac{1}{2}\mu_{\Lambda}e^{\mu_0+\mu_{\Lambda}}|b_v^0|\,|e^{-2iw_0}|.$$

Combining this inequality with (22), we obtain

$$|b_i(Z_1)| < |b_i^0| + \tfrac{1}{2}\mu_\Lambda e^{\mu_0+\mu_\Lambda}|b_v^0|\,|e^{-2iw_0}| + \mu_\Lambda^2 e^{\mu_\Lambda}(M_i/8). \tag{23}$$

Let Z_m denote the point on Λ where $b_i(z)$ becomes equal to M_i, and let μ_Λ' denote the quantity $1/\lambda\int_{Z_0}^{Z_m}|Q/p|ds$, where the integration is carried out along Λ. Then $\mu_\Lambda' \leqslant \mu_\Lambda$. Clearly an equation similar to (23) applies to the point Z_m. Thus

$$M_i < |b_i^0| + (\mu_\Lambda'/2)e^{\mu_0+\mu_\Lambda'}|b_v^0|\,|e^{-2iw_0}| + \mu_\Lambda'^2 e^{\mu_\Lambda'}(M_i/8).$$

Transposing and neglecting terms of higher power in the small quantities μ_0, μ_Λ, we obtain $M_i < |b_i^0| + \tfrac{1}{2}\mu_\Lambda|b_v^0|\,|e^{-2iw_0}|$. It follows that in this approximation

$$|b_i(Z_1)-b_i^0| < |b_i(Z_1)-\tilde{b}_i(Z_1)| + |\tilde{b}_i(Z_1)-b_i^0| < \tfrac{1}{2}\mu_\Lambda|b_v^0|\,|e^{-2iw_0}| + \tfrac{1}{8}\mu_\Lambda^2|b_i^0|. \tag{24}$$

Consider next the change in a_i. We have

$$|a_i(Z_1)-a_i^0| = |e^{iF(Z_0,\,\xi)}|\,|b_i(Z_1)e^{i/2\lambda\int_\Lambda (Q/p)\,dz} - b_i^0|,$$

where

$$|F(Z_0,\xi)| < \tfrac{1}{2}\mu_0 \quad \text{and} \quad \left|\frac{1}{2\lambda}\int_\Lambda \frac{Q}{p}dz\right| < \tfrac{1}{2}\mu_\Lambda.$$

Hence, neglecting small quantities of higher order,

$$|a_i(Z_1)-a_i^0| < e^{\mu_0/2}\{e^{\mu_\Lambda/2}|b_i(Z_1)-b_i^0| + |b_i^0|(\mu_\Lambda/2)\} < \tfrac{1}{2}\mu_\Lambda[\,|b_i^0| + |b_v^0|\,|e^{-2iw_0}|\,].$$

Finally, it follows from (11) that to this same approximation $|b_i^0| - |a_i^0| < |a_i^0|(\mu_0/2)$. Consequently

$$|a_i(Z_1)-a_i^0| < \tfrac{1}{2}\mu_\Lambda[\,|a_i^0| + |a_v^0|\,|e^{-2iw_0}|\,]. \tag{25}$$

We conclude that the variation in a_i is small in comparison with the larger of the two quantities $|a_i^0|$ and $|a_v^0|\,|e^{-2iw_0}|$.

In applying the above result two special cases are to be considered. The first is that of a good uphill path restricted by the additional requirement that $|e^{iw}| \geqslant 1$ along its entire length. (It will be convenient to refer to regions in which $|e^{iw}| > 1$ as *mountains*, and to regions in which $|e^{iw}| < 1$ as *valleys*. Clearly f_i is dominant and f_v subdominant on the upper levels of the mountains. These roles are reversed for the lower levels of the valleys.) In this case $|e^{-2iw_0}| < 1$ and $|a_i(Z_1)-a_i^0|$ is small compared with the average of the quantities $|a_i^0|$ and $|a_v^0|$. Under these circumstances we shall say that a_i is sensibly constant along the path, although if $|a_i^0| \ll |a_v^0|$, it may vary by a large percentage of its initial absolute value.

In order to deal with the variation in a_i along a good path leading from Z_0 clear over a mountain to Z_1, but not entering the adjacent valleys, it is convenient to think of the path as made up of two parts leading to the crest from opposite sides. Applying the above argument to each part of the path we come to the conclusion that a_i is *sensibly constant* over the entire path in comparison with the largest of the four quantities $|a_i^0|$, $|a_v^0|$, $|a_i(Z_1)|$, $|a_v(Z_1)|$.

A second important case of the application of Eq. (25) is that of a good path leading uphill, but beginning in a valley, where $|e^{iw}| < 1$ and f_v is dominant. If the valley is deep $|e^{-2iw_0}|$ is a very large number, but if $|a_v^0|\,|e^{-2iw_0}| \leqslant |a_i^0|$, we have the inequality

$$|a_i(Z_1)-a_i^0| < \mu_\Lambda|a_i^0| \tag{26}$$

and can say that $a_i(z)$ is sensibly constant along the good path Λ. Evidently $a_i(z)$ will also be sensibly constant along a good path Λ extending

across a valley from one mountain to another, provided that $|a_v(z)|\,|e^{-2\iota w(z)}| \leqslant |a_i(z)|$ at the lowest point of the path.

Turning to $a_v(z)$, we readily derive formulas parallel to those for $a_i(z)$ provided that we perform the integrations in the opposite direction on Λ, i.e., downhill with respect to $|e^{\iota w}|$. Thus, if we take a_i^0 and a_v^0 as the values of a_i and a_v at the upper end of the path, we obtain instead of (25) the inequality

$$|a_v(Z_1)-a_v^0| < \tfrac{1}{2}\mu_\Lambda\{|a_v^0|+|a_i^0|\,|e^{2\iota w_0}|\}. \quad (27)$$

In general the coefficient of the dominant approximation f_i or f_v is sensibly constant over a good path Λ on which $|e^{\iota w}|-1$ does not change sign. The coefficient of the subdominant term is also sensibly constant over such a path provided that the absolute value of the dominant term at the point of maximum dominance is zero, or smaller than the product (evaluated at the same point) of the absolute value of the coefficient of the subdominant term multiplied by the smaller of the two quantities $|e^{\pm 2\iota w}|$. However, since we have defined the phrase "sensibly constant" somewhat loosely, it is perhaps best to base all rigorous arguments directly on the inequalities (25) and (27).

4. Derivation of the Connection Formulas

We assume that the potential function in the neighborhood of the classical turning point z' has the form indicated in Fig. 1. Introducing polar coordinates r, θ with the origin at z', we write p^2 in the form

$$p^2 = 2\mu(E-V) = re^{\iota\theta}\varphi(z),$$

where $\varphi(z)$ is assumed to be bounded from zero in a wide region of the complex plane about z'. We further assume the existence of a path passing around z' in the upper half plane (cf. Fig. 3) enclosing no complex zeros of p^2 and good in the technical sense that $\mu_\Lambda \ll 1$. Let P_1 and

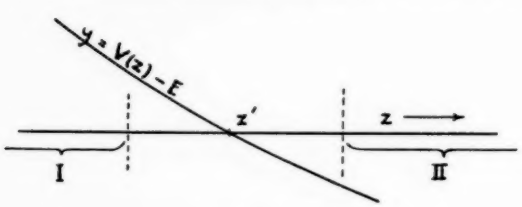

Fig. 1.

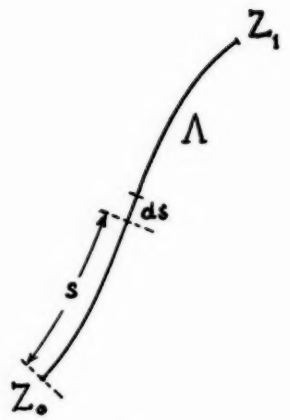

Fig. 2.

P_2 denote the end points of Λ located in regions I and II, respectively.

To avoid ambiguity due to the multiple-valued character of p, $p^{\frac{1}{2}}$, and w, we restrict the angle θ to the range $0 \leqslant \theta \leqslant 2\pi$ and define p and $p^{\frac{1}{2}}$ by the equations

$$p = r^{\frac{1}{2}}e^{\iota\theta/2}\varphi^{\frac{1}{2}}: \quad p^{\frac{1}{2}} = r^{\frac{1}{2}}e^{\iota\theta/4}\varphi^{\frac{1}{2}}.$$

$\varphi^{\frac{1}{2}}$ can be treated as single-valued. Let the point z_0 [Eq. (3)] be identified with z'. Then in the region I we have

$$\begin{gathered} p = \iota|p|: \quad p^{\frac{1}{2}} = e^{\iota\pi/4}|p|^{\frac{1}{2}}: \\ w = -\iota\lambda\textstyle\int_z^{z'}|p|\,d\zeta. \end{gathered} \quad (28)$$

In the region II to the right of z'

$$p = |p|; \quad p^{\frac{1}{2}} = |p|^{\frac{1}{2}}: \quad w = \lambda\textstyle\int_{z'}^{z}|p|\,d\zeta. \quad (29)$$

A cut extending from z' to the right along the axis of reals insures that we have a single branch of $w(z)$ to deal with.

In order to visualize the problem it is convenient to map the level lines of $|e^{\iota w}|$. Eqs. (28) and (29) show directly that the axis of reals passes through a mountain to the left of z', but that the portion of the axis of reals to the right of z' is a level line with $|e^{\iota w}| = 1$. Writing $z = x+\iota y$; $p = |p|e^{\iota\chi}$, the differential equation for the level lines is seen to be

$$dy/dx = \iota\frac{(p-p^*)}{(p+p^*)} = -\tan\chi, \quad (30)$$

where p^* is the complex conjugate of p. Treating φ in first approximation as constant over the

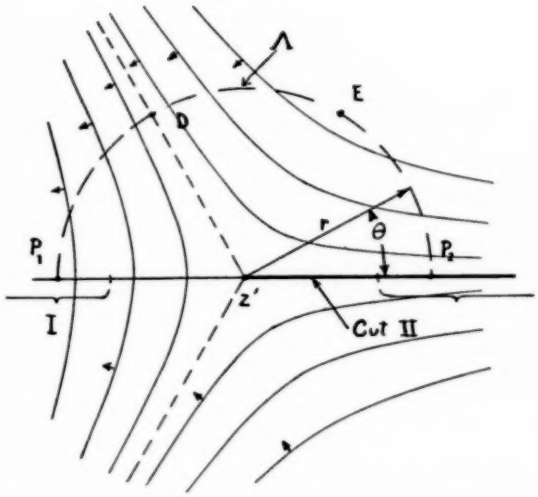

FIG. 3. Level lines of $|e^{iw}|$ for linear potential function. $|e^{iw}|$ is unity along cut and dotted lines radiating from Z'. Arrows indicate the uphill direction.

neighborhood of z' we obtain the equation $dy/dx = -\tan\frac{1}{2}\theta$ for the neighborhood in question. Fig. 3 shows the approximate form of the level lines derived from the above differential equation. Three lines radiate from the branch point z' and from every other simple zero point of $E-V(z)$. The exact forms of the contour lines will, of course, depend on $\varphi(z)$, but the distortion produced by φ is sure to be small if φ is smooth in the neighborhood of z'.

We identify the point ξ of Eqs. (11) with P_1, thus insuring that the a's and b's are sensibly equal on Λ. Let D denote the point where Λ crosses the line $|e^{iw}|=1$ which extends into the upper half plane. Then a_v will be sensibly constant between D and P_2 because f_v is dominant over this portion of Λ. It will also be constant over P_1D if a_i vanishes, or is very small, at P_1. It follows that if $\alpha_i \equiv a_i(P_1)=0$, $\alpha_v \cong \beta_v$. This fact, together with the reality condition gives the first connection formula.

Let us cast the argument in rigorous form. Denoting the point on Λ where $|e^{iw}|$ has its minimum value by E and the corresponding values of a_i and a_v by γ_i and γ_v, respectively, we apply Eq. (27) first to the arc P_1E and then to P_2E. Let μ_1 and μ_2 be the values of μ for these two sections of the path Λ. Then

$$\begin{aligned} |\gamma_v-\alpha_v| &< \tfrac{1}{2}\mu_1\{|\alpha_v|+|\alpha_i|\,|e^{2iw(P_1)}|\}, \\ |\gamma_v-\beta_v| &< \tfrac{1}{2}\mu_2\{|\beta_v|+|\beta_i|\}. \end{aligned} \tag{31}$$

Consider the application of these equations to a solution of Eq. (1) which is real on the axis of reals and which is of the f_v type at P_1. From the reality condition it follows that $\beta_i=\beta_v^*$ and $|\beta_i|=|\beta_v|$. If the function is to be of f_v type at P_1 we may assume that $|\alpha_i|\,|e^{2iw(P_1)}| \leqslant |\alpha_v|$. Hence

$$\begin{aligned} |\alpha_v-\beta_v| &< |\gamma_v-\alpha_v|+|\gamma_v-\beta_v| \\ &< \mu_1|\alpha_v|+\mu_2|\beta_v| < \mu_\Lambda\{|\alpha_v|+|\beta_v|\}. \end{aligned}$$

We can accordingly identify α_v and β_v in first approximation.

It follows from (28) that if α_v is given the value $e^{i\pi/4}$ the product $\alpha_v f_v$ is real in I and describes a real ψ function. Then $\beta_v=\beta_i^*=e^{i\pi/4}$. Thus the connection formula

$$\underbrace{e^{i\pi/4}f_v \equiv |p|^{-\frac{1}{2}}e^{-\lambda\int_{z'}^{z}|p|\,d\zeta}}_{\text{Region I}} \rightarrow \underbrace{2p^{-\frac{1}{2}}\cos\left[\lambda\int_{z'}^{z}p\,d\zeta-\frac{\pi}{4}\right]}_{\text{Region II}} \tag{32}$$

is established.

In this formula, following Langer, we draw the arrow from left to right to indicate that the approximate validity of the left-hand member implies that of the right, but that the converse statement is not true. In order to make clear the justification of this one-way street sign and to prepare the way for the derivation of the second connection formula, we observe that in virtue of the homogeneous linear character of Eqs. (9) and (10), the functions $a_i(z)$, $a_v(z)$ must be homogeneous linear in the constants of integration α_i, α_v. Hence β_i and β_v must be homogeneous linear functions of α_i and α_v. Thus a complete exact solution of the whole connection problem would involve a complete and exact determination of the matrix $\|g\|$ of the equations

$$\beta_i=g_{ii}\alpha_i+g_{iv}\alpha_v, \qquad \beta_v=g_{vi}\alpha_i+g_{vv}\alpha_v. \tag{33}$$

Our approximate solution of Eqs. (9) and (10) for the special case that $\alpha_i=0$ shows that

$$g_{vv}=1+\delta; \qquad g_{iv}=-i(1+\delta^*), \tag{34}$$

where δ is a small quantity of the order of magnitude of μ_A which we have neglected in (32).

Additional information regarding the matrix $\|g\|$ is obtainable from the fact that the Wronskian of any two exact solutions of the Schrödinger equation, say ψ and $\bar{\psi}$, is constant along the axis of reals.[7] Thus if

$$\psi=\alpha_i f_i+\alpha_v f_v; \qquad \bar{\psi}=\bar{\alpha}_i f_i+\bar{\alpha}_v f_v$$

in I, it follows that in I

$$W[\psi,\bar{\psi}]\equiv\psi\frac{\partial\bar{\psi}}{\partial z}-\bar{\psi}\frac{\partial\psi}{\partial z}=2\iota\lambda(\alpha_v\bar{\alpha}_i-\alpha_i\bar{\alpha}_v)=\text{constant}.$$

The Wronskian of the same pair of solutions in II takes the form

$$W[\psi,\bar{\psi}]=2\iota\lambda(\alpha_v\bar{\alpha}_i-\alpha_i\bar{\alpha}_v)(g_{vv}g_{ii}-g_{iv}g_{vi}).$$

Equating these two expressions for the Wronskian, we see that *the determinant of* $\|g\|$ *is unity*. Hence the inverse equations to (33) are

$$\alpha_i=g_{vv}\beta_i-g_{iv}\beta_v, \qquad \alpha_v=-g_{vi}\beta_i+g_{ii}\beta_v. \quad (35)$$

It follows from the reality condition that if $\beta_i=\beta_v^*$, the quantities $\alpha_i e^{\iota\pi/4}$ and $\alpha_v e^{\iota\pi/4}$ are real. Hence

$$g_{vi}=-\iota g_{ii}^*; \qquad g_{iv}=-\iota g_{vv}^*. \quad (36)$$

Combining the last relation with the requirement that $|g|$ be equal to unity, we obtain the following relation between g_{ii} and δ:

$$g_{ii}(1+\delta)+g_{ii}^*(1+\delta^*)=1. \quad (37)$$

If we neglect small quantities of the order of μ_A in comparison with unity, we may conclude that the real part of g_{ii} is $\frac{1}{2}$. The imaginary part of g_{ii} cannot be determined even approximately without an explicit evaluation of an integral of the form given in Eq. (17) over a path on which the exponential factor is very large. However, if we apply the inequalities (31) to the evaluation of $|\beta_v|$ when $\alpha_v=0$ we can derive the upper bound

$$|g_{ii}|=|g_{vi}|<\mu_A|e^{2\iota w(P_1)}|=\mu_A\exp\left[2\lambda\int_{P_1}^{z'}|p|d\zeta\right].$$

It does not seem necessary to include the details of this simple proof here.

Let us now consider the validity of the inverse of Eq. (32). If the relation in question were exact, we could, of course, invert it; but it is actually only approximate. We know from the derivation that if the left-hand member fits the function $\psi(z)$ exactly at P_1, the right-hand member fits the same function approximately at P_2 and along the neighboring portion of the axis of reals. The inverse relation would be the statement that if the right-hand member fits $\psi(z)$ exactly at P_2, the left-hand member is approximately correct at P_1. With the aid of our partial determination of the matrix $\|g\|$ we can test the validity of this statement. We accordingly assume as in the right-hand member of (32) that $\beta_i=\iota\beta_v=e^{\iota\pi/4}$. It follows that the corresponding values of α_v and α_i are not $e^{\iota\pi/4}$ and 0, but $e^{\iota\pi/4}[1-\delta^*+g_{ii}(\delta^*-\delta)]$ and $(\delta-\delta^*)e^{-\iota\pi/4}$. Although the correction to the value of α_i is small, its product by the dominant approximation function f_i is not necessarily small. Hence the left-hand member of (32) may be entirely incorrect if the right-hand member is exact.

The second connection formula is a direct consequence of (35) and our information regarding $\|g\|$. Consider an exact solution of (1) which has the form

$$\psi(x)=2p^{-\frac{1}{2}}\cos(w+\gamma)=e^{\iota\gamma}f_i+e^{-\iota\gamma}f_v$$

in the neighborhood of P_2. By (35) the corresponding values of α_i and α_v are, if we neglect small quantities of the order of μ_A,

$$\alpha_i=2e^{\iota\pi/4}\cos\left(\gamma-\frac{\pi}{4}\right):$$

$$\alpha_v=e^{\iota\pi/4}\left[2x\cos\left(\gamma-\frac{\pi}{4}\right)-\sin\left(\gamma-\frac{\pi}{4}\right)\right].$$

Here we have introduced the symbol x, for the unknown, but finite, imaginary part of g_{ii}. If γ is not too close to the critical value $-\pi/4$ (cf. the *first* connection formula) so that $|\cos(\gamma-\pi/4)|$ is not *much* smaller than $|\sin(\gamma-\pi/4)|$, the product $\alpha_v f_v$ is small compared with $\alpha_i f_i$. Hence we have the connection formula

[7] The writer is indebted to Dr. Eugene Feenberg for the observation that the second connection formula can be derived from the first by means of the properties of the Wronskian.

$$\underbrace{\cos\left(\gamma-\frac{\pi}{4}\right)|p|^{-\frac{1}{2}}e^{+\lambda\int_{z}^{z'}|p|\,d\zeta}}_{\text{Region I}}\leftarrow\underbrace{p^{-\frac{1}{2}}\cos\left[\lambda\int_{z'}^{z}p\,d\zeta+\gamma\right]}_{\text{Region II}}. \tag{38}$$

This is usually specialized by writing $\gamma=\pi/4$, but the possibility of a generalization has been indicated by Langer (last reference, Note 3).

In addition to the restriction on γ, the only condition for the validity of (32) and (38) is that there shall exist a path Λ in the upper half plane connecting P_1 with P_2, enclosing no complex zeros of p^2 and having the property that $\mu_\Lambda \ll 1$.

Both connection formulas in the form given above presuppose that the slope of the real curve $y=V(z)$ is negative at z'. In order to obtain the connection formulas for the case in which $V(z)$ has a positive slope at the classical turning point z' it is only necessary to make the transformation $z\rightarrow -z$ in (32) and (38) and to interchange the roles of the regions I and II.

5. Limiting Case Where One of the Connected Points Is at Infinity

So far we have assumed that the points P_1 and P_2 are located at finite distances from z' and can be connected by a good path Λ of finite length. In applying the B. W. K. method to energy level problems, however, we frequently wish to assume that $\psi(z)$ vanishes at $z=\pm\infty$. In this case it becomes necessary to discuss the changes in the coefficients a_i, a_v which occur in a path which extends to infinity along the axis of reals. Consider, for example, a case in which $p(z)$ is imaginary and bounded from zero for all real values of z to the left of the turning point z' of Fig. 1. Let it be required to find the values of β_i, β_v appropriate to P_2 when a_i is known to vanish at $z=-\infty$. The required transformation of the a's can be thought of as made in two steps, of which the first gives the values at P_1 in terms of those at $-\infty$ and the second is the one already studied giving the values at P_2 in terms of those at P_1.

Consider first the value of a_i at P_1, which as before we shall call α_i. It follows from Eq. (9) that

$$\alpha_i=\frac{\iota}{2\lambda}\int_{-\infty}^{P_1}Qf_i\psi dz. \tag{39}$$

As both f_v and ψ approach zero exponentially for large negative values of z, $|\alpha_i|$ is clearly very small. We compute an upper limit. Let z_1 denote the value of z at P_1. Eq. (39) is equivalent to

$$\alpha_i=\frac{\iota}{2\lambda^2}\int_{w(-\infty)}^{w(z_1)}\frac{Qe^{-\iota w}}{p^{\frac{1}{2}}}\psi dw.$$

Hence

$$|\alpha_i|<\tfrac{1}{2}\int_{w(-\infty)}^{w(z_1)}\left|\frac{Q}{\lambda^2p^{\frac{1}{2}}}\right|e^{-|w|}|\psi|\,|dw|.$$

Let m denote the maximum value of $|Q/\lambda^2p^{\frac{1}{2}}|$ in the range of integration. This we may assume to be small. Since $|\psi(z)|$ decreases monotonically as we pass from z_1 out to $-\infty$ along the axis of reals,

$$\begin{aligned}|\alpha_i|&<\frac{m}{2}|\psi(z_1)|\int_{w(z_1)}^{w(-\infty)}e^{-|w|}d|w|\\&<\frac{m}{2}|\psi(z_1)|e^{-|w(z_1)|}\\&<\frac{m}{2|p(z_1)^{\frac{1}{4}}|}[|\alpha_i|+|\alpha_v|e^{-2|w(z_1)|}].\end{aligned} \tag{39a}$$

If $m/|p(z_1)^{\frac{1}{4}}|$ is much less than unity, $|\alpha_i|\ll|\alpha_v|e^{-2|w(z_1)|}$.

By analogy with the corresponding problem for a finite path one expects that α_v is sensibly equal to the limiting value of $a_v(z)$ as z moves out to $-\infty$. It is not necessary, however, to investigate this point in order to deal with the eigenvalue-eigenfunction problem.

Consider the application of Eqs. (33) to the determination of β_i and β_v when $a_i(z)$ vanishes at the negative end of the axis of reals. In view of the upper bounds on $|\alpha_i|$ and $|g_{vi}|$

$$|g_{vi}\alpha_i|<\frac{m}{2|p(z_1)^{\frac{1}{4}}|}\mu_\Lambda|\alpha_vg_{vv}|.$$

Thus, by Eqs. (33), if P_1 is connected with P_2

by a good path, and if $|Q(z)/\lambda^2 p(z)^{\frac{1}{2}}p(z_1)^{\frac{1}{2}}|$ is small between P_1 and $-\infty$, β_v has sensibly the same value as if α_i were zero, i.e., β_v is sensibly equal to α_v. We conclude that the connection formula (32) remains valid when the point P_1 is moved out to infinity along the negative axis of reals, provided that $m/|p(z_1)^{\frac{1}{2}}| \ll 1$.

6. Evaluation of the Low Energy Levels of a One-Dimensional Oscillator

The usual wave mechanics derivation of the Sommerfeld "phase integral" quantum condition (with half-integral quantum numbers) is based on the use of the connection formulas and loses its validity when applied to the lower energy levels. Thus in the case of the Planck ideal linear oscillator, where $V(z)=\frac{1}{2}kx^2$, we have

$$Q=k(E+6V)/(E-V)^2. \tag{40}$$

The minimum value of $|Q/\lambda^2 p^2|$ consistent with the reality of p occurs at the origin and is $k/(8\lambda^2\mu E^2)$. In the case of the lowest energy level the value is $\frac{1}{2}$ and the corresponding minimum value of $\lambda^{-1}\int|Q/p|ds$ for any path joining the region of classical vibration with any point outside this region is $\frac{1}{3}$. As this is of the order of unity, appreciable departures from the connection formulas are to be expected for this lowest energy level, and it is surprising to note that the value of E given by the phase integral formula is in *exact* agreement with the rigorous value obtained by other methods. Thus one is led to inquire whether there is not some way of validating the Sommerfeld formula without assuming the existence of good paths joining the region of classical vibration with the regions of imaginary momentum on the axis of reals.

Birkhoff[8] has recently sketched a proof of the phase integral formula applicable to the lower energy levels. Partly, however, due to the fact that Birkhoff's technique is unfamiliar to physicists, and partly because his proof rests on a plausible, but as yet unverified assumption, it seems worth while to give an independent derivation here.

Let the problem under discussion be that of finding the discrete energy levels of a one-dimensional oscillator with the fundamental interval $-\infty<z<+\infty$ and a single potential valley in which the classical local momentum $p(z, E)$ takes on real values. We shall assume at first that $V(z)$ has the special parabolic form $V=\frac{1}{2}kz^2$ and consider later on the modification of the argument for an anharmonic oscillator.

Let the complex z plane have a cut extending from the left-hand classical turning point z' through the right-hand turning point z'' to $+\infty$ along the axis of reals. The functions p, $p^{\frac{1}{2}}$ and w are uniquely defined over the cut plane by the requirement that they conform to Eqs. (28) for all negative real values of $z-z'$. They will then conform to Eqs. (29) on the upper lip of the cut between z' and z''. For positive real values of $z-z''$ we have

$$\begin{aligned}
&\text{Upper lip:}\quad p=-\imath|p|;\quad p^{\frac{1}{2}}=e^{-\imath\pi/4}|p^{\frac{1}{2}}|;\qquad w=\lambda\int_{z'}^{z''}|p|d\zeta-\imath\lambda\int_{z''}^{z}|p|d\zeta;\\
&\text{Lower lip:}\quad p=-\imath|p|;\quad p^{\frac{1}{2}}=-e^{-\imath\pi/4}|p^{\frac{1}{2}}|;\quad w=-\lambda\int_{z'}^{z''}|p|d\zeta-\imath\lambda\int_{z''}^{z}|p|d\zeta.
\end{aligned} \tag{41}$$

We designate by III that portion of the region of imaginary momentum on the axis of reals to the right of z'' where $|Q/\lambda^2 p^2|\ll 1$ (cf. Fig. 4). It follows from Eqs. (41) that $|e^{\imath w}|$ is very large in both of the regions I and III. The level lines of $|e^{\imath w}|$ are readily sketched in and show that any path connecting I with III and avoiding the classical portion of the axis of reals must cross a single valley between the ridges on which it terminates. This is true whether the path lies in the upper or lower half plane.

Let z_1 and z_3 be any two points on the axis of reals in I and III, respectively. It follows from (40) that in the case of the parabolic potential function under consideration it is always possible to join z_1 and z_3 by a path Λ for which $\mu_\Lambda\ll 1$. In more general cases such a path will exist provided

[8] G. D. Birkhoff, Bull. Am. Math. Soc. **39**, 696 (1933).

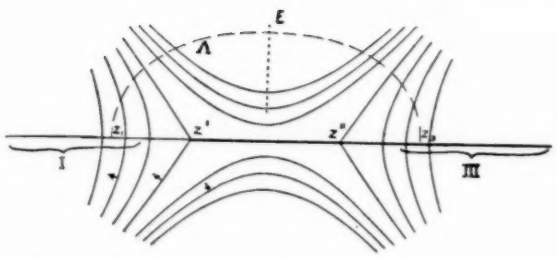

FIG. 4. Level lines of $|e^{iw}|$ for harmonic oscillator.

there are no complex zeros of $V-E$ near to z' and z''.

Let us now assume that we have to do with an eigenvalue of the energy $E=E_n$ and a corresponding eigenfunction $\psi_n(z)$. Then ψ_n vanishes at both ends of the axis of reals. Since $f_i(z)$ becomes infinite at both ends of this axis, a_i must vanish there. It follows from our previous analysis that a_i is very small at both of the points z_1 and z_3. Let E denote the point where the path Λ crosses the bottom of the valley, i.e., the point on Λ where $|e^{iw}|$ takes on its minimum value. Integration from z_1 to E shows that a_v is sensibly constant along the corresponding portion of Λ. Similarly integration from z_3 to E shows that it is constant along the rest of Λ. If we reflect the path Λ in the axis of reals we get a second path connecting z_1 with z_3 along which a_v is constant neglecting small quantities of the order of $\mu_\Lambda a_v(z_1)$. The existence of these two paths shows that a_v takes on the same values on the upper and lower edges of the cut at z_1. ψ_n is, of course, single-valued along the entire axis of reals. Hence $f_v(z)$ must have the same value on the upper and lower edges of the cut at z_3. Equating the two values of f_v in question and using the corresponding values of $p^{\frac{1}{2}}$ and w given in Eqs. (41), we obtain

$$\exp\{\lambda\textstyle\int_{z'}^{z''}|p|d\zeta\}=-\exp\{-\lambda\int_{z'}^{z''}|p|d\zeta\},$$

or the familiar equation

$$\oint p\,dz=(n+\tfrac{1}{2})h. \tag{42}$$

The accuracy of the result is limited only by the quality of the path Λ. But in the case of the ideal linear oscillator it is possible to reduce the value of μ_Λ below any assignable quantity by choosing the path Λ as a semicircle of sufficiently large radius with the origin as its center. Hence the above equation is *exact* for the case under discussion.

Turning now to the problem of the *anharmonic oscillator*, we observe that in order to secure single-valued functions f_i, f_v it is necessary to introduce cuts extending from the complex roots of $E-V$ to infinity. The argument then goes through exactly as in the case of the harmonic oscillator except that the path Λ must lie inside all the roots above mentioned in order to avoid crossing the cuts. Consequently it is not possible to reduce the value of μ_Λ below a certain minimum determined by the location of the roots of $E-V$. The formula (42) is essentially inexact for anharmonic oscillators.

The uncertainty δE in the energy due to the fact that μ_Λ and m do not actually vanish is readily calculated if we retain terms of the first order in these two infinitesimals. Let $\bar{a}_i(z_3)$ and $\bar{a}_v(z_3)$ denote the values of $a_i(z)$ and $a_v(z)$ on the lower edge of the cut at z_3. Equating the approximate expressions for ψ on the two edges of the cut at z_3 in terms of f_i, f_v we obtain

$$e^{i(\pi+\lambda J)}=\frac{a_v(z_3)+e^{2\lambda\int_{z''}^{z_3}|p|d\zeta}\bar{a}_i(z_3)}{\bar{a}_v(z_3)+e^{2\lambda\int_{z''}^{z_3}|p|d\zeta}a_i(z_3)}.$$

Let ϵ_v and $\bar{\epsilon}_v$ denote the small quantities $a_v(z_3)-a_v(z_1)$, $\bar{a}_v(z_3)-a_v(z_1)$, respectively. To a first approximation

$$i(\pi+\lambda J)=\log_e\left\{1+\frac{\epsilon_v-\bar{\epsilon}_v+[\bar{a}(z_3)-a_i(z_3)]e^{2\lambda\int_{z''}^{z_3}|p|d\zeta}}{a_v(z_1)}\right\}.$$

Introducing appropriate upper bounds for ϵ_v, $\bar{\epsilon}_v$, $|a_i(z_3)|$, $|\bar{a}_i(z_3)|$ from the inequalities (27) and (39a), we obtain

$$|\pi+\lambda J-2\pi k|<\mu_\Lambda+m/|p(z_3)^{\frac{1}{2}}|,\quad k=0,\ 1,\ 2,\ \cdots,$$

where m is the maximum value of $|Q/\lambda^2p^{\frac{1}{2}}|$ between z_3 and $+\infty$. Let ΔE denote the quantity $h\partial E/\partial J$ which measures the approximate spacing of the energy levels given by the Sommerfeld formula. Then

$$\frac{\delta E}{\Delta E}=\frac{1}{2\pi}\left(\mu_\Lambda+\frac{m}{|p(z_3)^{\frac{1}{2}}|}\right).$$

The writer has carried through a calculation of μ_Λ and $m/|p(z_3)^{\frac{1}{2}}|$ for the Morse curve potential function corresponding to the normal state of the

II_2 molecule. For simplicity of computation the energy E was so chosen as to bring the classical turning points z' and z'' together. Λ was taken to be a semicircle with radius equal to half the distance from z' to the nearest complex root of $p^2(E, z)$. Under these circumstances μ_Λ is approximately 0.015 and $m/|p(z_3)^3|$ is 7.5×10^{-5}. The corresponding value of $\delta E/\Delta E$ is 0.0025, showing that the B. W. K. approximation should give the energy correct to at least two or three tenths of a percent of the spacing of adjacent levels. Of course the actual error involved should be appreciably less than this upper limit.

7. Higher Order Approximations

It is well known that our functions f_i, f_v can be obtained from (1) by making the transformation $\psi=e^{i\lambda\int y dz}$, expanding y formally in powers of h, or $1/\lambda$, and taking only the first two terms of the series. By taking n terms of the series, one obtains functions $f_i^{(n)}$, $f_v^{(n)}$ having properties similar to those of f_i and f_v. The series are semiconvergent and hence the $f^{(n)}$'s, regarded as approximate solutions of (1), at first improve in quality as n increases, and then grow worse. They obey equations of the form

$$\frac{d^2f^{(n)}}{dz^2}+[\lambda^2p^2-Q^{(n)}]f^{(n)}=0,$$

where $Q^{(n)}(z, E)$ is a polynomial in $1/\lambda$ beginning with a term of degree $n-2$. If $Q\equiv Q^{(2)}$ is small at any point of the complex plane, $|Q^{(n)}|$ will be smaller than $|Q|$ provided that $n>2$, but not too large. Thus if $|Q/p^2|$ is small along a path Λ joining z_1 and z_3, $|Q^{(n)}/p^2|$ will be still smaller. We infer that the argument used to prove that, in the case of an anharmonic oscillator and an eigenvalue of E, the function f_v has sensibly the same values on the upper and lower edges of the cut in the region III, is applicable with a higher degree of precision to $f_v^{(n)}$. It follows at once that the energy level condition[9]

$$\oint y_v^{(n)}dz=mh, \quad m=0, 1, 2, \cdots \qquad (43)$$

is even more accurate than (42) for small values of n greater than 2.

[9] Cf. J. L. Dunham, Phys. Rev. **41**, 713 (1932). Dunham's derivation of (43) is fundamentally sound, though no more rigorous than Zwaan's proof of the connection formulas.

8. Modification of the B. W. K. Method for the Radial Equation in the Two-Body Problem

In applying the B. W. K. method to the radial equation of the two-particle problem one meets with an apparent difficulty in that the B. W. K. approximations do not have the right character to fit the exact solutions of the differential equation at the left-hand boundary point $r=0$. As Kramers has pointed out, however, it is possible to fit the boundary conditions at both ends of the fundamental region if we modify the approximation formulas by the addition of the term $h^2/32\pi^2\mu r^2$ to the potential energy. The added term is negligible except in the immediate neighborhood of the origin, and it is ordinarily possible to find a good path Λ leading from the origin around the classical turning points (there is only one when the angular momentum is zero) in the complex plane to a point on the axis of reals outside the region of classical motion where the approximation function is good. In this manner it is possible to apply to the two-particle problem essentially the same reasoning as we have used above for the anharmonic oscillator in the interval $-\infty<z<+\infty$. One obtains the energy level formula (42) with $p(r, E)$ modified by the substitution of $(l+\frac{1}{2})^2$ for $l(l+1)$ in the term which gives the contribution of centrifugal force to the effective potential energy of the radial vibration. Further details regarding this application of our technique will be published elsewhere.[10]

9. The Transmission of Progressive Matter Waves Through a Potential Barrier

The transmission of matter waves through potential barriers has been the subject of much discussion,[11] but so far as the writer has been able to discover there has been no application of the B. W. K. method to this problem that is properly applicable to cases in which the energy of the incident particles is not very different from the maximum potential energy of the barrier.

Let us assume a rounded potential hill of approximately parabolic form. Consider first the

[10] In a book on the general principles of quantum mechanics now in preparation.

[11] Cf., e.g., N. H. Frank and L. A. Young, Phys. Rev. **38**, 80 (1931).

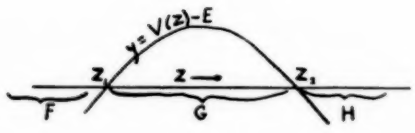

FIG. 5.

case in which the top of the hill projects above the energy level of the incident particles. We divide the axis of reals of the complex z plane into three parts F, G, H, separated by the classical turning points z_1, z_2 as indicated in Fig. 5. Single-valued functions f_i, f_r are obtained by introducing a cut along the axis of reals from z_1 to $+\infty$ and by choosing those branches of p and $p^{\frac{1}{2}}$ which are negative real and negative imaginary, respectively, in F. p, $p^{\frac{1}{2}}$, and w are to be analytic over the cut plane. p is then real and positive in H and positive imaginary in G. On both sides of the hill the function

$$f_r e^{-2\pi i Et/h} = p^{-\frac{1}{2}} \exp\left\{\frac{2\pi i}{h}\left[\int_{z'}^{z} p\,d\zeta - Et\right]\right\}$$

describes an outgoing wave, while $f_r e^{-2\pi i Et/h}$ describes an incoming wave. The level lines of e^{iw} for a parabolic potential function are shown in the figure. f_r is dominant in most of the first and third quadrants, while f_i is dominant in most of the second and fourth quadrants.

Let us assume that progressive waves are incident on the potential hill from the left side only. There will then be reflected as well as incident waves in F, but only transmitted waves in H. We accordingly assume that a_r vanishes in the first quadrant where f_r is dominant. Let the regions F and H be connected by a good path Λ. Then a_i will be sensibly constant along this path. Thus we have a connection formula of the type

$$f_i + c f_r \rightarrow f_i, \tag{44}$$

where c is a constant whose value has yet to be determined. As a matter of fact we can evaluate only the modulus of c. This is done by using the constancy of the current density

$$D[\psi] = \frac{h}{4\pi i}\left(\psi^* \frac{d\psi}{dz} - \psi \frac{d\psi^*}{dz}\right)$$

on the axis of reals. Choosing z_1 as the origin of the integral w, we give e^{iw} the absolute value 1 in the region F and the absolute value e^{-K} in H where K denotes the integral $(2\pi/h)\int_{z_1}^{z_2} |p|\,d\zeta$. The right-hand member of (40) now represents a current of density e^{-2K} in the direction of the positive z axis, while the left-hand member represents a current with the density $cc^* - 1$ in the same direction. Equating these two currents, we find that $cc^* = 1 + e^{-2K}$. The corresponding transmission coefficient is

$$T = e^{-2K}/cc^* = 1/(1+e^{2K}). \tag{45}$$

This formula is free from all restrictions depending on the height of the hill provided that $E - V_{\max} < 0$. Like Eq. (42) it is easily seen to hold for any analytic potential hill which yields no zeros of $E - V$ near z_1 and z_2 and hence permits a good path Λ joining the regions F and H.

If the maximum potential energy is less than the energy of the incident particles, a parabolic potential function yields two imaginary roots of $E - V(z)$, $z = \pm i\{2(E - V_{\max})/k\}^{\frac{1}{2}}$, where k denotes the negative of V''. Denoting these roots by z_1 and z_2 and the integral $(2\pi/h)\int_{z_1}^{z_2} |p|\,|d\zeta|$ by K', it is not difficult to prove that the transmission coefficient is

$$T = 1/(1+e^{-2K'}). \tag{46}$$

The reader will observe that the formulas (45) and (46) join continuously in the limiting case where $z_1 = z_2 = 0$, giving the common value $\frac{1}{2}$ for T.

The writer is greatly indebted to Dr. Eugene Feenberg, Professor G. D. Birkhoff and Professor J. H. Van Vleck for helpful suggestions.

A Theory of Liquid Surface Rupture by a Uniform Electric Field

LEWI TONKS, *Research Laboratory, General Electric Company*

(Received June 28, 1935)

Surface distortion and rupture permits field emission from liquid surfaces at field strengths less than those effective for equally smooth solid surfaces. An approximate mathematical theory of the rupture of a plane liquid surface in a uniform electric field has been developed. The relation between initial distortion, rupture time, and field strength has been calculated for fields large compared to that which just renders the surface unstable. This critical field is $E_m = 2\pi^{1/2}(\rho g T)^{1/4} = 53$ kv cm^{-1} for mercury, where ρ is density and T is surface tension. Typically, the theory shows that a hump initially 4×10^{-5} cm high and of diameter 9×10^{-4} cm will lead to rupture in 5×10^{-6} sec. in a field of 10^6 v cm^{-1}. Relative to initial humps in the surface whose linear dimensions vary inversely as the square of the field, the time to rupture varies inversely as the cube of the field strength. This calculation shows that a lowered sparking potential to liquid mercury can be ascribed to surface rupture and shows that it is possible that surface rupture plays a part in Beams' low field emission from liquid mercury. Possible application of the theory to the high field condition at the cathode spot of the Hg arc is not clear.

IN the course of a study I have been making on the breakdown between a metal electrode and a liquid (Hg) surface close to it, I have observed that sparking occurs at considerably lower voltages just above the freezing point than below it. This suggested that the plane surface of the liquid might be deformed by the mechanical force accompanying the electric field, thereby concentrating the field, augmenting the disruptive force, finally building up a point sharp enough to give field emission and initiating the discharge. The same theory might apply to experiments performed by J. W. Beams[1] in which he applied 1 microsecond pulses of increasing voltage across an iron-mercury vacuum gap. Whereas theory requires 3×10^7 v/cm for appreciable field emission, he found that an arc started at 1.8×10^6 v/cm with clean mercury. The duration of the voltage pulse was deemed too short for the liquid to respond mechanically, but no analysis supporting this view was offered. According to the following approximate treatment, a field of 1.8×10^6 v/cm^{-1} would suffice to give field emission in 10^{-6} sec., so that it is quite possible that point formation on the liquid was responsible for initiating the arc.

Furthermore, as Dr. Langmuir has suggested, peak formation may be occurring in the intense field at the cathode spot of the Hg arc.

The bursting condition, $E^2 > 16\pi T/R$, for a liquid droplet of radius R and surface tension T subjected to a radial surface field E is well known, and the distortion and disruption of bubbles has been frequently investigated.[2] The present problem differs essentially from the older one in that the stability of a surface of zero curvature is to be investigated and we are interested in the development of distortion as a function of time.

The problem can be considered in two parts; first, what is the relation between applied field, surface distortion and resulting net pressure on the surface; and second, what will the motion of the liquid be under the influence of this pressure?

The rigorous solution is impossibly complicated, so that an approximate treatment will be followed from the very start. Consider an axially symmetrical hump in the liquid surface as indicated in Fig. 1. Let us use the three quantities, R, y and r to characterize it, R being the radius of curvature at the vertex of the hump, y the height of the vertex above the undisturbed

[1] J. W. Beams, Phys. Rev. **44**, 803 (1933). In a very recent letter J. W. Beams describes tests performed by Mr. Quarles which indicate that in the time duration and field strength range where he was working surface rupture of the kind discussed here was not occurring. It is too early to say just what the relation is between those experiments and the present theory.

Note added in proof: Since submission of this paper, an article by L. R. Quarles, Phys. Rev. **48**, 260 (1935), describes experiments showing that at the high fields emission did not depend upon a time response of the surface. In a private communication, however, Professor Beams states that the sparking voltage did begin to decrease markedly for application times of several microseconds, so that it would be there that the theory developed in the present paper should find application.

[2] C. T. R. Wilson and G. I. Taylor, Proc. Camb. Phil. Soc. **22**, 728 (1925); J. J. Nolan, Proc. Roy. Irish Acad. **37**, 28 (1926); W. A. Macky, Proc. Camb. Phil. Soc. **26**, 421 (1930); Proc. Roy. Soc. **A133**, 565 (1931); J. J. Nolan and J. G. O'Keeffe, Proc. Roy. Irish Acad. **40**, 86 (1932); G. D. West, Proc. Phys. Soc. **44**, 336 (1932); J. Zeleny, Phys. Rev. **16**, 102 (1920); **47**, 638 (1935).

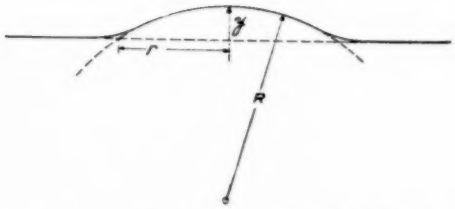

FIG. 1. Shape of hump assumed in liquid surface.

level, and $2r$ the effective diameter of the hump, taken here as the diameter of the small circle cut from the $y=0$ plane by the sphere R. By geometry

$$yR=\tfrac{1}{2}(r^2+y^2). \tag{1}$$

We now analyze the component pressures on the vertex of the hump. The impressed uniform field will be denoted by E_0 and the enhanced field at the vertex by E. The pressure transmitted to the vertex from the undisturbed portion of the liquid surface is made up of three components, (1) the pressure A of any atmosphere above the liquid, (2) the hydrostatic pressure $-\rho gy$, ρ being the density of the liquid, and (3) the electric pressure $-E_0^2/8\pi$, with a total value for the three of $A-\rho gy-E_0^2/8\pi$. This is the upward pressure exerted against the hump vertex by the liquid beneath it. The downward pressure there also has three components; (1) that of the atmosphere, (2) that arising from surface tension, $2T/R$, where T is the surface tension of the liquid, and (3) the electric pressure, $-E^2/8\pi$, totaling $A+2T/R-E^2/8\pi$. Subtracting the latter from the former gives the net upward pressure P at the vertex:

$$P=(E^2-E_0^2)/8\pi-\rho gy-2T/R. \tag{2}$$

If P is positive for any assumed conditions, then the surface tends to greater distortion; if negative, it tends to flatten out.

To relate E to y and r we note that for $y=r$, that is, for a hemispherical boss on a plane, the field is three times the normal. Accordingly, we assume the linear relation

$$E=E_0(1+2y/r) \tag{3}$$

which fits the two values $y/r=0$ and $y/r=1$ and lies sufficiently close to the theoretical values for our treatment.

Substitution into Eq. (2) of Eq. (3) to eliminate E, and of Eq. (1) to eliminate R gives

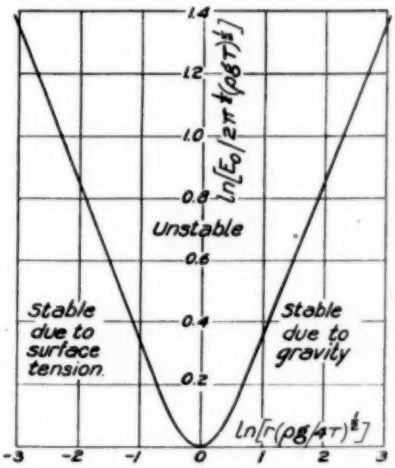

FIG. 2. Stability of surface relative to impressed field E_0 and hump radius r. Exponent of (ρgT) should be $\frac{1}{4}$.

$$P=yE_0^2/\pi\left[\frac{y+r}{r^2}-\frac{4\pi T/E_0^2}{y^2+r^2}-\frac{\pi\rho g}{E_0^2}\right]. \tag{4}$$

This equation shows that we are dealing with a disturbance that has no equilibrium condition. When the bracket is positive, y tends to increase, which in turn increases the value of the bracket. When the bracket is negative and y decreases as a result, the bracket becomes still more negative.

We must suppose that the disturbance arises as a continuous transition, so that in investigating the incipient distortion, $y \ll r$, and we may neglect y in the brackets. Thus we find that the growth or subsidence of a small distortion ensues according as

$$1/r > \text{or} < (4\pi T/E_0^2)/r^2+\pi\rho g/E_0^2$$

or, in terms of the field, as

$$E_0^2 > \text{or} < 4\pi T/r+\pi\rho gr. \tag{5}$$

The stable and unstable regions in the E_0r plane are mapped in Fig. 2. The minimum value E_m of E_0 which will cause instability and the corresponding value r_m of r are seen to be

$$E_m=2\pi^{\frac{1}{4}}(\rho gT)^{\frac{1}{2}},\ r_m=2(T/\rho g)^{\frac{1}{2}}. \tag{6}$$

Taking $T=450$ dynes cm^{-1} and $\rho=13.6$ g cm^{-3} for mercury and $g=980$ cm sec.$^{-2}$, the numerical values are 52,700 v/cm^{-1} (176 e.s.u.) for E_m and 0.367 cm for r_m. The interpretation to be made of the plot is that on a large free surface subjected to a given E_0 which is greater than E_m, only those distortions will grow those radii lie within

the limits indicated. This suggests an experimental test in which r is limited to values less than that given by Eq. (6).

The answer to the first portion of the problem is now seen to be: Below a certain field strength, E_m, no distortion of the surface arises, but above that field strength the distortion increases progressively under the net unbalanced pressure P.

In particular, it can easily be shown that for $r=r_m$, the bracket in Eq. (4) becomes

$$(1-(E_m/E_0)^4)/2A, \tag{7}$$

where $A=8\pi T/E_0^2$. As the $(E_m/E_0)^4$ term represents the gravitational force, it is evident that when $E_0^4 \gg E_m^4$ gravitation can be neglected, a condition which is sufficiently well satisfied when $E_0 > 3E_m$.

As the hump develops, liquid flows into it from its immediate neighborhood. On the average, this flow will extend over a distance comparable with r, so that associated with a surface area a at the vertex of the hump, a volume of liquid ar is in motion with a velocity $\dot{y}$. The corresponding momentum is thus $\rho ar\dot{y}$. Its rate of increase is equal to the force acting, whence

$$aP=\rho a d(r\dot{y})/dt.$$

By substituting from Eq. (4), we find for the equation of motion

$$d(r\dot{y})/dt=B^2 y\left(\frac{r+y}{r^2}-\frac{A/2}{r^2+y^2}-\frac{\pi\rho g}{E_0^2}\right), \tag{8}$$

where $B^2=E_0^2/\pi\rho$. If we confine attention to fields greater than $3E_m(=0.158$ MV/cm for mercury) the gravitational term can be neglected in accordance with Eq. (7). If, further, new variables

$$\tau=(B/A)t,\ w=y/A,\ \sigma=r/A \tag{9}$$

be substituted, Eq. (8) becomes

$$d(\sigma\dot{w})/d\tau=w\left(\frac{\sigma+w}{\sigma^2}-\frac{1/2}{\sigma^2+w^2}\right) \tag{10}$$

where, as later, the dot represents the derivative with respect to the time-like variable.

To solve this equation, the relation between σ (r) and w (y) must be known. It seems reasonable to assume that r varies in such manner as to give the right member of Eq. (8), and hence of Eq. (10), the maximum value. In other words, the development of the disturbance "follows the path of least resistance."

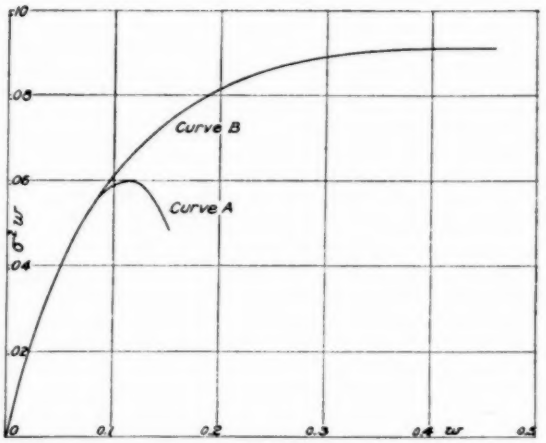

FIG. 3. Method of determining relation between hump height ($\sim w$) and radius ($\sim\sigma$).

The routine analysis for this condition leads to the parametric equations

$$w=\lambda^4/(1+\lambda^2)^2(2+\lambda),\ \sigma=\lambda w. \tag{11}$$

It is certainly to be expected that as the deformation progresses, the volume of the hump shall not decrease. But plotting $\sigma^2 w$, as a measure of the volume, against w, these equations lead to curve A of Fig. 3. We must, accordingly, modify our original assumption so as to have it apply only to the initial stage of deformation. Subsequent to this we postulate that the volumetric change approaches zero as y (w) approaches r (σ). This anticipates the second stage in the surface deformation which begins when y (w) exceeds r (σ), and throughout which it will be assumed that the hump volume is constant. The extrapolation of the beginning of curve A, Fig. 3 in accordance with this change in assumption was carried out by plotting first differences along A up to $w=0.08$, and from there fairing in a first difference curve to cross the axis where $\sigma=w$, which occurs at about $w=0.45$. Curve B is the continuation of curve A based on this method. The values of σ which have been calculated from curve B are shown plotted against w in Fig. 4. This made it possible to plot $f(w)$, the right member of Eq. (10), as a function of w in Fig. 5.

We can now proceed to solve Eq. (10). In so doing we shall confine ourselves to that solution whose initial condition is $w=0$ and $\dot{w}=0$ at

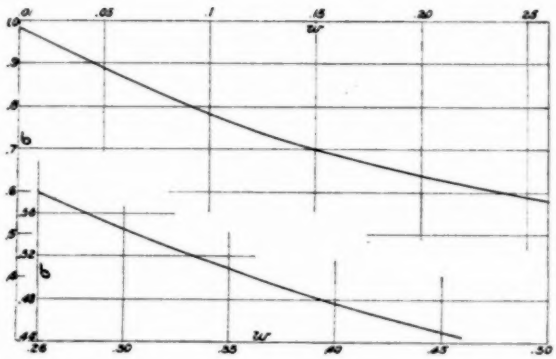

FIG. 4. Hump radius ($\sim\sigma$) as a function of height ($\sim w$).

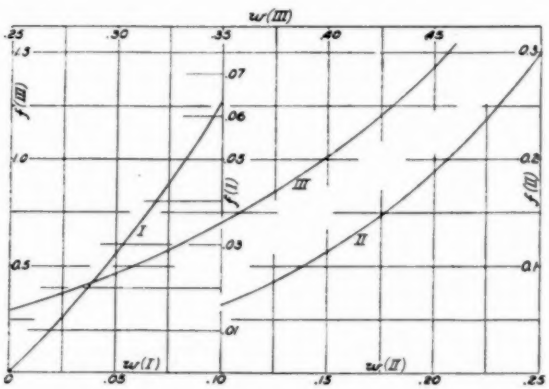

FIG. 5. The function $f(w)$.

$\tau=-\infty$. the magnitude of the time interval for disruption will not depend markedly enough on the initial relation of velocity to displacement to warrant carrying out a number of numerical integrations for different initial conditions.

For small values of w the solution

$$w=w_0 \exp(\tau/2^{\frac{1}{2}}) \tag{12}$$

is exact to the degree that $2w_0$ is negligible compared to unity. This equation therefore serves to establish the initial conditions, $w=w_0$, $\dot{w}=w_0/2^{\frac{1}{2}}$ at $\tau=0$, for the numerical integration, and to permit extrapolation to find the times involved when the initial disturbance is less than w_0.

For the numerical integration the value

$$w_0=0.04, \text{ so that } \dot{w}_0=0.0283 \tag{13}$$

was chosen, and the calculation was carried out by well-known methods.[3] Fig. 6 shows the height of the hump as a function of time. Denoting the values of w, σ and τ when $w=\sigma$ by the subscript 1, it was found that $w_1=\sigma_1=0.450$, $\tau_1=2.41$, and $\dot{w}_1=0.431$. These are the initial conditions for the second phase of the rupture in which no new liquid enters the hump but the concentration of force at the vertex creates a rapid peaking. Thus, at the beginning of the second stage we have for y, R, r, and $\dot{y}$:

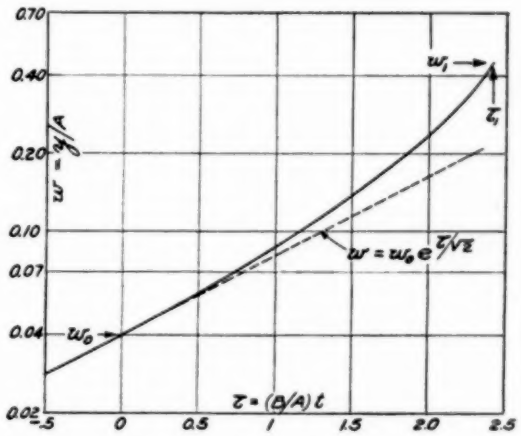

FIG. 6. Hump height as a function of time.

$$\begin{aligned} y_1=R_1=r_1=w_1A=0.450A \\ t_1=\tau_1A/B=2.41A/B, \\ dy_1/dt=\dot{w}_1B=0.431B. \end{aligned} \tag{14}$$

In this second stage we shall suppose that the shape of the hump near the vertex is that of a cylinder terminated by a sphere, as shown in Fig. 7, and that the growth of the peak is by the upward flow of liquid from the cylindrical zone of altitude, $R/2$, just below the base of the hemisphere to form an additional segment of narrower cylinder capped by a smaller hemisphere. Again this is a rough approximation, for the assumption itself leads to a cone frustum rather than a cylinder below the hemisphere.

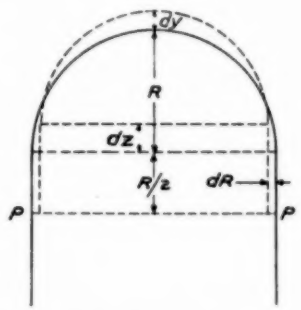

FIG. 7. Hump vertex assumption in second stage.

[3] R. E. Root, *Mathematics of Engineering* (1927), § 74.

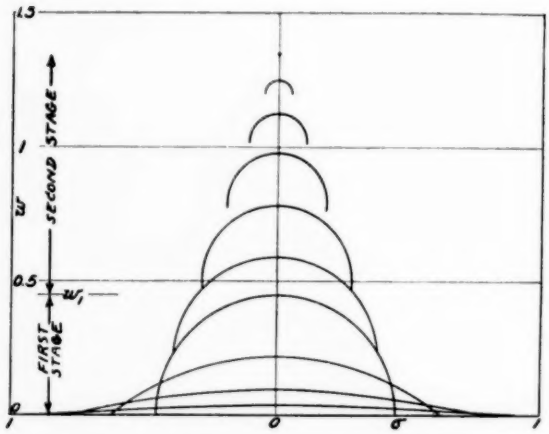

FIG. 8. Evolution of hump.

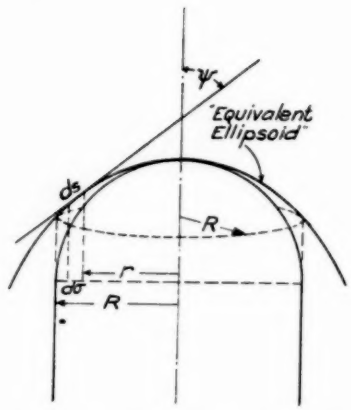

FIG. 9. Method of calculating force on the vertex.

Of more importance will be the neglect of differences in velocity at different points of the hump through treating the motion as that of a rigid body of variable mass when the equation of motion is written. It appears probable that taking this factor into account would explain the thread and ultimately the drop formation which has been observed in the bubble and droplet disruption experiments. The present hypothesis, however, leads to an infinitely sharp peak when y reaches $3y_1$, as shown by Eq. (24), and it is this condition which shall be deemed to be surface rupture.

Incidentally, this relation permits the delineation of the sequence of hump shapes from the initial small distortion of stage one through to rupture itself. This is illustrated in Fig. 8 where no attempt has been made to show regular time intervals.

Although the postulated shape of the hump peak during the second stage is that of a hemisphere upon a cylinder, the configuration left by the termination of the first stage is a hemisphere upon a plane. Yet it does not seem worth while to devise a special treatment for this transitional phase, particularly as the whole duration of stage two is but a fraction of that of stage one.

Equating of volumes above the PP plane of Fig. 7 before and after deformation gives

$$dy = -2dR, \tag{15}$$

dR being intrinsically negative. The volume is $(5/6)\pi R^3$ and its center of gravity moves upward $-(3/2)dR$, so that its momentum is

$$-(3/2)dR(5/6)\pi R^3(\dot{y}/dy)\rho = (5/8)\pi\rho R^3\dot{y}. \tag{16}$$

To calculate the force increasing this momentum we shall treat the hump as an ellipsoid of semi-major axis y and radius of curvature at the end of this axis R. The force will then be taken as the resultant acting on the portion of the equivalent ellipsoid within a circle of radius R on its surface, as indicated in Fig. 9.

The semi-minor axis, b, of the ellipse and the eccentricity e are given, respectively, by

$$b^2 = yR, \quad e^2 = 1 - R/y. \tag{17}$$

The charge density C at the vertex is

$$C = \frac{E_0}{4\pi} \frac{e^3}{(1-e^2)\{(1/2)\ln[(1+e)/(1-e)]-e\}}. \tag{18}$$

Elsewhere it is $C\sin\psi$. The vertical component of force acting on the surface element ds is

$$dF = 2\pi C^2 \sin^3\psi ds = 2\pi C^2 \sin^2\psi d\sigma. \tag{19}$$

Using r to denote distance from the hump axis, we have

$$\sin^2\psi = \frac{(1-e^2)[y^2(1-e^2)-r^2]}{[y^2(1-e^2)^2+e^2r^2]}. \tag{20}$$

Integration of dF from $r=0$ to $r=R$ after the substitution of Eq. (20) into (19) gives

$$F = \frac{E_0^2y^2}{8} e^2 \frac{\ln(1+e^2)-e^2(1-e^2)}{\{(1/2)\ln[(1+e)/(1-e)]-e\}^2}. \tag{21}$$

By equating this to the rate of change of the momentum given by Eq. (16), we obtain the equation of motion:

$$d(R^3\dot{y})/dt=(1/5)B^2y^2g(e), \tag{22}$$

where

$$g(e)=e^2\frac{\ln(1+e^2)-e^2(1-e^2)}{\{(1/2)\ln[(1+e)/(1-e)]-e\}^2}. \tag{23}$$

The relation between y and R is given by integrating Eq. (15) and using the condition imposed by Eq. (14). It is

$$2R=3y_1-y. \tag{24}$$

Transforming variables by substituting

$$\eta=y/y_1,\ T=(t-t_1)(8/5)^{\frac{1}{2}}B/y_1 \tag{25}$$

and using Eq. (24) to eliminate R from Eq. (21) we have

$$d(3-\eta)^3\dot{\eta}/dT=\eta^2g(e) \tag{26}$$

with $\eta=1$ at $T=0$. From Eqs. (17) and (24) we find

$$\eta=3/(3-2e^2). \tag{27}$$

Thus, by calculating η and $g(e)$ for a sequence of values of e from 0 to 1, values of the right member of Eq. (26) can be tabulated as a function of η, and the equation can be solved by numerical integration.

Such a tabulation appears in Table I and a plot is shown in Fig. 10. It is seen that at $\eta=2.51$ a tenfold increase of field is attained, and that up to this value of η, $\eta^2\,g(e)$ is fairly constant at the value 5. By using this value in Eq. (26), we can integrate directly to obtain an approximate solution

$$(3-\eta)^3\dot{\eta}=5T+c, \tag{28}$$

where c is a constant of integration. Now at $T=0$, we have $\eta=1$, and

$$\dot{\eta}_1=d\eta_1/dT=(dy_1/y_1)/dt(dT/dt)$$
$$=(dy_1/dt)(dt/y_1dT)=\dot{w}_1(5/8)^{\frac{1}{2}} \tag{29}$$

TABLE I.

e	y/R	E/E_0	η	$\eta^2g(e)$	T
0	1.00	3.00	1.00	4.50	0
0.4	1.19	3.24	1.12	5.10	0.257
0.6	1.56	3.63	1.32	5.44	.504
0.8	2.78	4.78	1.75	5.81	.746
0.9	5.26	6.70	2.17	5.12	.814
0.95	10.3	10.02	2.51	4.03	.829
0.98	25.2	18.1	2.78	2.81	—
1.00	∞	∞	3.00	0	.833

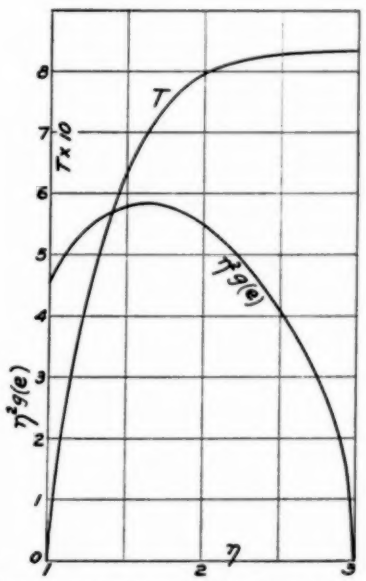

FIG. 10. The force function $\eta^2g(e)$ of Eq. (26) and elapsed time ($\sim T$) in second stage.

from Eqs. (14) and (25). Using these conditions gives for the first order equation

$$(3-\eta)^3\dot{\eta}=5T+2\dot{w}_1(10)^{\frac{1}{2}}.$$

Another integration, adjusted to initial conditions, gives

$$10T^2+8(10)^{\frac{1}{2}}\dot{w}_1T-16+(3-\eta)^4=0. \tag{30}$$

Values of T for different values of η are given in Table I and shown in Fig. 10. Whether we seek a sixfold or greater increase in field makes but little difference in the value of T which rapidly approaches its final value $T_2=0.83$.

In converting the mathematical quantities w, σ, τ and T into the physical quantities, y, r and t, we note from Eqs. (9) and (25) that the quantities A and B are of primary importance. Expressing field strength in megavolts cm^{-1}, denoted by E_{MV}, we have for mercury

$$A=8\pi T/E_0^2=1.02\times10^{-3}E_{MV}^{-2}, \tag{31}$$

$$B=E_0/(\pi\rho)^{\frac{1}{2}}=509E_{MV}. \tag{32}$$

We then obtain directly:

$$y_0=w_0A=4.08\times10^{-5}E_{MV}^{-2}, \tag{33}$$

$$r_0=0.913A=0.931\times10^{-3}E_{MV}^{-2}, \tag{34}$$

Eq. (23):

$$y_1=r_1=0.450A=0.459\times10^{-3}E_{MV}^{-2}, \tag{35}$$

$$dy_1/dt=0.431B=229E_{MV}, \tag{36}$$

$$t_1=\tau_1A/B=4.8\times10^{-6}E_{MV}^{-3}, \tag{37}$$

$$\text{Eq. (24)} \quad \left.\begin{aligned} t_2 - t_1 &= (5/8)^{\frac{1}{2}} \times 0.450 \times 0.83 A/B \\ &= 0.59 \times 10^{-6} E_{\text{MV}}^{-3}, \end{aligned}\right. \quad (38)$$

and it follows that

$$t_2 = 5.4 \times 10^{-6}\ E_{\text{MV}}^{-3}. \quad (39)$$

Thus an initial disturbance of height 4×10^{-5} cm and diameter 2×10^{-3} cm in a field of 1 megavolt cm^{-1} will give rise to surface rupture in 5.4μ sec. The increase in time attendant upon smaller initial unevenness y_a is found from Eq. (12) to be

$$t_0 = 2.83 \times 10^{-6} E_{\text{MV}}^{-3} \ln (y_0/y_a), \quad (40)$$

so that at 1 megavolt cm^{-1} again, the rupture time is increased 2.8μ sec. for every power of ϵ that y_a is less than y_0.

The striking feature of the result of this calculation is the extreme shortness of the time in which a marked mechanical response is achieved. To be sure, the peak which is raised is very small, being only $3y_1 = 1.4\times10^{-3} E_{\text{MV}}^{-2}$ cm high at rupture.

In the experiments on sparking between mercury and a solid electrode the mercury surface was so constrained by a meniscus that no short circuiting occurred when the sparking voltage was applied. Under these conditions there was a concentration of field at the mercury meniscus, and there was also an initial distortion of the surface. The field was produced by an Mo strip, edge down, 0.025 cm above the mercury. A 60-cycle a.c. voltage of somewhat over 11,000 v peak was required for sparking at room temperature. This rose about 20 percent as the mercury was cooled to its freezing point and there almost doubled when solidification occurred. At room temperature the sparking voltage rose 60 to 70 percent when a second Mo strip was substituted for the liquid mercury surface, so that the spark occurred between two solid electrodes. Thus the effect of lowering the sparking voltage by substituting a liquid for a solid electrode is definite.

But the geometry was too indefinite for a quantitative test of the theory. Suffice it to point out that the field of the order of 0.4 MV cm^{-1} gives a value of 80μ sec. to t_2, which is very short compared to the duration of 1/2 cycle.

In Beams' experiment a field of 1.8 MV cm^{-1} applied to a clean mercury surface caused electrical breakdown in 1μ sec. Eqs. (33) and (39) state that for this field an initial amplitude of 1.3×10^{-5} cm will give rupture in 0.93μ sec. It is impossible to say whether or not disturbances of this magnitude were present. The corresponding diameter, 5.7×10^{-4} cm by Eq. (34) is the wave length λ of capillary waves of frequency $(2\pi T/\rho)^{\frac{1}{2}}\lambda^{-\frac{3}{2}} = 10^6$ sec.$^{-1}$, a frequency usually considered as outside the range of mechanical vibrations. Certainly, experiments to determine the magnitude of the waves on the mercury surface and the dependence of electrical breakdown on pulse duration can be performed.

The possibility suggests itself that thermal roughness of the surface may account for the incipient rupture. R. Gans has calculated[4] the mean square amplitude by means of a Fourier analysis. The order of magnitude of the displacement for a hump is $(k\theta/T)^{\frac{1}{2}}/\pi$ independent of diameter, θ being the absolute temperature. At room temperature this is 3×10^{-9} cm. By Eq. (40), $t_0 \sim 30\mu$ sec. at 1 MV cm^{-1}. Further consideration shows that the thermal velocity rather than displacement is the pertinent quantity, and it seems possible at this writing that this may furnish "strong" enough nuclei. Nuclei of optimum diameter, which have been the only ones considered here, are still too "weak," but smaller nuclei may gain in strength (because of the operation of statistical laws) more than enough to compensate for what they lose in growth acceleration by the field.

The application of the results of the present calculation to the cathode spot is less clear. The cathode drop of 10 v in a distance of s cm, the cathode sheath thickness, would give a field strength $E_{\text{MV}} \sim 10^{-5}/s$. The height of peak at rupture would then be $3y_1 \sim 1.4\times10^{7} s^2$ by Eq. (35), and for the hump to lie entirely within the sheath at this stage $1 > 3y_1/s \sim 1.4\times10^{7} s$, whence $s < 7\times10^{-8}$ cm, a value far below that at which field emission would occur without peaking and also far below the 10^{-5} cm which has been calculated in other ways.

---

[4] R. Gans, Ann. d. Physik **74**, 231 (1934).

LETTERS TO THE EDITOR

Prompt publication of brief reports of important discoveries in physics may be secured by addressing them to this department. Closing dates for this department are, for the first issue of the month, the twentieth of the preceding month; for the second issue, the fifth of the month. The Board of Editors does not hold itself responsible for the opinions expressed by the correspondents.

The Photographic Absorption Spectrum of Gaseous Ammonia

The absorption spectrum of the ammonia molecule, which is of the symmetrical top type, has been investigated by many authors. The four bands in the photographic region, 10,230A, 7920A, 6470A and 5490A,[1] have generally been considered to be harmonics of the fundamental band at $3\mu(\nu_1)$. Because of the complexity of the structure, only partial analyses of these bands have been made. A higher resolution has been attained in the present work, but a satisfactory analysis has not yet been completed. Nevertheless a brief preliminary report will be given in the following.

The 10,230A band appears in the present work to consist of two separate bands which can be distinguished by their intensity in absorption and which slightly overlap at 10,150A. The one of longer wave-length is the stronger and its center is approximately at 10,230A, while the center of the weaker band appears to be at 9900A. In the former, there are several groups of strong lines on the high frequency side with intervals of about 10 cm^{-1}, half the spacing of the parallel type band. This suggests similarity to the perpendicular type band such as 1.97μ, studied by Stinchcomb and Barker.[2] The structure of the weaker band is relatively simpler.

In the 6470A band, a group of strong lines which are nearly equally spaced in the center of the band suggests the Q branch of a perpendicular type band, while there are also other groups of lines resembling P and R branches. Its appearance is similar to that expected for a perpendicular type band derived from rotation energy levels

$$E_r/hc = BJ(J+1)+\beta BK^2,$$

where $B=9.92$, $\beta B=1.4$ cm^{-1} (1.4 = half the average spacing of the lines in the Q group). There are, however, several discrepancies. For instance, the spacing of the lines due to changes of K with fixed J-values are smaller in the R branch and are larger in the P branch than those in the Q branch.

Recently Adel[3] proposed that the 6470A band is the fourth harmonic of the parallel type band, ν_1, with a doubling similar to the 10μ band. But the structure of the band does not agree with this type, even with different values of B and β in the normal and excited states. As already mentioned, the structure looks much more like that of a perpendicular type band, although it has not yet been possible to make it fit this type entirely.

In order to account for perpendicular type bands in the photographic region, the following possibilities may be considered. The first possibility is that, if the 1.97μ band is considered, as was done by Barker,[2] to be one of the fundamentals of the perpendicular type, ν_2, then the 10,230A band or else the 9900A band may be the first and the 6470A band the second harmonic of this fundamental. The second possibility is that, if ν_2 is in the neighborhood of 3300 cm^{-1} as suggested by Amaldi and Placzek,[4] then the four bands will be harmonics of this perpendicular type fundamental band. Although this 3300 frequency has been found only in the Raman spectrum of liquid ammonia, it should be noted that Howard[5] recently showed by calculations based on the valence force potential function that one of the perpendicular type fundamentals is probably approximately at 3450 cm^{-1}, which is very close to ν_1.

It has been shown[6] that the harmonics of perpendicular type bands in general include a set of several parallel and perpendicular type bands, so that their structure should be rather complex.

I wish to express my appreciation to Professor R. S. Mulliken for the proposal of the problem and for constant inspiration and valuable advice throughout the investigation.

SIU-HUNG CHAO

Ryerson Physical Laboratory,
University of Chicago,
August 23, 1935.

[1] P. Lueg and Hedfeld, Zeits. f. Physik **75**, 599 (1932); H. J. Unger, Phys. Rev. **43**, 123 (1933); R. M. Badger and R. Mecke, Zeits. f. physik. Chemie **B5**, 333 (1929); R. M. Badger, Phys. Rev. **35**, 1038 (1930).
[2] G. A. Stinchcomb and E. F. Barker, Phys. Rev. **33**, 305 (1929).
[3] A. Adel, Phys. Rev. **48**, 103 (1935).
[4] E. Amaldi and G. Placzek, Zeits. f. Physik **81**, 259 (1933); P. Daure, Ann. de Physique **12**, 375 (1929); R. G. Dickinson, R. T. Dillon and F. Rasetti, Phys. Rev. **34**, 582 (1929).
[5] J. B. Howard, J. Chem. Phys. **3**, 207 (1935).
[6] Cf. L. Tisza, Zeits. f. Physik **82**, 48 (1933).

Fine Structure in the K X-Ray Edge of Gallium

Previous investigations have shown no extended fine structure in the K x-ray absorption edge of Ga. In view of Hanawalt's work[1] on the fine structure in the K edge of Fe as a function of temperature, it was thought that a structure might exist in the Ga edge at temperatures sufficiently below the melting point, 30°C. Accordingly, absorption spectra in the vicinity of the Ga K edge were investigated at low temperatures, and a preliminary report of the results is given herewith.

The Ga absorber was a rolled foil 0.001 inch thick, supported on stiff paper. The source of x-rays was a tungsten target, water-cooled, metal tube run at 38 kv and 24 ma. A Société Génevoise double crystal spectrometer was used as a single crystal instrument, observations being made by the ionization method. Blank runs were taken to ensure

that the results were not spurious. The foil was cooled by a stream of vapor from boiling liquid air.

At the lowest temperature, −150°C, five peaks were found at energies greater than the drop at the main Ga K edge by 77, 127, 154, 201, and 248 volts, respectively. The peak at 127 volts appeared as an unresolved shoulder on the 154-volt peak and the 248-volt peak is weak and unverified. The other three peaks are quite strong and definite.

A single run through the structure at −67°C showed only peaks at 63 and 123 volts from the main edge, both of which were broader and less intense than the corresponding peaks at the lower temperature. Runs at room temperature agree with previous observations in showing no structure.

The crystal structure of Ga is unique, and an attempt is to be made to compare the experimental results with Kronig's theory for the Ga structure. A full report of the work will be published soon.

A value of the wave-length of the Ga K edge of 1192.5 X.U. is found, agreeing with the value given by Kievit and Lindsay[2] (1192.9 X.U.) rather than the accepted value of 1190.2 X.U.

W. W. Mutch

Sloane Physics Laboratory,
Yale University,
August 26, 1935.

[1] J. D. Hanawalt, Zeits. f. Physik **70**, 293 (1931).
[2] B. Kievit and G. A. Lindsay, Phys. Rev. **36**, 648 (1930).

On the Recombination of Neutrons and Protons

The process of the photoelectric disintegration of the deuteron, and the reverse process (recombination of a neutron and a proton with formation of a deuteron and emission of a γ quantum) have been treated theoretically by Bethe and Peierls.[1] These authors consider the emission or absorption of γ-rays by the ordinary mechanism of the electric dipole radiation. For the recombination cross section they obtain an expression which vanishes in the limit of low relative velocities of the neutron and the proton. This last result seems to be in contradiction with general experimental evidence, that slow neutrons are captured in hydrogenated materials such as paraffin or water. Recently the lifetime of a slow neutron in paraffin has been evaluated by a direct experiment and found to be of the order of magnitude of 10^{-4} second.[2]

I wish to point out that if we take into account also the radiation processes due to oscillations of the magnetic dipole of the neutron-proton system, one finds a probability of capture which is in satisfactory agreement with the above value. The theory is based on the customary assumption that the fundamental state of the deuteron is a ^3S (neutron and proton with parallel spins).

The ordinary theory of impact shows that in the case of slow neutrons only the capture from S states in the continuum is of importance. The usual radiative processes of electric dipole and quadripole are forbidden for these $S-S$ transitions. Instead transitions from a ^1S state in the continuum to the fundamental ^3S state can occur by the mechanism of magnetic dipole radiation.

The ordinary electromagnetic theory gives for the inverse mean life $1/\tau$ of a neutron with velocity v moving in a medium containing n protons per unit volume the following formula:

$$\frac{1}{\tau}=n\cdot\frac{64\pi^4h\nu^3}{c^3m^2v^2}\mu_0(g_p-g_n)^2\left|\int f\varphi r^2dr\right|^2.$$

m is the neutron mass: ν is the emitted frequency; μ_0 is the nuclear magneton; g_p and g_n are the nuclear g-factors for proton and neutron. The last integral contains the normalized eigenfunction $f(r)$ of the fundamental state and the continuum eigenfunction $\varphi(r)$. This last is normalized in such a way that for large r it goes over into $(1/r)$ sin $(2\pi pr/h+\text{const.})$.

This last integral can be evaluated numerically by methods similar to those used by Bethe and Peierls. The parameter needed for the description of the ^1S eigenfunction can be obtained on the assumption that the high elastic scattering cross section of slow neutrons in hydrogen is mainly due to the ^1S eigenfunction (real or virtual ^1S level close to energy zero). We find for slow neutrons

$$\frac{1}{\tau}=\frac{16\pi^3W^{5/2}}{h^3c^3m^{\frac{1}{2}}}\frac{\mu_0^2(g_p-g_n)^2}{l},$$

where l is the mean free path for the elastic scattering of slow neutrons (for paraffin about 0.5 cm)[3], and $W=2.1\times10^6$ e.v. is the binding energy of the deuteron. Assuming 3 and 1, nuclear magnetons, as magnetic moments of the proton and the deuteron,[4] we get $g_p=6$ and $g_n=-4$. This gives $1/\tau=5.2\times10^3$ in agreement with the experimental result.

The magnetic dipole radiation affects also the process of the photoelectric disintegration of the deuteron. The cross section for the photoelectric absorption of a γ-ray by a deuteron results on the same assumptions

$$\sigma_\gamma=\frac{4\pi^2a^2\alpha^2\mu_0^2(g_p-g_n)^2}{3hc}\frac{(\gamma-1)^{\frac{1}{2}}}{\gamma\{1+a^2\alpha^2(\gamma-1)\}},$$

where $$a^2=\frac{1}{\pi nl},\quad \alpha^2=\frac{4\pi^2mW}{h^2},\quad \gamma=\frac{h\nu}{W}.$$

The cross section must be added to that already calculated by Bethe and Peierls in order to give the total cross section.

Details of this theory will be published elsewhere.

Enrico Fermi

University of Michigan,
August 27, 1935.

[1] H. Bethe and R. Peierls, Proc. Roy. Soc. **A148**, 146 (1935).
[2] E. Amaldi, O. D'Agostino, E. Fermi, B. Pontecorvo and E. Segrè, Ricerca Scientifica, June, 1935.
[3] E. Amaldi, O. D'Agostino, E. Fermi, B. Pontecorvo, F. Rasetti and E. Segrè, Proc. Roy. Soc. **A149**, 522 (1935).
[4] O. Frisch and O. Stern, Zeits. f. Physik **85**, 4 (1933); Estermann and Stern, Zeits. f. Physik **85**, 17 (1933); Phys. Rev. **45**, 761 (1934); Rabi, Kellogg and Zacharias, Phys. Rev. **45**, 157, 163 (1934).

Alpha Radioactivity of Argon Formed by Radiochlorine

During a study of the beta-radiation from a sample of silver radiochloride by means of the screen-wall counters previously used in this laboratory[1] it was found possible to follow the decay of the radiochlorine when the sample was at a distance from the counter so that none of the beta-radiation could have reached the counter itself. However, the sample and counter were both enclosed in a chamber filled with argon at 2 or 3 cm of Hg pressure so that a gas evolved by the sample might have reached the counter. Following careful establishment of these observations direct evidence for the properties of the gas was obtained by passing gas which had stood for several minutes in contact with the hot silver radiochloride sample at a rate of a fraction of a liter per minute through a copper coil three or four feet in length immersed in liquid air. This gas was used to fill a solid wall tube counter which was immediately placed in operation. A fall in rate was observed which corresponded to an activity of half-life 1.9 ± 0.3 minutes. The initial effect was generally about fifty or seventy-five per minute superimposed on a background of fifty per minute. Changing the size and material construction of the counter had no appreciable effect on the behavior of the gas. From these results the conclusions were drawn that, first, the active gas must be formed by radiochlorine when it disintegrates and, secondly, that the gas must be argon because no other gas which radiochlorine might form would pass the liquid air trap used.

The character of the radiation from the gas was partially established by covering the screen-wall counter used in the first experiment with an aluminum foil of approximately 3 cm air equivalent and repeating the experiment in which the counts due to the diffused radioactive gas were used to follow the decay of the radiochlorine. The result was almost complete disappearance of the effect, indicating that the radiation from the gas had a range less than 3 cm of air and was therefore probably alpha in character.

To investigate further the gaseous radiation, a low pressure cloud chamber operating at 1/8 atmosphere of air and water vapor was used. The gas was passed from the warm silver radiochloride sample into the chamber and the chamber expanded at the rate of 20 expansions per minute. A polonium source was frequently placed near a mica window to furnish comparison alpha-particle tracks. In the course of the investigation of approximately two dozen silver radiochloride samples we obtained between 50 and 75 tracks with both ends located in the gas and approximately 1.5 to 2.5 cm in length. All the tracks were observed within 8 minutes after transference of the gas. The densities of the tracks were comparable with those of the polonium alpha-tracks and definitely greater than those of beta-tracks formed by recoil electrons from a strong gamma-radiation source.

Fig. 1 shows a picture of the direct and two mirror images of the chamber and one of the tracks. The pointer shown was being used to mark the position of a track in the preceding picture when the track shown occurred in almost exactly the same position. Reprojection of the three images showed the track to have had its upper end 6 mm from the top of the chamber and its lower end 12 mm from the bottom, to have been inclined at a vertical angle of 49.5° and to have been 22 mm long. Reduction to standard air gives 3.0 mm as the equivalent length of this track.

Data on four tracks gave standard air ranges of 2.9, 3.0, 3.1 and 3.2 mm, indicating a probable value of 3.1 ± 0.2 mm in rather close agreement with the prediction of 1 to 3 mm of the Gamow, Gurney and Condon theory for an alpha-particle from argon of 1.9 minutes half-life.

The silver radiochloride was prepared by precipitation from the water phase resulting from the extraction of

FIG. 1. Sample picture of track. Arrows indicate positions of the direct and two mirror images.

ethylene dichloride in which small amounts of $FeCl_2$ and $FeCl_3$ had been dissolved prior to irradiation by neutrons from a radon-beryllium source.

Because of the relative scarcity of A^{38} we suggest that it is the active argon isotope formed, the principal reactions in the series being

$$Cl^{38}=e^-+A^{38}, \quad A^{38}=\alpha+S^{34},$$

Cl^{38} being formed by $Cl^{37}+n=Cl^{38}$.

We wish to thank Dr. L. R. Taussig and the University of California Hospital for the donation of the several hundred millicuries of radon used in the course of this research. The members of the Radiation Laboratory, in particular Dr. F. N. D. Kurie and Dr. M. G. White, also have our thanks for the advice and assistance they have given us.

W. F. Libby
M. D. Peterson
W. M. Latimer

Department of Chemistry,
University of California,
Berkeley, California,
August 26, 1935.

[1] Libby, Phys. Rev. **46**, 196 (1934).

The Arc Spectrum of Tungsten

The structure of the arc spectrum of tungsten has been studied in this laboratory in connection with the remeasurement of the spectrum on plates made last year by the Bureau of Standards. The number of known levels is as follows:

j-Value	Even	Odd
0	3	2
1	5	29
2	7	53
3	9	62
4	8	51
5	7	41
6	2	13
Total	41	251

including those levels recently published by F. Poggio[1] which we could verify. Our list includes besides the levels published by Laporte in *Atomic Energy States*,[2] those found by Dr. J. E. Mack and kindly communicated by him.

Approximately 3000 lines are accounted for, but about 2000 arc lines remain unclassified, including about a dozen which show self-reversal or furnace of underwater spark absorption. Some lines of the latter class arise from rather high levels with j-values greater than the lowest ^7D term; for instance, from the 5-level at 15,069.94 cm^{-1}, which was discovered by Laporte and Mack but remains unpublished. Other important even levels found more recently by the author are:

4—16431.30	5—19535.00	5—49354.58
6—17008.46	6—19648.48	4—51123.08
4—17107.01	4—47975.45	5—55333.03.

The last four of these account for some of the most intense lines in the spectrum and an odd level has been found at 26,676.38 with j-value equal to 5 which combines with the first of these to account for an intense line which King[3] lists as possibly showing absorption in the electric furnace.

D. D. Laun

Marquette University,
August 24, 1935.

[1] F. Poggio, Anales Sociedad Española de Fisica y Quimica **33**, 171 (1935).
[2] Bacher and Goudsmit, *Atomic Energy States* (1932), p. 590.
[3] A. S. King, Astrophys. J. **75**, 379 (1932).

THE AMERICAN INSTITUTE OF PHYSICS

INCORPORATED

GOVERNING BOARD

For The American Physical Society:

KARL T. COMPTON, *Chairman*
Massachusetts Institute of Technology

GEORGE B. PEGRAM, *Secretary*
Columbia University

JOHN T. TATE
University of Minnesota

For The Optical Society of America:

E. C. CRITTENDEN
Bureau of Standards

PAUL D. FOOTE
The Gulf Companies

F. K. RICHTMYER
Cornell University

For The Acoustical Society of America:

HARVEY FLETCHER
Bell Telephone Laboratories

VERN O. KNUDSEN
University of California at Los Angeles

WALLACE WATERFALL
The Celotex Company

For The Society of Rheology:

E. C. BINGHAM
Lafayette College

A. STUART HUNTER
du Pont Rayon Company

S. E. SHEPPARD
Eastman Kodak Company

For The American Association of Physics Teachers:

HOMER L. DODGE
University of Oklahoma

PAUL E. KLOPSTEG
Central Scientific Company

FREDERIC PALMER
Haverford College

ADMINISTRATIVE STAFF

HENRY A. BARTON, *Director* JOHN T. TATE, *Adviser on Publications*

MADELINE M. MITCHELL, *Editorial Secretary*

Office: 11 East 38th Street, New York, New York

JOURNALS

THE PHYSICAL REVIEW

REVIEWS OF MODERN PHYSICS

PHYSICS

JOHN T. TATE, *Editor*
J. W. BUCHTA, *Assistant Editor*
E. C. BINGHAM, *Rheology Editor*

THE JOURNAL OF THE OPTICAL SOCIETY OF AMERICA

THE REVIEW OF SCIENTIFIC INSTRUMENTS WITH PHYSICS NEWS AND VIEWS

F. K. RICHTMYER, *Editor*

JOURNAL OF THE ACOUSTICAL SOCIETY OF AMERICA

F. R. WATSON, *Editor*

THE JOURNAL OF CHEMICAL PHYSICS

HAROLD C. UREY, *Editor*

THE AMERICAN PHYSICS TEACHER

DUANE ROLLER, *Editor*

The American Institute of Physics is a membership corporation of which five societies are the founding members. These five societies are the principal national societies devoted to pure and applied physics in America. Their names, and those of their representatives who form the Governing Board of the Institute, are given above. The principal work of the Institute is the publication of journals sponsored by the societies or by itself. The names and the editors of the journals are also listed above.

The broad purpose of the Institute is to represent, in all matters of wide or common interest, the five thousand or more members and subscribers associated with the Founder Societies and the journals. It aims to advance the science and profession of physics, and to promote cooperation between pure research, the applied sciences and the industries. To achieve these aims, it is greatly in need of an endowment and is empowered by law to administer grants and funds of any kind.

CONTENTS

PHYS. REV. 48 (1935) SEPTEMBER 15

Diffraction of X-Rays by Liquid Na-K Alloy in a Magnetic Field. C. W. HEAPS 491

Transmutation Functions for Some Cases of Deuteron-Induced Radioactivity . ERNEST O. LAWRENCE, EDWIN MCMILLAN AND R. L. THORNTON 493

Note on the Transmutation Function for Deuterons. . . . . .J. R. OPPENHEIMER AND M. PHILLIPS 500

Radioactivity of Solids Determined by Alpha-Ray Counting. . . . . GLADYS D. FINNEY AND ROBLEY D. EVANS 503

Double Beta-Disintegration. . . . . M. GOEPPERT-MAYER 512

Infrared Absorption Spectra of the Linear Molecules Carbonyl Sulphide and Deuterium Cyanide. . . PAUL F. BARTUNEK AND E. F. BARKER 516

Absorption Spectrum of Tin Sulphide . . . . . E. N. SHAWHAN 521

Mass Spectrum Analysis of the Products of Ionization by Electron Impact in Nitrogen, Acetylene, Nitric Oxide, Cyanogen and Carbon Monoxide. . . . . .JOHN T. TATE, P. T. SMITH AND A. L. VAUGHAN 525

Effect of a Magnetic Field Upon the Polarization of Impact Radiation. . . . . .W. H. MCCORKLE 532

Atomic Energy States for Excited Helium . . . . . WM. S. WILSON 536

Dielectric Constant of Water Vapor . . . . . J. D. STRANATHAN 538

Rate of Change of Electron Temperature in the Mercury Afterglow. . . . . .ROBERT H. RANDALL AND HAROLD W. WEBB 544

Contribution to the Theory of the B. W. K. Method. . .EDWIN C. KEMBLE 549

Theory of Liquid Surface Rupture by a Uniform Electric Field . LEWI TONKS 562

Letters to the Editor:

Photographic Absorption Spectrum of Gaseous Ammonia . . SIU-HUNG CHAO 569

Fine Structure in the *K* X-Ray Edge of Gallium . . . . . W. W. MUTCH 569

On the Recombination of Neutrons and Protons . . . . . ENRICO FERMI 570

Alpha Radioactivity of Argon Formed by Radiochlorine . . . . . W. F. LIBBY, M. D. PETERSON AND W. M. LATIMER 571

Arc Spectrum of Tungsten . . . . . D. D. LAUN 572

LANCASTER PRESS, INC., LANCASTER, PA.